Carnegie Mellon University

CARNEGIE INSTITUTE OF TECHNOLOGY

THESIS

SUBMITTED IN PARTIAL FULFILLMENT OF THE REQUIREMENTS

FOR THE DEGREE OF Doctor of Philosophy

TITLE **Scalable and Robust Designs of Model-Based Control Strategies for Energy-Efficient Buildings**

PRESENTED BY **Clarence Agbi**

ACCEPTED BY THE DEPARTMENT OF

Electrical and Computer Engineering

Bruce Krogh — ADVISOR, MAJOR PROFESSOR — 5/14/14 — DATE

Jelena Kovacevic — DEPARTMENT HEAD — 5/14/14 — DATE

APPROVED BY THE COLLEGE COUNCIL

Vijayakumar Bhagavatula — DEAN — 5/14/14 — DATE

Scalable and Robust Design of Model-Based Control Strategies for Energy-Efficient Buildings

Submitted in partial fulfillment of the requirements for

the degree of

Doctor of Philosophy

in

Electrical and Computer Engineering

Clarence E. Agbi

B.S., Electrical Engineering, Yale University
M.S., Electrical and Computer Engineering, Carnegie Mellon University

Carnegie Mellon University
Pittsburgh, PA

May 2014

Abstract

In the wake of rising energy costs, there is a critical need for sustainable energy management of commercial and residential buildings. Buildings consume approximately 40% of total energy consumed in the US, and current methods to reduce this level of consumption include energy monitoring, smart sensing, and advanced integrated building control. However, the building industry has been slow to replace current PID and rule-based control strategies with more advanced strategies such as model-based building control. This is largely due to the additional cost of accurately modeling the dynamics of the building and the general uncertainty that model-based controllers can be reliably used in real conditions.

The first half of this thesis addresses the challenge of constructing accurate grey-box building models for control using model identification. Current identification methods poorly estimate building model parameters because of the complexity of the building model structure, and fail to do so quickly because these methods are not scalable for large buildings. Therefore, we introduce the notion of parameter identifiability to determine those parameters in the building model that may not be accurately estimated and we use this information to strategically improve the identifiability of the building model. Finally, we present a decentralized identification scheme to reduce the computational effort and time needed to identify large buildings.

The second half of this thesis discusses the challenge of using uncertain building models to reliably control building temperature. Under real conditions, building models may not match the dynamics of the building, which directly causes increased building energy consumption and poor thermal comfort. To reduce the impact of model uncertainty on building control, we pose the model-based building control

problem as a robust control problem using well-known H_∞ control methods. Furthermore, we introduce a tuning law to reduce the conservativeness of a robust building control strategy in the presence of high model uncertainty, both in a centralized and decentralized building control framework.

Acknowledgments

First and foremost, I would like to thank God, without whom my journey through graduate school would not have been possible. I am deeply grateful for the opportunity to realize my dreams, for the important lessons that I have learned, and for the cast of the characters that I have met along the way.

I would like to express my profound gratitude to my advisor Professor Bruce H. Krogh for advising me through this journey. He was tough when he needed to be and celebrated all of my accomplishments no matter how small. I am forever grateful for the time he has taken to make me better. Thank you for seeing me through to the end! I would like to specially thank my committee member Dr. Zhen Song at Siemens Corporate Research for his encouragement to pursue this topic and his constant input and collaboration. I also acknowledge and thank Professor Bruno Sinopoli and Professor Mario Berges, for serving on my thesis committee.

I acknowledge the financial support of The National Science Foundation Graduate Research Fellowship. I would like to thank Dr. Yan Lu and the researchers at Siemens Corporate Research for the opportunity to do some very interesting work on building energy efficiency, out of which was born this dissertation. I would like to thank The Center for Building Performance and Diagnostics, and I am deeply grateful for the collaboration and friendship of researchers at the Intelligent Workplace, in particular the (soon to be Dr.) Erica Cochran and her family, Azizan Aziz, Dr. Vivian Loftness, Flore Marion, Bertrand Lasternas, and Dr. Yuebin Yu.

I want to express my gratitude to Dr. Suzanne Laurich-McIntyre for her encouragement and advice throughout this process. I am grateful to know Dr. Jessica Porter, Dr. Portia Taylor, Dr. Sanna Gaspard, and Dr. Britney McCoy who have served as examples on how to navigate this process and have been a source of in-

spiration and encouragement for me at every stage of my process. Murakoze to the numerous students, staff, and faculty at CMU-R that I have had the pleasure to meet and befriend during my time in Rwanda.

I would like to thank Sergio Pequito for his friendship and support throughout this process, and for being a sounding board for my research. I would also like to thank Claire Baurle, Dr. Akshay Rahjans, Dr. Ajinkya Bhave, Dr. Luca Parolini, Nikos Arechiga and the rest of Porter Hall B-Level. Finally, I would like to thank my undergraduate advisor Professor Roman Kuc whose course sparked my curiosity in all things automated, smart, and decentralized. I would also like to thank Professor Kumpati Narendra for the impetus to continue studying in the area of control.

I would also would like to thank my friends outside of my scholarly activities who have put up with me through graduate school: Prep for Prep, Sage Sevilla and my friends at The Dalton School, friends at Yale University, and the numerous friends I have made in Pittsburgh both inside and outside of CMU.

Finally, this thesis is dedicated to my family, in particular my parents, whose prayers have been heard, and answered.

Contents

List of Tables

List of Figures

List of Algorithms

Chapter 1

Introduction

Managing energy consumption in building environments has become an increasingly difficult and complex problem. Often times, the energy needed to keep a building environment comfortable and operational outweighs behavioral strategies for energy conservation. In recent years, there has been an increase in automated energy management software and control solutions to address this problem. However, there is a general reluctance to retrofit old buildings with newer automated strategies or include advanced control strategies in newer buildings. Part of this reluctance stems from capital costs due to the installation of a new building control system, the cost of commissioning this new system, training personnel to learn the new equipment, the cost of maintenance, and the long-term returns on investment. Admittedly, some of these costs are inevitable and cannot be completely eliminated from the equation. However, this dissertation endeavors to tackle some of the costs associated with commissioning model-based building control strategies.

Model-based control strategies are very difficult to instrument in real building environments because of the complexity and size of the building dynamics to be

modeled. Furthermore, depending on the type of control model employed, building control models may have to be regularly retuned, maintained, and monitored to ensure the model-based control strategy still works accurately. These activities all come at a cost to the building owner and the companies employed to maintain these systems. To tackle these challenges, we investigate two major questions related to the commissioning and implementation of model based building control:

1. *How do we accurately and efficiently model building environments?*

2. *How do we control buildings using uncertain building models?*

This dissertation explores each of these questions in depth. We provide practical strategies to efficiently and accurately create a control-oriented building model, and we consider robust control approaches to deal with model uncertainty.

This chapter introduces some of the current and state-of-the-art approaches to advanced building control. We motivate our discussion of model-based building control by highlighting current trends to reduce building energy consumption and the potential for energy savings through advanced control strategies such as model-based control. We balance this discussion with the potential problems of implementing a model-based controller for real buildings, and we summarize our efforts to address these issues.This chapter is organized as follows. Section 1.1 provides an overview of the energy trends for building environments in the U.S. Section 1.2 reviews current approaches to advanced building control strategies, including conventional and model-based control strategies for real building environments. Finally, Section 1.3 summarizes the contributions and the organization of this dissertation.

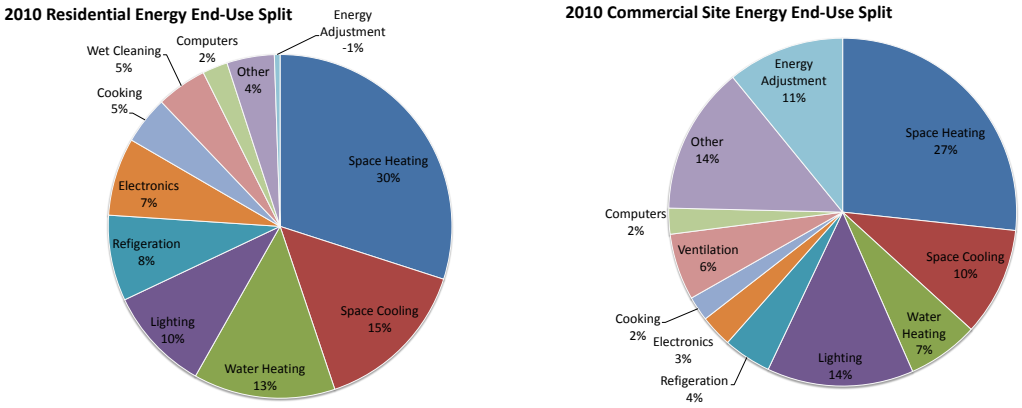

(a) Residential Buildings (b) Commercial Buildings

Figure 1.1: Breakdown of energy consumption in residential and commercial buildings in 2010 created from building energy data in [29].

1.1 Trends in Building Energy Consumption

Building environments are broadly classified as either residential or commercial buildings, and this classification generally determines how energy is consumed in the building. Residential buildings such as apartment buildings, condominiums, and single family homes cater to the general population and function primarily to shelter people. Therefore, residential buildings primarily consume energy in the form of electricity and fossil fuels to keep people comfortable through proper heating, cooling, and ventilation. Commercial buildings such as schools, stores, office buildings, warehouses, and hospitals cater to select segments of the population and serve different needs. Consider a museum building which serves to store and showcase artwork for the general population. Then, lighting and cooling are the primary uses of energy in the building, and likely consume a majority of the energy consumed in the museum.

According to the U.S. Department of Energy (DOE), energy consumption of residential and commercial buildings constitute about 40% of the total energy consumed in the U.S, where commercial buildings make up 22% of the total energy consumption

[29]. Energy audits of residential and commercial buildings in [16, 29] reveal the top five ways energy is consumed: space heating, space cooling, water heating, lighting, and electrical plug loads. Fig. 1.1a and 1.1b illustrate the breakdown of energy use in residential and commercial buildings, respectively. Space and water heating, space cooling, and ventilation alone make up about 50% of total energy consumption for both building classifications. Given these statistics, we observe heating, cooling, and ventilating buildings significantly impact national energy consumption, contributing to approximately 20% of total U.S. energy consumption. This observation, coupled with increased energy costs and carbon emissions, has motivated policy makers and some building owners to actively reduce building energy consumption, particularly in commercial buildings.

The Building Technologies Office at the DOE has identified significant potential for energy savings in controlling systems that regulate building heating, cooling, and ventilation known as HVAC (Heating, Ventilation & Air Conditioning) systems. HVAC systems are composed of boilers, chillers, air handling units (AHU), variable air volume (VAV) terminal units and auxilliary devices (pumps, fans, valves, etc.) [62]. The goal of HVAC systems is to convert primary energy sources such as electricity, gas, and coal into secondary energy sources, and distribute these secondary energy sources in the form of heated and cooled air (or water) through the building. The DOE is committed to shaving about 30% - 40% of total building energy consumption through cost-effective control and coordination of HVAC systems,[1] which we refer to as *advanced building control strategies*.

[1] `www1.eere.energy.gov/buildings/technologies/sensors_controls_research.html`

1.2 Building Control Strategies

Commercial buildings are often equipped with large, centralized automated systems to monitor and regulate the building *indoor air quality* (IAQ). These systems are generally known as *building automation systems* (BASs) [8, 9, 84], and they implement advanced building control strategies to accomplish building-level tasks such as heating, cooling, and ventilation. Typically, an advanced control strategy used in a BAS has two levels of control denoted as *local control* and *supervisory control*. Local building control regulates lower-level processes specific to HVAC equipment such as maintaining boiler temperature, chiller sequencing control, and changing fans speed. Supervisory building control denotes the coordination of lower level processes to acheive a building-level task. Wang classifies the different types of local and supervisory building control strategies in Fig 1.2. This section briefly highlights advanced and conventional building control approaches currently used in building environments.

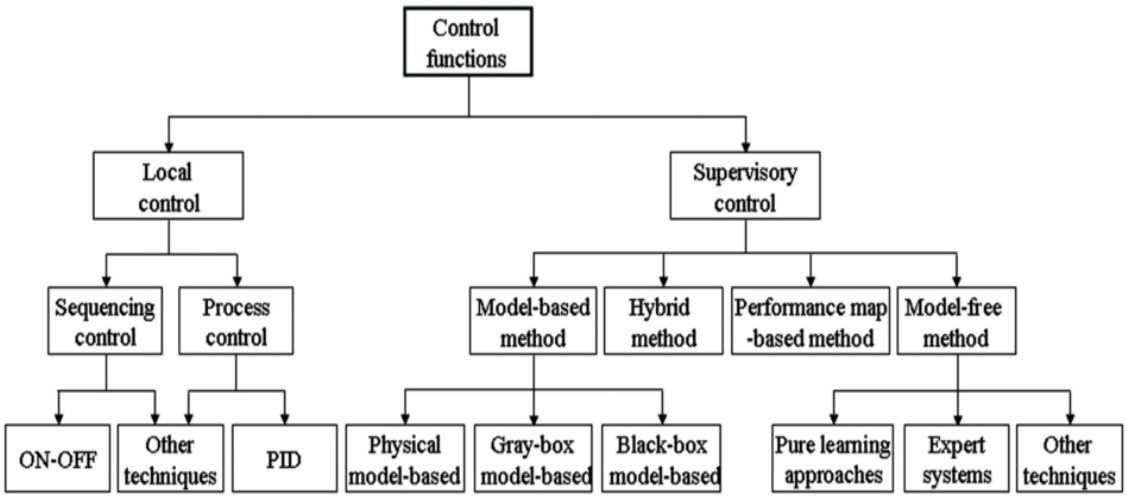

Figure 1.2: Classification of Building Control Strategies [84].

1.2.1 Conventional Building Control Strategies

Conventional building controls use *rule-based control* (RBC) at the supervisory level in combination with a local controller (such as PID control, bang-bang, ON-OFF, etc) to maintain building IAQ. RBC can be defined as a set of user-defined rules derived from human expertise and knowledge of the building to govern building operation [37, 84]. This type of supervisory control requires expert users, particularly facility managers, to understand the rule semantics and the limitations of HVAC equipment. These expert users can easily add or remove rules to the system to appropriately adjust the building IAQ. However, as buildings become larger and more complex, RBC becomes increasingly harder to scale and too complex to use.

At the local level, proportional-integral-derivative (PID) control has become the popular and standard way of controlling local HVAC equipment. Generally, local building controllers such as PID are packaged as part of the equipment, and users are generally able to tune these local controllers. However, individual PID controllers are quite difficult to tune especially in highly dynamic environments [28, 76]. Several studies show that this conventional strategy wastes a lot of energy and poorly satisfy occupant demands for comfort [28, 32, 84]. In one study, nearly 50% of occupants questioned were dissatisfied with HVAC and the comfort of the building environment [32]. Another study found conventional building thermostats act as bang-bang controllers with dead zone and suffer from overshoot, which increases building energy consumption [28].

1.2.2 Model-Based Building Control Strategies

Many studies have demonstrated that improvements to the supervisory and local levels of a building control strategy can significantly reduce overall building energy

consumption [7, 37, 76, 84, 85]. As a result, current research investigates promising alternatives to the conventional building control such as RBC and PID [60]. One such alternative is using model-based supervisory control, in combination with local level controllers such as PID, and these controllers have shown to perform better than model-free approaches because they leverage knowledge of the building to determine optimal control actions. *Model-predictive control* (MPC) is a popular example of current model-based strategies being actively studied and applied in buildings [10, 28, 59, 69, 76, 84].

Model-based control strategies require accurate models of the building environment [60, 84]. However, high-fidelity models of the dynamics in a building are difficult to create and are likely too computationally complex to be integrated on low-cost, resource constrained hardware used in buildings [76]. Therefore, a common solution to the problem of building modeling has been to create simpler, parametric models from known thermodynamic principles and estimate those model parameters with collected building data [76, 84]. The difficulty with this approach is that these building models can be costly to construct and unreliable to use for control [76]. Specifically, simple building models can contain a large number of parameters can be unreliably estimated due to complexity of the model and the nonlinearities in the building operation. Finally, there is the additional problem of controlling the building environment using the estimated model.

1.3 Dissertation Contributions & Organization

As mentioned earlier, this dissertation seeks to address two main challenges: accurately modeling building environments and reliably controlling building environments with inaccurate building models. These questions are central to the feasibility of im-

plementing model-based control strategies in real building environments, particularly large-scale commercial buildings. This dissertation makes the following key contributions to make model-based control a more feasible strategy for large-scale buildings:

I. Parameter Identifiability of Grey-Box Building Models

One of the main advantages of grey-box building models is the flexibility to fit the model to a set of building data by adjusting the model parameters. However, this process of estimating the right parameters to fit the model is not without difficulty. Grey-box building models are classified as unidentifiable if some or all of the model parameters cannot be accurately estimated. Chapter 3 broadly defines this notion of model identifiability, and presents metrics taken from [24–26] to qualitatively and quantitatively measure it. Embedded within this notion of model identifiability is the idea that not all parameters are equally identifiable. It means that even among those parameters that can be estimated, some are better estimated than others. In Chapter 3, we build on the previous metrics for identifiability and we use new metrics to quantitatively determine which parameters are least likely to be accurately estimated or identified. This concept is known as *parameter identifiability*, and we use this concept to find poorly identifiable building model parameters. Exposing the unidentifiable parameters in a model allows us to apply heuristics to improve the identifiability of the model. This contribution is detailed in Chapter 3.

II. Design-Driven Building Model Identification Process

The current model identification process is largely open loop in that users arbitrarily design and test different models and inputs in the hopes of accurately estimating the dynamics of a building. This is primarily because there is little feedback given about *why* model identification fails for a particular

model or set of data. Given the notion of parameter identifiability, we propose a design-driven identification process that exposes unidentifiable parameters. This design-driven approach to identification gives the user key problem areas to improve upon in the model. Based on some the structural challenges to building models exposed in this process, we develop a heuristic to improve the structure of the model used for identification. This heuristic improves the identifiability of the building model by mapping the unidentifiable set of parameters to a reduced set of aggregate parameters that can be better estimated. This technique is known as *parameter aggregation* and is outlined at length in Chapter 3. Additionally, we demonstrate through a focused case study that using identification with parameter aggregation improves the identifiability of building models. This contribution is also presented in Chapter 3.

III. Decentralized Identification of Control-Oriented Building Models

The proposed approach to construct identifiable building models is not scalable to the size of the building environments. Specifically, buildings that are larger in size take longer to be identified and often times are unidentifiable. This makes it especially difficult to run the identification procedure introduced above. Therefore, we address the scalability of the identification scheme described above by splitting the building model into building zone models. In doing so, we reduce the total time of identification and make the identification procedure more practical for large-scale buildings. The proposed decentralized identification scheme accomplishes two key tasks. First, it uses graph theory to represent building model structure in order to analyze the reachability of building models. We use digraphs of building models to define several important substructures such as air-based subsystems (or building rooms), building maps,

and building zones. Second, we present an efficient decomposition algorithm to partition the building digraph into subgraphs that represent room and building zone models. The proposed algorithm creates a non-unique set of 'identifiable' building zones. These contributions are presented in Chapter 4.

IV. Robust Model-Based Supervisory Control

Although the accuracy for simple control-oriented building models can be improved, the performance of model-based building control strategies such as model-predictive control is vulnerable to modeling mismatch and inaccuracies. This can lead to energy-efficient control strategies that degrade over time if they are not properly maintained. To address this challenge, we consider the use of robust control strategies to better control dynamic systems given uncertainties in the control-oriented model. One robust control strategy of interest is the receding horizon H_∞ controller which attenuates the impact of disturbances on the overall performance of a controlled closed-loop system below a factor γ. In Chapter 5, we develop a framework that integrates this receding horizon H_∞ controller with a performance-based control strategy such as MPC. However the power of this system lies in choosing a value of γ that is not overly conservative. Therefore, we propose a method to automatically tune γ over time in order to reduce the conservativeness of the controller and to improve the controller performance. Details of this contribution can be found in Chapter 5.

V. Hierarchical and Robust Model-Based Supervisory Control

Given the framework for robust model-based supervisory control, we impose a hierarchical structure on the proposed robust model-based control in order to achieve robust and decentralized model-based building control. Decentralized control is an attractive control approach because it is scalable for large

buildings and allows for modular control design. Our approach to decentralized building control builds on the hierarchical control framework posed in [64, 74, 75], which introduces smaller low-level controllers and a high level supervisor. Our proposed decentralized approach delegates the tasks of robust control to the local controllers using local information and tasks the supervisor only with the task of coordinating the local controllers. One major outcomes of this control structure is that the level of robustness needed to minimize uncertainty is given locally, independent of what the other local controllers may be doing. Therefore, we propose a method to independently tune the robustness γ for each local controller. This contribution is presented in Chapter 6.

VI. MATLAB Simulator & Case Study

A key contribution of this work is the implementation and evaluation of the proposed strategies proposed above, using examples of real building environments. Chapter 2 introduces two building environments that are used to demonstrate the main contributions in this thesis. The first example stems from a real building environment known as the Intelligent Workplace. The second example is a 12 floor reference building that typifies large-scale commercial buildings found in the in the United States. We construct grey-box models of these building environments using the developed MATLAB Simulator.

Finally, Chapter 7 concludes this work and presents interesting directions for future work in the area of model-based building control.

Chapter 2

Background on Building Environments

Buildings are highly complex and dynamic environments that are difficult to model. Energy simulation software such as EnergyPlus [31] use large sets of partial differential equations and finite element analysis to model building environments. These simulation models are high-fidelity approximations of building dynamics and are often used to accurately quantify building energy consumption over long periods of time. In recent years, tools such as MLE+ have been developed to use simulation models for building control [68]. However, these models are often too complex and too difficult to be integrated in current model-based building control strategies.

Consequently, control-oriented building models are designed to be simpler than simulation-oriented building models so that they can be easily implemented in model-based building control strategies. These control-oriented models can be constructed as either white-box, black-box, or grey-box building models. A *white-box building model* uses first-principle equations to approximate the dynamics of a building. A *black-box*

building model is created by constructing a mathematical relationship between the building inputs and the building outputs using experimental data collected or measured from the building. A *grey-box building model* is a hybrid model that is derived from the first-principle thermodynamic equations in white-box building models. The difference between a grey-box building model and a white-box building model is that grey-box model parameters are estimated using collected building measurements.

This chapter proposes a framework to construct grey-box control-oriented building models using the resistive-capacitive (RC) modeling. This approach is commonly used to approximate building dynamics [2, 10, 18, 19, 60, 82]. The chapter is organized as follows. Section 2.1 reviews the first principles of heat transfer used to model building thermodynamics; Section 2.2 reviews the RC modeling approach; and Section 2.4 introduces the building case study considered throughout this work.

2.1 Heat Transfer in Building Environments

In this section, we briefly review the different types of heat transfer that occur in building environments [2, 67, 71, 81]. The *heat* stored in a material is the quantity of energy (J) transferred to that material from the ambient environment. We denote the heat in the material as $Q(t)$. *Heat flow* is the rate of heat (W) being transferred from one material to another. We denote heat flow as $\dot{Q}(t)$, where $\dot{Q}(t) > 0$ is heat flowing into the material and $\dot{Q}(t) < 0$ is heat flowing out of the material. The computation of $\dot{Q}(t)$ is determined by the type of heat transfer: *advection*, *conduction*, *convection*, *radiation*.

2.1.1 Advective Heat Transfer

Advection (or mass transfer) occurs when heat is transferred by moving mass with heat from one location to another. An example of advection in buildings is an air handling unit (AHU) blowing hot air into a cold room. Then, heat is transferred to the room simply by moving air with more heat into the room. Likewise, advection occurs when cold air is blown into a hot room and heat is removed from the room. Suppose the room air temperature is $T_i(t)$, the temperature of the air leaving the AHU is $T_j(t)$, and the air leaving the AHU flows into the room at a rate of $\dot{v}_j(t)$. Then, the rate of heat transferred to the room is

$$\dot{Q}(t) = \rho_a \dot{v}_j(t) c_a (T_j(t) - T_i(t)) \tag{2.1}$$

where ρ_a is the density of air (kg/m^3) and c_a is the specific heat of the air ($\frac{J}{kg \cdot K}$). We note that ρ_a varies slightly with temperature and c_a varies with pressure. The air density ρ_a and the specific heat c_a are assumed to be constant for the range of building temperatures given the pressure in the building is held constant.

2.1.2 Conductive Heat Transfer

Conduction occurs when materials in direct contact transfer heat to reach thermal equilibrium. Consider a wall separating the i^{th} and j^{th} rooms in a building with air temperatures $T_i(t)$ and $T_j(t)$, respectively, where $T_i(t) < T_j(t)$. As the air in the j^{th} room heats one side of the wall, conduction takes place when heat is transferred through the wall to heat the air in the i^{th} room. Fourier's Law claims the rate of heat transfer is proportional to the negative gradient of the temperature in the wall. Consequently, a partial differential equation can be written to compute the rate of

heat transfer. We assume the following simplified version of Fourier's law, to compute the rate of conductive heat transfer to the i^{th} room,

$$\dot{Q}(t) = k_w A_w \frac{T_j(t) - T_i(t)}{\ell_w} \tag{2.2}$$

where A_w is the cross sectional area of the wall (m^2), ℓ_w is the thickness of the wall (m), and k_w is the thermal conductivity of the wall ($\frac{W}{m \cdot K}$). Furthermore, we assume the parameter k_w is constant for the normal range of building temperatures.

2.1.3 Convective Heat Transfer

Convection occurs as a result of heat transferred by the movement of air over a building surface. An example of convection is the heat transferred from a hot building wall due to the natural (or forced) movement of cooler air that passes across the wall surface. Let $T_i(t)$ be the temperature of cool air and $T_w(t)$ be the temperature of the building wall. Using Newton's law of cooling, the rate of heat transferred from the wall to the air is

$$\dot{Q}(t) = h_w A_w (T_w(t) - T_i(t)) \tag{2.3}$$

where h_w is the convective heat transfer coefficient ($\frac{W}{m^2 \cdot K}$) and A_w is the surface area of the wall (m^2). This equation holds only for laminar air movement and breaks down for turbulent air flow. Furthermore, the coefficient h_w is subject to changing over time as the flow of air over the wall changes with time. Therefore, this dissertation assumes that air movement in building environments is always laminar and the convective heat transfer coefficient is assumed constant.

2.1.4 Radiative Heat Transfer

Radiation occurs when heat is transferred to a material through the absorption of electromagnetic waves. A common example of radiation is an exterior building wall with temperature $T_i(t)$ heated through the absorption of solar rays with solar temperature $T_s(t)$. The rate of heat transferred to the building wall is governed by the Stefan-Boltzmann Law and yields a nonlinear, fourth order equation. We approximate radiative heat transfer with the following linearized equation,

$$\dot{Q}(t) = \epsilon_i \sigma h_r A_i (T_s(t) - T_i(t)) \tag{2.4}$$

where ϵ_i is the emissivity of the wall surface, σ is the Stefan-Boltzmann constant, A_i is the surface area of the building wall (m^2), and h_r is the linearized radiation heat transfer coefficient ($\frac{W}{m^2 \cdot K}$). We note that h_r is a nonlinear function of the temperatures, $T_i(t)$ and $T_s(t)$, but we will assume a constant value of h_r.

2.2 RC Modeling of Heat Transfer

Resistance capacitance (RC) models are commonly used to describe heat transfer in building environments [2, 19, 82]. These lumped capacitance models assume materials with thermal mass have spatially uniform temperatures $T(t)$, and they approximate the heat flow between these uniform materials as described in Section 2.1. The main advantage of RC modeling is that this approach exploits the natural analogies between electrical RC circuits and the dynamics of the system to be modeled, making it easier to mathematically approximate the thermodynamics of a building using circuit theory. We highlight these parallels below.

$Q(t)$:	Electrical Charge (C)	$\Longleftrightarrow$	$Q(t)$:	Heat (J)
$I(t)$:	Electrical Current (A)	$\Longleftrightarrow$	$\dot{Q}(t)$:	Heat Flow (W)
$V(t)$:	Voltage (V)	$\Longleftrightarrow$	$T(t)$:	Temperature $(^\circ K)$
R^e :	Electrical Resistance (Ω)	$\Longleftrightarrow$	R^t:	Thermal Resistance $(^\circ K/W)$
C^e :	Electrical Capacitance (F)	$\Longleftrightarrow$	C^t:	Thermal Capacitance $(^\circ K/J)$

In this section, we use the analogies between electrical circuits and heat transfer in buildings to create a parametric, state-space model of a building's thermodynamics.

2.2.1 Thermal Resistances and Capacitances

Thermal resistance R^t denotes the resistance to heat transfer $\dot{Q}$ that occurs between materials. The value for R^t can be computed differently based on the type of heat transfer, building geometry, and properties of the materials in the building construction.

- The *advective thermal resistance* is $R^t(t) = 1/\rho_a c_a \dot{V}_j(t)$ given the advective heat flow equation in (2.1). We note that advective resistance varies with time as the volumetric flow $\dot{v}_j(t)$ rate varies with time.

- The *conductive thermal resistance* is $R^t = \ell_w / k_w A_w$ given the conductive heat flow equation in (2.2).

- The *convective thermal resistance* is $R^t = 1/h_w A_w$ given the convective heat flow equation in (2.3). We assume that the convective heat transfer constant, h_w, is constant.

- The *radiative thermal resistance* is $R^t = 1/\epsilon_i \sigma h_r A_i$ given the radiative heat flow equation in (2.4).

Thermal capacitance C^t is defined as the ability to store heat in a material. Typically, the thermal capacitance of the i^{th} material is $C_t = \rho_a c_a v_i$ where c_a is the specific heat of the material, ρ_a is the density of the material, and v_i is the volume of the material.

2.2.2 Parametric State-Space Model

Dynamics of an RC circuit can be written as a set of differential equations by applying Kirchhoff's current law (KCL). Essentially, KCL states the sum of currents entering a node must be equal to the sum of currents exiting the node, $\sum I_{in}(t) - \sum I_{out}(t) = 0$. This is analogous to saying the net heat flowing into the i^{th} material must be balanced, $\sum \dot{Q}_{in}(t) - \sum \dot{Q}_{out}(t) = 0$. We define the heat flowing from $T_i(t)$ to $T_j(t)$ across thermal resistance R^t as

$$\dot{Q}_i^r(t) = \frac{T_i(t) - T_j(t)}{R^t} \tag{2.5}$$

according to Ohm's Law. Likewise, the rate of heat being stored in the i^{th} material with thermal capacitance C^t is determined by the following equation,

$$\dot{Q}_i^c(t) = C^t \dot{T}_i(t). \tag{2.6}$$

Therefore, the balanced heat equation for the i^{th} material is

$$\dot{Q}_i^c(t) - \sum_{j \neq i} \dot{Q}_{R,ij}(t) = 0. \tag{2.7}$$

Buildings are physically made of many building elements (e.g. air, walls, roofs, floors, etc.) and each element can be made of several materials, where the thermodynamics of each material are determined by (2.7). Therefore, we can characterize the dynamics

of a building as the set of thermodynamic equations for all materials, and we can represent this set of equations as the following linear state-space system,

$$\dot{\mathbf{T}}(t) = A_c(\theta)\mathbf{T}(t) + B_c(\theta)\mathbf{u}(t) + G_c(\theta)\mathbf{w}(t) \tag{2.8}$$

where $\theta \in \mathbb{R}^q$ is the set of all thermal resistors and capacitors, $\mathbf{T}(t)$ is the vector of all building material temperatures, $\mathbf{u}(t)$ is the vector of controllable heat inputs to the building, and $\mathbf{w}(t)$ is the vector of uncontrollable heat inputs to the building. We illustrate the parallels between circuit theory and thermodynamics in the following example.

Example 1 (RC Model of a Building Wall)

Consider a single building wall that separates two rooms with uniform air temperatures $T_1(t)$ and $T_2(t)$. Furthermore, assume the wall is made of a single material with spatially uniform temperature $T_w(t)$. Fig. 2.1 depicts both the physical wall and the RC circuit used to describe the dynamics of the wall.

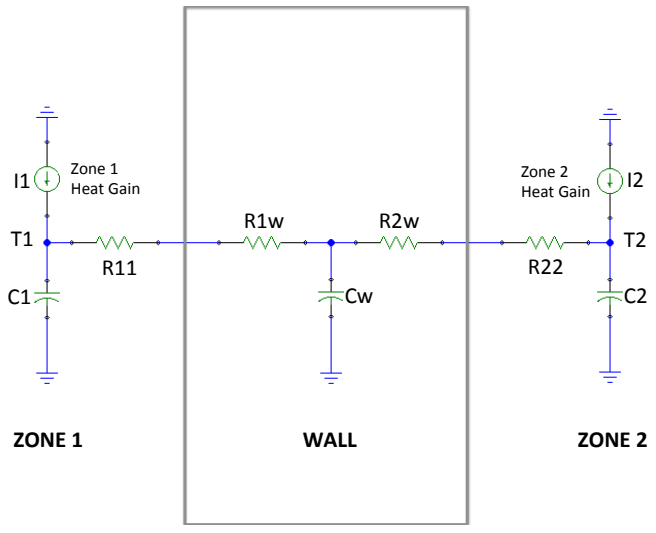

Figure 2.1: The RC circuit models heat transfer to a building wall

We define the thermal resistances and capacitances as follows:

- R_{1w} and R_{2w} model conductive thermal resistance to heat transfer from the surface of the wall to the midpoint of the wall.
- R_{11} and R_{22} model the convective resistance to heat transferred from the room air to the wall.
- $I_1(t)$ and $I_2(t)$ model convective and conductive heat transfer from the room air, $T_1(t)$ and $T_2(t)$, to the wall $T_w(t)$ according to (2.5)
- $I_w^c(t)$ models the rate of heat being stored in the building wall due to the thermal capacitance of the wall C_w according to (2.6).

Then, the balanced heat equation is $I_w^c(t) - I_1(t) - I_2(t) = 0$, and this can be expanded to

$$\underbrace{C_w \dot{T}_w(t)}_{I_w^c(t)} \quad - \quad \underbrace{\frac{T_1(t) - T_w(t)}{R_1}}_{I_1(t)} \quad - \quad \underbrace{\frac{T_2(t) - T_w(t)}{R_2}}_{I_2(t)} \quad = \quad 0 \tag{2.9}$$

where $R_1 = R_{11} + R_{1w}$ and $R_2 = R_{22} + R_{2w}$. Then, we can represent the dynamic equation in (2.9) as the following state-space model

$$\dot{\mathbf{T}}(t) = \begin{bmatrix} -\frac{1}{R_1 C_w} - \frac{1}{R_2 C_w} \end{bmatrix} \mathbf{T}(t) + \begin{bmatrix} \frac{1}{R_1 C_w} & \frac{1}{R_2 C_w} \end{bmatrix} \mathbf{w}(t) \tag{2.10a}$$

where $\theta = \begin{bmatrix} R_1 & R_2 & C_w \end{bmatrix}^T$, $\mathbf{T}(t) = T_w(t)$, and $\mathbf{w}(t) = \begin{bmatrix} T_1(t) & T_2(t) \end{bmatrix}^T$.

2.2.3 RC Model of Building Elements

Building elements such as walls, roofs, and floors are made from of a number of materials that can store heat such as air, wood, concrete, plaster, etc. Therefore, the RC model of a building element depends on the number of materials with heat capacitance used to construct the element. We use the following shorthand notation to describe RC models of building elements.

1R0C RC Model: A building element modeled as a single thermal resistor. The model assumes the building element is made of a single material that does not store heat, but resists heat flow. Windows and glass materials are typically modeled as 1R0C RC models.

2R1C RC Model: A building element modeled as 2 thermal resistors and 1 thermal capacitor. The model assumes the building element is made of a single material that stores heat and resists heat flow across it. We assume all materials with thermal mass like air, wood, concrete, plaster, and tar, etc. are modeled as '2R1C' RC models. The RC circuit in Fig. 2.1 can be designed more simply as a network with two resistors, $R_1 = R_{11} + R_{1w}$ and $R_2 = R_{22} + R_{2w}$, and a capacitor, C_w. Therefore, we denote the circuit shown in Fig. 2.1 as a 2R1C RC model of the wall.

3R2C RC Model: A building element modeled as 3 thermal resistors and 2 thermal capacitors. The model assumes the building element is made of two adjacent materials that each store heat and resists heat flow across it. Fig 2.2 shows a building wall modeled as a 3R2C RC model.

4R3C RC Model: A building element modeled as 4 thermal resistors and 3 thermal capacitors. The model assumes the building element is made of three adjacent

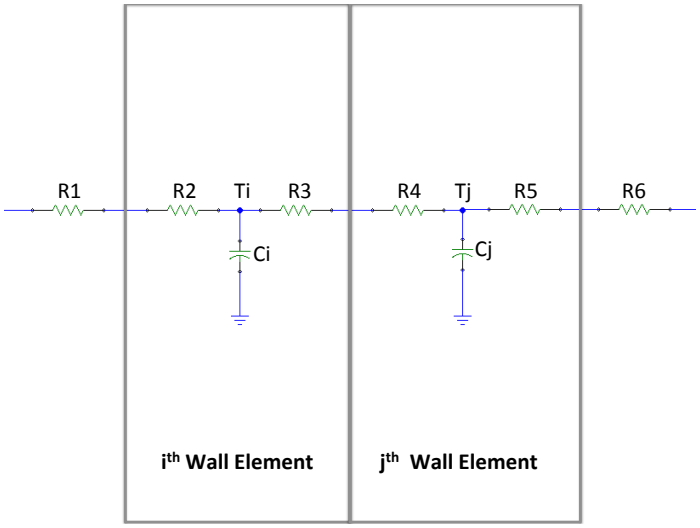

Figure 2.2: An illustration of a 3R2C RC wall model

materials that each store heat and resists heat flow across it. We assume that this is the highest order RC model used to model a single building element.

In order to accurately model the dynamics of a building element, knowledge of the number of materials that store heat in the building element is needed. Materials such as glass that resist heat flow but do not store significant heat are modeled as a single resistor or a 1R0C model. Likewise, those materials that are assumed to store heat are assumed to have at least a 2R1C RC model or higher. Depending on the complexity of the data, higher order RC models may be needed to accurately fit the model output to the actual building output.

2.3 Dynamics of Building Environments

2.3.1 Continuous-Time Building Dynamics

We assume the continuous-time dynamics of the building environments introduced above are described by the following linear, parametric system

$$\mathcal{S}: \quad \begin{aligned} \dot{\mathbf{T}}(t) &= A_c(\theta)\mathbf{T}(t) + B_c(\theta)\mathbf{u}(t) + G_c(\theta)\mathbf{w}(t) \\ \mathbf{y}(t) &= C\mathbf{T}(t) + \mathbf{e}(t) \end{aligned} \tag{2.11}$$

where $\theta \in \mathbb{R}^q$ is the set of all building parameters values, $\mathbf{T}(t) \in \mathbb{R}^n$ is the thermal state of the building temperatures, $\mathbf{u}(t) \in \mathbb{R}^m$ is the vector of thermal inputs to the building, $\mathbf{w}(t) \in \mathbb{R}^p$ is the vector of thermal disturbance inputs to the building, $\mathbf{y}(t) \in \mathbb{R}^o$ is the vector of building measurements, and $\mathbf{e}(t) \in \mathbb{R}^o$ is the vector of measurement errors. Furthermore, $A_c(\theta) : \theta \in \mathbb{R}^q \rightarrow \mathbb{R}^{n\times n}$, $B_c(\theta) : \theta \in \mathbb{R}^q \rightarrow \mathbb{R}^{n\times m}$, and $G_c(\theta) : \theta \in \mathbb{R}^q \rightarrow \mathbb{R}^{n\times p}$. Given (2.11), we make the following simplifying assumptions.

A1) Building temperatures can be broadly split into two categories: air temperatures of open spaces and temperatures of materials in walls, roofs, floors, etc. Therefore, we assume the temperature vector $\mathbf{T}(t)$ can be written as

$$\mathbf{T}(t) = \begin{bmatrix} \mathbf{T}_a(t) \\ \mathbf{T}_w(t) \end{bmatrix}$$

where $\mathbf{T}_a(t) = \begin{bmatrix} T_1(t) & \dots & T_a(t) \end{bmatrix}^T \in \mathbb{R}^a$ is the vector of air temperatures and $\mathbf{T}_w(t) \in \mathbb{R}^{n-a}$ is the vector of non-air temperatures for $a \leq n$.

A2) Given the input vector $\mathbf{u}(t) = \begin{bmatrix} u_1(t) & \dots & u_m(t) \end{bmatrix}^T \in \mathbb{R}^m$, let the input variable $u_i(t)$ represent the total rate of heat applied to a building air temperature due to controllable heating and cooling devices, where $u_i(t) \geq 0$ is a controllable heating input and $u_i(t) \leq 0$ is a controllable cooling input. We assume that no two inputs $u_i(t)$ and $u_j(t)$ for $i \neq j$ are applied directly to the same building air temperature. Furthermore, not all building air temperatures are directly influenced by a controllable input which implies, $m \leq a$.

A3) Then, the input matrix $B_c(\theta)$ is assumed to be

$$B_c(\theta) = \begin{bmatrix} B_A(\theta) \\ 0_{n-a \times m} \end{bmatrix} \in \mathbb{R}^{n \times m}$$

where $B_A(\theta) \in \mathbb{R}^{a \times m}$. Furthermore, we assume rows and columns of $B_a(\theta)$ have at most one non-zero entry, which implies $u_i(t)$ is applied to at most one distinct, building air temperature.

A4) The disturbance vector $\mathbf{w}(t)$ represents the vector of signals that are uncontrollable and directly influence the dynamics of the buildings. We consider two types of building disturbances: ambient outdoor temperature $T_o(t)$ and uncontrollable heat sources $\dot{q}_i(t)$ applied to the building air temperature $T_i(t)$. Then, the disturbance vector is assumed to be $\mathbf{w}(t) = \begin{bmatrix} T_o(t) & \dot{q}_1(t) & \dots & \dot{q}_a(t) \end{bmatrix}^T \in \mathbb{R}^p$ for $p = a + 1$.

A5) We assume the building output $y_i(t)$ measures exactly one building air temperature $T_i(t)$, such that $\mathbf{y}(t) = \begin{bmatrix} y_1(t) & \dots & y_a(t) \end{bmatrix}^T \in \mathbb{R}^o$ and the output matrix is $C = \begin{bmatrix} I_{a \times a} & 0_{o \times n-a} \end{bmatrix} \in \mathbb{R}^{o \times n}$ where $o = a$.

2.3.2 Discrete-Time Building Dynamics

Assume the continuous-time signals of $\mathcal{S}$ can be discretely sampled, for sampling period T_s, such that $\mathbf{T}[k] = \mathbf{T}(kT_s)$, $\mathbf{u}[k] = \mathbf{u}(kT_s)$, $\mathbf{w}[k] = \mathbf{w}(kT_s)$, $\mathbf{y}[k] = \mathbf{y}(kT_s)$, and $\mathbf{e}[k] = \mathbf{e}(kT_s)$ where the integer k represents a discrete time step. Then, (2.11) can be written as the following discrete-time system,

$$\mathcal{S}_d : \begin{aligned} \mathbf{T}[k+1] &= A_d(\theta)\mathbf{T}[k] + B_d(\theta)\mathbf{u}[k] + G_d(\theta)\mathbf{w}[k] \\ \mathbf{y}[k] &= C\mathbf{T}[k] + \mathbf{e}[k] \end{aligned} \tag{2.12}$$

where the discretized matrices are $A_d(\theta) = e^{A_c(\theta)T_s}$, $B_d(\theta) = \left(\int_0^{T_s} e^{A_c(\theta)\tau} d\tau\right) B_c(\theta)$, and $G_d(\theta) = \left(\int_0^{T_s} e^{A_c(\theta)\tau} d\tau\right) G_c(\theta)$. Often, the following approximation

$$\int_0^{T_s} e^{A(\theta)\tau} d\tau \approx A_c(\theta)^{-1}(A_d(\theta) - I_{n\times n})$$

is used to compute the discretized system matrices $A_d(\theta)$, $B_d(\theta)$, and $G_d(\theta)$. Approximation of $\int_0^{T_s} e^{A(\theta)\tau} d\tau$ introduces some approximation error between $\mathcal{S}$ and $\mathcal{S}_d$. Finally, we assume **A1) - A2)** and **A4)- A5)** hold for the discrete-time signals $\mathbf{T}[k]$, $\mathbf{u}[k]$, $\mathbf{w}[k]$, and $\mathbf{y}[k]$ as well. On occasion, we may use $A(\theta)$, $B(\theta)$, and $G(\theta)$ to denote the discretized matrices $A_d(\theta)$, $B_d(\theta)$, and $G_d(\theta)$, respectively. In those cases, we will clearly note the abuse of notation.

2.4 Case Studies of Buildings Environments

One of the major contributions of this dissertation is the demonstration of our proposed strategies for real and large-scale building scenarios. We focus our case studies on two real building environments, specifically the Intelligent Workplace at Carnegie

Mellon University and a commercial office building. This section provides some background on these real building environments and provides some simplifying assumptions that we make about these building environments throughout the dissertation.

2.4.1 Intelligent Workplace

The Robert L. Preger Intelligent Workplace (IW) sits on the top of the Margaret Morrison building at Carnegie Mellon University in Pittsburgh, Pennsylvania.[1] The IW provides 600 sq. ft of open office space and is dubbed a 'living laboratory' because the space is equipped with cutting-edge building technologies that are constantly being studied, tweaked, and tested. These technologies include window shading, occupancy-based sensing, energy monitoring, automatic thermal and lighting control [23, 34, 57]. We focus our attention on the thermal conditioning of the IW, which uses a system water mullions or pipes to radiantly heat and cool the space [34, 57]. The water mullions are run along the edge of the IW as can be seen in the floor plan for the north bay of the IW in Fig.2.3. In colder weather, hot water is run through the water mullion system to warm the air around the pipes and radiantly heat the building air. This heating system mimics traditional steam radiators used to heat current building environments [34]. Similarly, cold water is run through the water mullion system in warmer weather to absorb heat from the space and provide additional energy-efficient cooling. Finally, we note the IW can be split into a north bay known as the 'IW-North' and a south bay (not depicted) known as the 'IW-South'. For this case study, we will only consider the thermal modeling and control of the IW-North depicted in Fig. 2.3.

We will make the following set of simplifying assumptions about both the IW-North and the heating systems at work.

[1] `http://www.cmu.edu/iwess/about-us/iw.html`

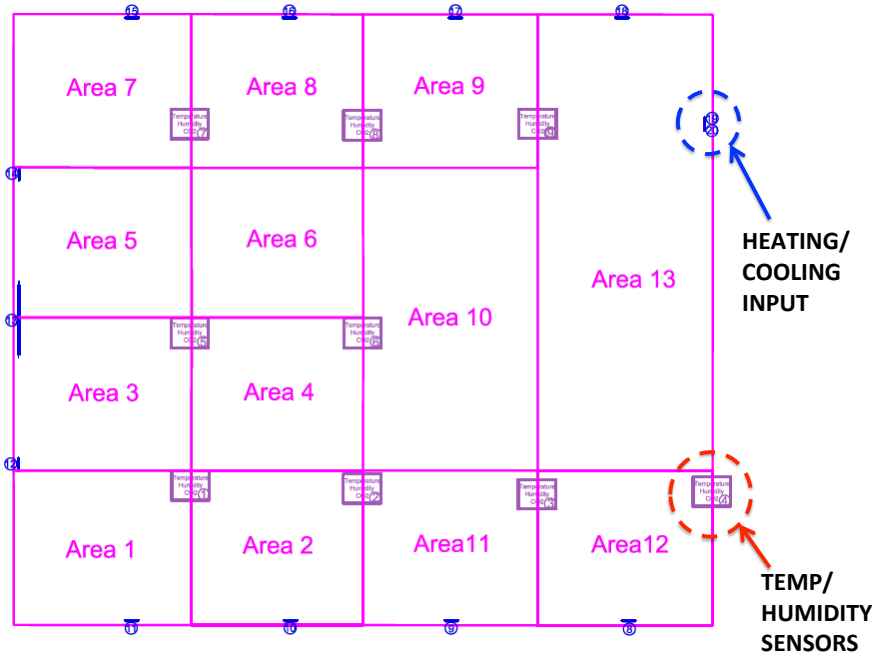

Figure 2.3: Floor Plan of the North Bay of the Intelligent Workplace [57]

B1) The materials used in the IW-North construction have the following thermal properties shown in Table 2.2.

Building Element	RC Model	Resistivity $(\frac{m^2K}{W})$	Capacitivity $(\frac{J}{Wm^2})$
Interior Walls	1R0C	0.24	-
Exterior Walls	2R1C	1.60	81,320
Windows	1R0C	0.82	-
Roof	2R1C	3.30	104,870
Floors	2R1C	0.18	72,000

Table 2.2: Thermal Properties of IW-North Construction. We note the exterior walls separate the outdoors from the indoors, while the interior walls partition the indoor air spaces.

B2) The air temperature $T_i(t)$ of each building area in the IW-North is measured for all $i \in [1, 13]$. Furthermore, because the water mullion system is run along the facade of the building, we will assume the perimeter areas in the IW-North

which are Areas $1-3, 5, 7-9, 11-13$ have access to a controllable thermal input.

B3) There are three major sources of disturbance to the air temperatures of the IW-North: occupancy, outdoor air temperature $T_o(t)$, and the IW-South air temperature, $T_s(t)$. For this case study, we will assume the roofing and flooring border the outdoors and $T_s(t) = T_o(t)$. Finally, the occupancy schedules and the outdoor air temperatures in Pittsburgh during the month of January are given in Table 2.4

2.4.2 Large Commercial Office Building

The Office of Energy Efficiency and Renewable Energy (EERE) at the U.S. Department of Energy has developed a set of reference buildings to describe the current population of commercial and residential buildings within the U.S. and across all weather climates. This classification is useful to building research because it allows users to benchmark energy consumption of a real building against similar buildings in similar climates. For this case study, we are interested in the segment of U.S. buildings that are classified as large commercial office building. E.E.RE. classifies the typical large commercial office building as a space of about $500,000$ sq. ft. total with 12 floors and 5 building areas per floor [30]. Fig. 2.4 and Fig. 2.5 depict the reference building that represents typical large commercial office spaces.

We will make the following assumptions about this reference building:

C1) The building is located within a climate similar to the climate in Pittsburgh, which is outlined in Table 2.4. Furthermore, assume the thermal properties of the building are outlined in Table 2.3.

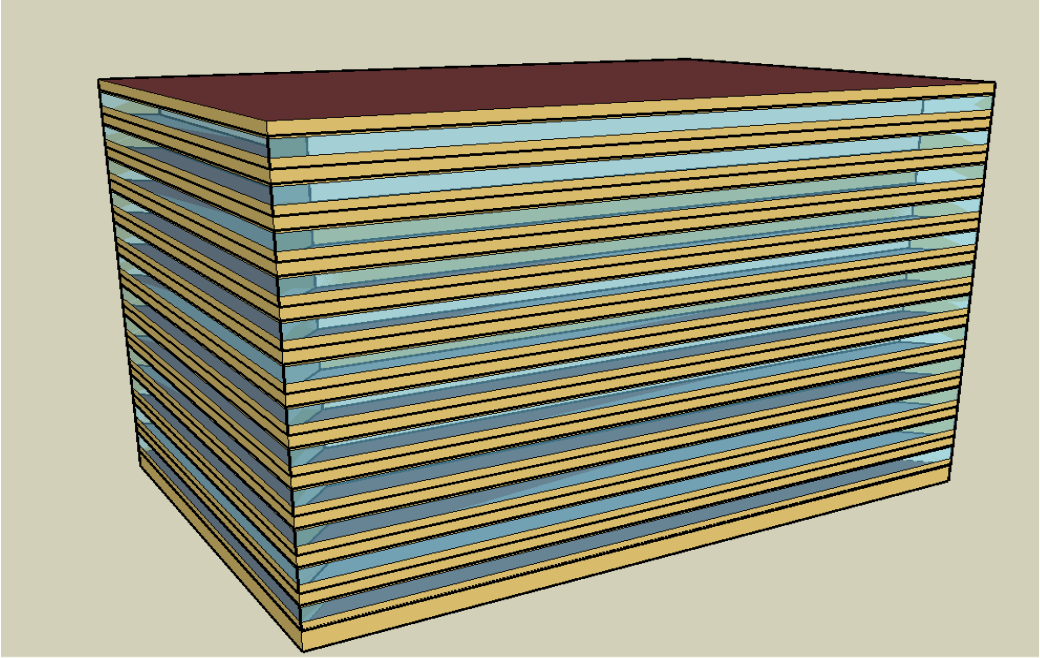

Figure 2.4: Exterior View of Large Office Building [30]

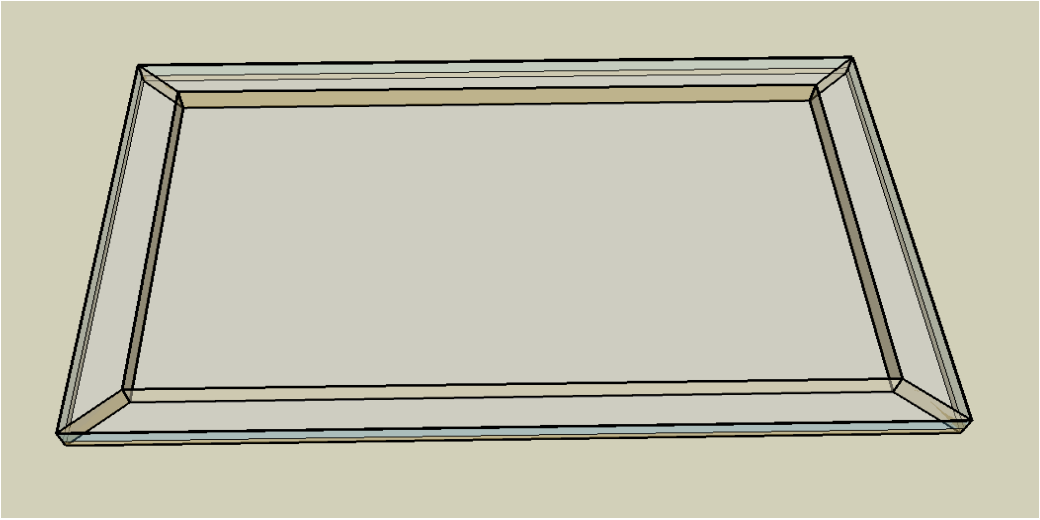

Figure 2.5: Floor Plan of Large Office Building [30]

Building Element	RC Model	Resistivity $(\frac{m^2K}{W})$	Capacitivity $(\frac{J}{Wm^2})$
Interior Walls	2R1C	0.24	3600
Exterior Walls	2R1C	1.17	102,000,000
Windows	1R0C	$\frac{1}{3.24}$	-
Roofs	2R1C	2.85	104,870
Floors	2R1C	1.11	72,000

Table 2.3: Thermal Properties of Large Office Building Construction. We note the exterior walls separate the outdoors from the indoors, while the interior walls partition the indoor air spaces. Furthermore, windows comprise 40% of the exterior building wall areas.

C2) The air temperature $T_i(t)$ of each building area is measured for $i \in [1, 60]$, and the core areas contain a controllable thermal input.

C3) Building occupancy and outdoor air temperature are major sources of disturbance to large commercial office buildings. Table 2.4 is a combination of Pittsburgh weather data and occupancy schedules for large office buildings taken from the Office of Energy Efficiency and Renewable Energy website [30]

Time of Day (hrs)	Ave. Outdoor Temperature in January (K)	Weekday Occupancy Schedule (%)	Saturday Occupancy Schedule (%)
0:01 - 1:00	272.05	0	0
1:01 - 2:00	271.85	0	0
2:01 - 3:00	271.75	0	0
3:01 - 4:00	271.55	0	0
4:01 - 5:00	271.35	0	0
5:01 - 6:00	271.15	0	0
6:01 - 7:00	271.05	10	10
7:01 - 8:00	270.95	20	10
8:01 - 9:00	271.35	95	50
9:01 - 10:00	271.95	95	50
10:01 - 11:00	272.75	95	50
11:01 - 12:00	273.45	95	50
12:01 - 13:00	274.15	50	50
13:01 - 14:00	274.75	95	50
14:01 - 15:00	274.95	95	10
15:01 - 16:00	275.05	95	10
16:01 - 17:00	274.45	95	10
17:01 - 18:00	273.75	70	0
18:01 - 19:00	273.35	40	0
19:01 - 20:00	272.85	40	0
20:01 - 21:00	272.65	10	0
21:01 - 22:00	272.35	10	0
22:01 - 23:00	271.95	5	0
23:01 - 24:00	271.75	5	0

Table 2.4: Average Weather Temperature and Occupancy Data . Each entry in the weather column represents the average daily temperature during that time of day for the month of January in Pittsburgh. The occupancy schedules are taken from the reference data for large scale building models. Each entry of the occupancy schedule columns represent the percentage of maximum occupancy in a large commercial building at that time of day. Note the occupancy schedules differ based on the day of the week. Sunday is not given, so we will assume the Sunday occupancy schedule is the same as Saturday occupancy.

2.5 Summary

This chapter provides some preliminary background on building environments and the types of heat transfer that takes place in a building. Given information about the building geometry, building construction, and first principle heat flow equations, we can construct control-oriented grey-box models using a well known lumped capacitance approach called resistance capacitance (RC) modeling. RC modeling of building dynamics have several advantages over the conventional black-box approaches including flexibility to changes in the environment and the ability to retain the physical meaning of the model. Furthermore, we define some standard notation used to mathematically represent the dynamics of these real building environments, and we state some simplifying assumptions. Finally we introduce two case studies that will be used in subsequent chapters to demonstrate our approach to building model identification and model-based building control.

Chapter 3

Identification of Building Control Models

The main advantage of using an RC model to approximate building dynamics is the flexibility of the model to map a set of building inputs to building outputs. Flexible RC building models assume an RC model (e.g. 1R0C, 2R1C, etc.) for each building element a priori, and the model parameters are estimated to fit the model output to the collected building data. As the number of parameters and the size of the model state vector are increased, the building model becomes more flexible to fit nuances found in the building data. This process of choosing a model structure to describe a set of input/output data and estimating the model parameters from the data is known as *model identification* [54]. Because building models need to be flexible, the challenge of model identification in the context of building environments is the increased model size and complexity, which leads to ill-conditioning.

Identification of ill-conditioned models is a difficult problem because there is insufficient data to sufficiently estimate all of the model parameters or the model is struc-

tured such that parameters may not be independently distinguished. One method to alleviate this issue is to model highly dynamic processes in the frequency domain, and provide heuristics to improve estimation of the low gain directions of the model [4, 39, 79, 87]. Stec et. al consider the impact of different model structures and identification tests on the model of a high purity distillation column [79]. They observe poor estimation of low gain directions is due to poor data, and conclude identification data needs to be chosen to sufficiently excite the low-gain direction of the model. In [87], Zhu et. al extend [79] to consider test inputs that sufficiently excite the low gain directions of the model. Chaplais offers a slightly different approach by first separating the model into fast and slow time-scales, and then identifying the transfer function of each time-scale separately [11]. This time-scale separation approach is applied to the identification of building models in [61], where ARX models are used to describe the dynamics of the building.

Another method to eliminate ill-conditioning is to reduce the size of the model since high model order and over parameterization lead to ill-conditioned models [42]. This is known as *model reduction*, and has been used in [3, 17, 19, 35] to improve identification of thermal building models. In [20], the physical RC model is reduced using a balanced truncation method, known as Moore's reduction, which keeps the dominant components of the model and retains the large time constants in the building. Dautin compares several truncation techniques on thermal building models in [17], and Goyal extends the balanced truncation method to nonlinear building models [36]. The drawback of these truncation methods is that the physical meaning of the model is lost. To deal with this drawback, several new reduction methods known as *lumping* or *aggregation-based* methods are introduced to preserve the physical meaning of the model by combining a number of state variables affinely (and in some cases nonlinearly) into a single state [3, 19]. In [19], Deng aggregates certain building states

together, and estimates the thermal resistance and capacitance between these new aggregated states.

This chapter addresses the deficiency of standard model identification to accurately estimate the parameters of ill-conditioned building models. We propose a new process called *design-driven model identification* that implements two key tasks. First, this proposed approach uses the notion of *model identifiability* to quantitatively determine the building model parameters that cannot be sufficiently estimated from the measured building data. The topic of model identifiability is a mature area [15, 21, 22, 24, 25, 27, 33, 44, 52, 54, 55, 72], and is more thoroughly presented later in this chapter as the framework to determine poorly estimated model parameters caused by ill-conditioning. Second, we introduce a re-parameterization method that reduces the number of parameters, improves estimation of poorly estimated parameters, and preserves the physical meaning of the model. We demonstrate that implementing these approaches to the standard model-identification process improves the identifiability of ill-conditioned models.

The chapter is organized as follows. Section 3.1 defines a building model and provides some assumptions about these models. Section 3.2 poses the model identification problem in the context of building environments, and Section 3.3 introduces the framework of model identifiability. Section 3.4 presents our proposed design-driven approach to identification, and Section 3.5 demonstrates our approach for the Intelligent Workplace. Finally, Section 3.6 summarizes the contributions of this chapter.

3.1 Assumptions & Notations

Consider a building environment with discrete-time dynamics $\mathcal{S}_d$, given in (2.12), and assume $\mathcal{S}_d$ satisfies the building conditions and assumptions detailed in the previous

chapter. Then, we define a *model* of $\mathcal{S}_d$ as the following discrete-time system

$$M(\theta): \quad \begin{aligned} \mathbf{x}[k+1] &= A(\theta)\mathbf{x}[k] + B(\theta)\mathbf{u}[k] + G(\theta)\mathbf{w}[k] \\ \hat{\mathbf{y}}[k] &= C\mathbf{x}[k] \end{aligned} \tag{3.1}$$

where $\mathbf{x}[k] \in \mathbb{R}^n$ is the modeled building state vector, $\mathbf{u}[k] \in \mathbb{R}^m$ is the vector of controllable heating inputs, $\mathbf{w}[k] \in \mathbb{R}^p$ is the vector of uncontrollable heating inputs, and $\hat{\mathbf{y}}[k] \in \mathbb{R}^o$ is the modeled building output. With slight abuse of notation, we will use the notation $A(\theta)$, $B(\theta)$, and $G(\theta)$ in this chapter to denote the structured matrices $A_d(\theta)$, $B_d(\theta)$, and $G_d(\theta)$ in (2.12), respectively. We will assume the model output $\hat{\mathbf{y}}[k]$ can be represented by the following input-output function $\hat{\mathbf{y}}[k] = g(k; \theta, \mathbf{x}[0], U^k)$, where

$$g(k; \theta, \mathbf{x}[0], U^k) = CA(\theta)^k\mathbf{x}[0] + \sum_{\tau=0}^{k-1} CA(\theta)^{k-1-\tau}\Big(B(\theta)\mathbf{u}[\tau] + G(\theta)\mathbf{w}[\tau]\Big) \tag{3.2}$$

given θ, the initial condition $\mathbf{x}[0]$, and the set of building inputs, $U^k = \{\mathbf{u}[\tau], \mathbf{w}[\tau] : \forall \tau \in [0, k-1]\}$, Occasionally, we will use (3.2) in lieu of $\hat{\mathbf{y}}[k]$ to show an explicit relationship between the model output $\hat{\mathbf{y}}[k]$, the initial value $\mathbf{x}[0]$, the model parameter value θ, and the set of input data U^k. Furthermore, let the *transfer function* of the building model $M(\theta)$ be

$$G(z, \theta) = \begin{bmatrix} C(zI - A(\theta))^{-1}B(\theta) & C(zI - A(\theta))^{-1}G(\theta) \end{bmatrix} \tag{3.3}$$

where z is a complex number in the discrete frequency domain.

Furthermore, consider the discrete-time signals $\mathbf{u}[k]$, $\mathbf{w}[k]$, and $\mathbf{y}[k]$ defined in Chapter 2. Then, we will assume the following notation:

U^N $\quad U^N = \{\mathbf{u}[k], \mathbf{w}[k] : k \in [0, N-1]\}$.

Y^N	$Y^N = \{\mathbf{y}[k] : k \in [0, N-1]\}$.
Z^N	The *building data set* is $Z^N = U^N \cup Y^N$.
$\|\mathbf{s}[k]\|_P$	$\|\|\mathbf{s}[k]\|\|_P = \sqrt{\mathbf{s}[k]^T P \mathbf{s}[k]}$ for matrix $P = P^T$ and vector $\mathbf{s}[k]$.
$\|\mathbf{s}[k]\|$	$\|\mathbf{s}[k]\| = \|\mathbf{s}[k]\|_I$ where I is an identity matrix.

Consider a signal $\{s[k]\}$. Then, $s[k]$ is *quasi-stationary* if $\mathbf{s}[k]$ is bounded for all k and the *autocorrelation* of $s[k]$ given by $R_{ss}(\tau) = \lim_{N\to\infty} \frac{1}{N} \sum_{k=0}^{N-1} \mathbf{s}[k]\mathbf{s}[k-\tau]^T$ exists for all τ [54]. We will assume the signals $\{\mathbf{u}[k]\}$, $\{\mathbf{w}[k]\}$, and $\{\mathbf{y}[k]\}$ are *quasi-stationary*.

3.2 Building Model Identification

This section introduces the standard model identification process [2, 54], in the context of building environments. Alg. 1 summarizes the current process of identifying a model in the following three stages: *choice of model and data*, *parameter estimation*, and *model validation*. We expand on each of these stages in the following subsections.

Algorithm 1 Standard Identification Process

I. Choice of Model and Data
   A) Choose a building model $M(\theta) \in \mathcal{M}$ such that $\mathcal{S}_d \in \mathcal{M}$.
   B) Choose a building data set Z^N that captures the building dynamics.

II. Parameter Estimation: Solve (3.6) for the parameter estimate $\hat{\theta}_N$.

III. Model Validation:
   A) Choose a different building data set L^N for validation.
   B) Compute the mean squared error, $V_N(\hat{\theta}_N, L^N)$ in (3.5).
   C) If $V_N(\hat{\theta}_N, L^N) < \epsilon$, then the model $M(\hat{\theta}_N)$ is identified.

3.2.1 Choosing a Model for Identification

Consider a building model $M(\theta)$ that will be identified to model the dynamics of a building, $\mathcal{S}_d$. According to [54], one of the major requirements to accurately identify $M(\theta)$ is to guarantee the dynamic process $\mathcal{S}_d$ belongs to the *model structure* of $M(\theta)$.

Definition 1 (Model Structure [54]). *The model structure of* $M(\theta)$ *is* $\mathcal{M} = \{M(\theta) : \forall\theta \in \Theta\}$ *where* $\Theta \subseteq \mathbb{R}^q$ *is the set of all possible parameter values.* ♠

Assuming $\mathcal{S}_d$ belongs to the model $\mathcal{M}$ (or $\mathcal{S}_d \in \mathcal{M}$), then the building model $M(\theta)$ is guaranteed to sufficiently describe the dynamics of the building and model the set of building data Z^N provided the correct set of parameter values θ are chosen. We can make this claim because both the building model $M(\theta)$ in (3.1) and the building dynamics $\mathcal{S}_d$ in (2.12) use the same structured matrices $A(\theta)$, $B(\theta)$, $G(\theta)$, and C, which are based on knowledge of the building geometry and heat transfer. Since $\mathcal{S}_d$ and $M(\theta)$ have the same structure, then $\mathcal{S}_d$ and $M(\theta)$ are said to be *equivalent* when the set of model parameter values is chosen to be the set of true parameters values, $\theta = \theta_S$. This notion of model equivalence is defined below.

Definition 2 (Model Equivalence [54]). *For parameter values* θ_1 *and* θ_2*, the model* $M(\theta_1)$ *is equivalent to the model* $M(\theta_2)$*, denoted as* $M(\theta_1) \overset{M}{=} M(\theta_2)$*, if* $G(z, \theta_1) = G(z, \theta_2)$ *where* $G(z, \theta)$ *is defined in* (3.3). ♠

Given the implication, $M(\theta_S) \overset{M}{=} \mathcal{S}_d$, then the objective of model identification is to find the set of true parameter values for which this implication holds.

3.2.2 Choosing a Data Set for Identification

Given a model $M(\theta) \in \mathcal{M}$ and system $\mathcal{S}_d \in \mathcal{M}$, Ljung notes the data set Z^N also needs to be *informative with respect to* $\mathcal{M}$ in order to successfully identify the model $M(\theta)$ from the set Z^N.

Definition 3 (Informative Data Set, [54]). *A set of quasi stationary signals Z^N is informative with respect to the model structure $\mathcal{M}$ if, for $M(\theta) \in \mathcal{M}$ and $\theta_1 \neq \theta_2$, then*

$$\frac{1}{N}\sum_{k=0}^{N-1} \|\hat{\mathbf{e}}(k;\theta_1,\mathbf{x}[0],Z^N) - \hat{\mathbf{e}}(k;\theta_2,\mathbf{x}[0],Z^N)\|^2 = 0$$

implies $M(\theta_1) \overset{M}{=} M(\theta_2)$, where $\hat{\mathbf{e}}(k;\theta,\mathbf{x}[0],Z^N) = \mathbf{y}[k] - g(k;\theta,\mathbf{x}[0],U^N)$. ♠

Intuitively, this means the building data set Z^N sufficiently capture the dynamics of the building $\mathcal{S}_d$. Ljung also shows in [54] that one of the ways to ensure the data set Z^N is informative enough is to excite the dynamics of the building using a sufficiently "rich" input signal. Ljung refers to this type of input as a *persistently exciting signal*.

Definition 4 (Persistently Exciting Signal [54]). *A quasi-stationary signal $\{\mathbf{s}[k]\}$ with spectrum $\Phi_{ss}(\omega)$ is persistently exciting if*

$$\Phi_{ss}(\omega) > 0, \qquad \text{for almost all } \omega.$$

where $\Phi_{ss}(\omega) = \sum_{\tau=-\infty}^{\infty} R_{ss}(\tau)e^{-j\omega\tau}$ and $R_{ss}(\tau)$ is the autocorrelation of $s[k]$. ♠

Typical persistently exciting signals used for identification include pseudo-random binary signals (PRBS), sinusoidal or the sum of sinusoidal signals (SINE), and random Gaussian distributed signals (RGS) [54, 55]. We will assume for this work that the building input signal $\mathbf{u}[k]$ and the building disturbance signal $\mathbf{w}[k]$ are persistently exciting. This means significant planning is needed to take into account uncontrollable conditions such as occupancy and outdoor weather when modeling real building environments.

3.2.3 Parameter Estimation Problem

As stated earlier, the objective of model identification is to find the set of model parameter values such that $\theta = \theta_S$. Since equivalent models yield equivalent outputs for the same inputs, then the objective is to estimate the parameter θ that drives the model output $\hat{\mathbf{y}}[k]$ to match the building output $\mathbf{y}[k]$.

Given the input-output model in (3.2) and the building data set Z^N, let the error between the building output $\mathbf{y}[k]$ and the model output $\hat{\mathbf{y}}[k] = g(k; \theta, \mathbf{x}[0], U^N)$ be

$$\hat{\mathbf{e}}(k; \theta, \mathbf{x}[0], Z^N) = \mathbf{y}[k] - g(k; \theta, \mathbf{x}[0], U^N) \tag{3.4}$$

where $\mathbf{y}[k] \in Z^N$ and $U^N \subset Z^N$, θ. Furthermore, let the *mean squared error* between the building output $\mathbf{y}[k]$ and the model output $\hat{\mathbf{y}}[k] = g(k; \theta, \mathbf{x}[0], U^N)$ be

$$V_N(\theta, Z^N) = \frac{1}{N} \sum_{k=1}^{N} \|\hat{\mathbf{e}}(k; \theta, \mathbf{x}[0], Z^N)\|_Q^2 \tag{3.5}$$

where $Q = Q^T > 0$. Typically, $Q = P_e^{-1}$ where $P_e \in \mathbb{R}^{o \times o}$ is the covariance of the measurement noise on the building output, $\mathbf{y}[k]$. Using (3.5), Ljung poses the

parameter estimation problem as the following convex optimization problem [54],

$$\min_{\theta} \quad \frac{1}{2} V_N(\theta, Z^N) \quad \text{s.t.} \quad \theta_{min}(i) \leq \theta(i) \leq \theta_{max}(i) \quad \forall \theta(i) \in \theta \tag{3.6}$$

where $\theta(i) \in \theta$ is the i^{th} parameter value, and $\theta_{min}(i) \in \mathbb{R}^1$ and $\theta_{max} \in \mathbb{R}^1$ are the i^{th} the parameter constraints. We denote the set of parameter values that solve (3.6) as the parameter set $\hat{\theta}_N \in \mathbb{R}^q$. A common approach to solve (3.6) is the prediction error method (PEM) which uses a numerical gradient-based algorithm to find the estimated set of parameter values $\theta = \hat{\theta}_N$ that minimizes the predicted output error $\hat{\mathbf{e}}(k; \theta, \mathbf{x}[0], Z^N) = \mathbf{y}[k] - g(k; \theta, \mathbf{x}[0], U^N)$ [54].

3.2.4 Model Validation

After the set of parameter estimate $\hat{\theta}_N$ is obtained, a different set of informative building data L^N is used to validate that the output of the model $M(\hat{\theta}_N)$ is equivalent to the output of $\mathcal{S}_d$. We compute the mean squared error of the model output, $V_N(\hat{\theta}_N, L^N)$ in (3.5). If the mean squared error between $\mathbf{y}[k]$ and $\hat{\mathbf{y}}[k]$ is below a threshold such that, $V_N(\hat{\theta}_N, L^N) < \epsilon$, then the estimated model $M(\hat{\theta}_N)$ is considered to be *validated*, which means $M(\hat{\theta}_N)$ accurately approximates the building dynamics $\mathcal{S}_d$. This also implies the set of estimated parameter values $\hat{\theta}_N$ is approximately equal to the set of true parameter value θ_S given $\mathcal{S}_d$ and $M(\hat{\theta}_N)$ belong to the same model structure. For models $M(\hat{\theta}_N)$ that cannot be validated with different data sets L^N, then the structure of the model or the data set used for identification have to be adjusted.

3.3 Building Model Identifiability

In order to choose an appropriate model or data set for identification, we must first determine and define the metrics that qualify a model or data set to be "good enough" for identification. Several papers have introduced the concept of *model identifiability* as a criteria to determine if the parameter estimation problem in (3.6) can be solved given a model $M(\theta)$ and a data set Z^N [1, 21, 22, 24, 25, 27, 41]. In the following subsections, we explore the concept of model identifiability and review the two types of model identifiability used to qualify building models and and building data sets: *structural identifiability* and *output identifiability*.

3.3.1 Structural Identifiability

Consider the following definition of structural identifiability.

Definition 5 (Structural Identifiability, [25]). *Let $\mathcal{M}$ be a model structure, and let $M(\theta) \in \mathcal{M}$ be a building model. Then, the model $M(\theta)$ is structurally identifiable at $\theta = \theta^*$ if, for all θ_1, θ_2 in a neighborhood of θ^*,*

$$M(\theta_1) \stackrel{M}{=} M(\theta_2) \implies \theta_1 = \theta_2$$

where $M(\theta_1) \in \mathcal{M}$ and $M(\theta_2) \in \mathcal{M}$. ♠

Structural identifiability implies there is a unique mapping from θ to $M(\theta)$, such that distinct parameter values $\theta = \theta^*$ yield distinct models $M(\theta^*)$ for models in an identifiable model structure $M(\theta^*) \in \mathcal{M}$. Since a distinct model $M(\theta^*)$ uniquely maps

the building inputs U^N to the modeled building outputs, Y^N, then changes to the model parameter value θ^* can be easily observed in the output and distinguished from models with different model parameter values. This ability to distinguish between models in a model structure is important because this impacts how well (3.6) estimates the model parameter values.

Suppose $M(\theta)$ is not structurally identifiable at $\theta = \theta^*$. Then, by Definition 5, there exists distinct parameter values $\theta_1 \neq \theta_2$ that yield an equivalent model $M(\theta_1) \stackrel{M}{=} M(\theta_2)$. This means that there exists more than one possible solution for the identification problem in (3.6), which makes it very difficult to distinguish between models. In [24, 25], Van Doren defines a metric to quantitatively test for this one-to-one mapping of θ to $M(\theta)$, and infers the identifiability of the model structure given that test. Using Lemma 1 below and Definition 5, we present this test for structural identifiability in Proposition 1.

Lemma 1 ([25]): *Let Ω be an open set in $\mathbb{R}^n$ and $f : \Omega \to \mathbb{R}^m$ be a k-times continuously differentiable map with $k \geq 1$. If $\frac{\partial f(\theta)}{\partial \theta}\big|_{\theta_m}$ has constant rank p in a neighborhood of θ_m, then f is locally injective at θ_m if and only if $p = n$.*

Proposition 1 (Test for Structural Identifiability, [25, 26]): *Assume the discrete-time building model $M(\theta)$ in (3.1), where $\theta \in \mathbb{R}^q$, belongs to a model structure $M(\theta) \in \mathcal{M}$. Let $C_i \in \mathbb{R}^{1\times n}$ be the i-th row of $C \in \mathbb{R}^{o\times n}$. Furthermore, let the mapping $s(k, \theta) : \theta \in \mathbb{R}^q \to \mathbb{R}^{1\times(om+op)}$ be defined as*

$$s(\tau, \theta) := \begin{bmatrix} C_1 A(\theta)^\tau D(\theta) & C_2 A(\theta)^\tau D(\theta) & \dots & C_o A(\theta)^\tau D(\theta) \end{bmatrix} \tag{3.7}$$

where $D(\theta) = \begin{bmatrix} B(\theta) & G(\theta) \end{bmatrix} \in \mathbb{R}^{n\times(m+p)}$, and let the mapping $S_k(\theta) : \theta \in \mathbb{R}^q \to$

$\mathbb{R}^{1\times(kom+kop)}$ *be defined as*

$$S_k(\theta) := \begin{bmatrix} s(0,\theta) & s(1,\theta) & \dots & s(k-1,\theta) \end{bmatrix}. \tag{3.8}$$

Given (3.8)*, let the mapping* $F_k(\theta) : \theta \in \mathbb{R}^q \to \mathbb{R}^{q\times q}$ *be defined as*

$$F_k(\theta) = \frac{\partial S_k(\theta)}{\partial \theta}\frac{\partial S_k(\theta)}{\partial \theta}^T. \tag{3.9}$$

Then, $M(\theta)$ *is structurally identifiable at* $\theta = \theta^*$ *if* $rank(F_k(\theta)) = q$ *for* $k \geq 2n$. ♣

Proof The proof of Prop. 1 follows directly from Lemma 1 and Definition 5. Given the mapping $S_k(\theta)$ in (3.8) that describes the structure of the model $M(\theta)$, then $S_k(\theta)$ is a unique or injective mapping if Lemma 1 is satisfied for $rank\left(\left.\frac{\partial S_k(\theta)}{\partial \theta}\right|_{\theta=\theta^*}\right) = q$. We note that $rank\left(\left.\frac{\partial S_k(\theta)}{\partial \theta}\right|_{\theta=\theta^*}\right) = rank(F_k(\theta^*))$. ■

3.3.2 Output Identifiability

Output identifiability highlights the importance of choosing a data set Z^N that can distinguish between different models. In [54], Ljung defines this type of data set Z^N as an *informative data set*, which is defined as follows. Given $\hat{\mathbf{y}}[k] = g(k;\theta,\mathbf{x}[0],U^k)$ in (3.2), consider the following definition of output identifiability.

Definition 6 (Ouptut Identifiability [25, 26]). *Let* $\hat{\mathbf{y}}[k] = g(k;\theta,\mathbf{x}[0],U^k)$ *be the output of the model* $M(\theta) \in \mathcal{M}$*. Then, the model* $M(\theta)$ *is output identifiable at* $\theta = \theta^*$ *given the initial condition* $\mathbf{x}[0]$ *and the input data* U^k *if, for all*

θ_1, θ_2 *in a neighborhood of* θ^*,

$$g(k;\theta_1,\mathbf{x}[0],U^k) = g(k;\theta_2,\mathbf{x}[0],U^k) \implies \theta_1 = \theta_2$$

where $g(k;\theta_1,\mathbf{x}[0],U^k)$ *is the output of* $M(\theta_1) \in \mathcal{M}$ *and* $g(k;\theta_2,\mathbf{x}[0],U^k)$ *is the output of* $M(\theta_2) \in \mathcal{M}$. ♠

Definition 6 implies the model $M(\theta) \in \mathcal{M}$ is output identifiable at $\theta = \theta^*$ if the model output $\hat{\mathbf{y}}[k] = g(k;\theta^*,\mathbf{x}[0],U^k)$ is distinct given a distinct parameter value, $\theta = \theta^*$ and input data U^k. Output identifiability differs from structural identifiability because it accounts for the impact of U^k on being able to distinguish between models $M(\theta)$ from the output $\hat{\mathbf{y}}[k] = g(k;\theta,\mathbf{x}[0],U^k)$.

Suppose $M(\theta)$ is structurally identifiable but not output identifiable given poor input data, $\bar{U}^k$. Then, the model output $g(k;\theta,\mathbf{x}[0],\bar{U}^k)$ is not distinct for the parameter value $\theta = \theta^*$, which implies there could exist another parameter value $\theta_M \neq \theta^*$ such that $g(k;\theta^*,\mathbf{x}[0],U^k) = g(k;\theta_M,\mathbf{x}[0],U^k)$ for all k. Van Doren defines a metric in [25, 26] to quantitatively test for this one-to-one mapping of θ to $g(k;\theta,\mathbf{x}[0],U^k)$, and infers the output identifiability of $M(\theta)$ at $\theta = \theta^*$ given the input data U^k. We present this test for output identifiability in Proposition 2.

Proposition 2 (Test for Output Identifiability, [25, 26]): *Given the cost function* $V_N(\theta, Z^N)$ *defined in* (3.5)*, let the hessian* $\left.\frac{\partial^2 V_N(\theta,Z^N)}{\partial\theta^2}\right|_\theta$ *be approximated by the following function,*

$$H_N(\theta, U^N) = \frac{1}{N}\sum_{k=0}^{N-1} \frac{\partial\hat{\mathbf{y}}[k]}{\partial\theta} Q \frac{\partial\hat{\mathbf{y}}[k]}{\partial\theta}^T \tag{3.10}$$

where $\hat{\mathbf{y}}[k] = g(k;\theta,\mathbf{x}[0],U^N)$ *and* $Q = Q^T > 0$. *Then, the model structure* $\mathcal{M}$ *is output identifiable given* U^k *at* $\theta = \theta^*$ *if* $rank(H_N(\theta^*, U^N)) = q$. ♣

PROOF This proof is given in [25]. Since (3.6) is convex, then the solution $\hat{\theta}_N$ is unique if the hessian of the cost function $V_N(\theta, Z^N)$ in (3.5) is positive definitive at $\theta = \hat{\theta}_N$, or

$$\left.\frac{\partial^2 V_N(\theta, Z^N)}{\partial\theta^2}\right|_{\theta=\hat{\theta}_N} > 0. \tag{3.11}$$

Then, based on Definition 6 and the approximation $H_N(\theta, U^N)$, we note that

$$rank\left(\left.\frac{\partial^2 V_N(\theta, Z^N)}{\partial\theta^2}\right|_{\theta}\right) = rank\left(H_N(\theta, U^N)\right) = q \tag{3.12}$$

implies the condition in (3.11) for $\theta = \hat{\theta}_N$. ■

Remark 1 Van Doren notes $H_N(\theta, U^N)$ is a Fisher information matrix in [24–26]. A *Fisher information matrix* bounds the covariance of the estimated parameter value $\hat{\theta}_N$ according to the following inequality,

$$\frac{1}{N}\sum_{k=0}^{N-1} \|\hat{\theta}_N - \theta_S\|^2 \geq H_N(\hat{\theta}_N, U^N)^{-1} \tag{3.13}$$

where θ_S is the true parameter value. The inequality in (3.13) is known as the Cramér-Rao inequality, and indicates the minimum possible covariance of any unbiased estimator. In other words, maximizing the information matrix $H_N(\hat{\theta}_N, U^N)$ minimizes the covariance of the estimated parameter $H_N(\hat{\theta}_N, U^N)^{-1}$, which improves the estimated parameter value, $\hat{\theta}_N$.

3.3.3 Linking Structural and Output Identifiability

Output identifiability implies distinct changes in the model parameter value yield distinct changes in the model output $g(k;\theta,\mathbf{x}[0],U^N)$ given an informative data set Z^N. Implicit in this inference is that the model structure $\mathcal{M}$ yields a distinct model $M(\theta)$ for a distinct parameter value θ, which means $M(\theta)$ is structurally identifiable by Definition 5. Therefore, we present and prove Proposition 3, which establishes a relationship between structural identifiability and output identifiability.

Proposition 3: *$M(\theta)$ is output identifiable for an informative data set Z^N if $M(\theta)$ is structurally identifiable.* ♣

PROOF Suppose $M(\theta^*) \in \mathcal{M}$ is structurally identifiable at θ^*. Then, by Definition 5, for any two parameters θ_1 and θ_2 in the neighborhood of θ^* and for models $M(\theta_1) \in \mathcal{M}$ and $M(\theta_2) \in \mathcal{M}$, then

$$M(\theta_1) \overset{M}{=} M(\theta_2) \implies \theta_1 = \theta_2.$$

Furthermore, given (3.4), let the model output errors for $M(\theta_1)$ and $M(\theta_2)$ be $\hat{\mathbf{e}}(k;\theta_1,\mathbf{x}[0],Z^N)$ and $\hat{\mathbf{e}}(k;\theta_2,\mathbf{x}[0],Z^N)$, respectively. Since Z^N is an informative data set, then by Definition 3,

$$\frac{1}{N}\sum_{k=1}^{N-1} \|f_e(k,\theta_1,\theta_2,Z^N)\|^2 = 0,$$

where $f_e(k,\theta_1,\theta_2,Z^N) = \hat{\mathbf{e}}(k;\theta_1,\mathbf{x}[0],Z^N) - \hat{\mathbf{e}}(k;\theta_2,\mathbf{x}[0],Z^N)$. This leads to the following observation

$$f_e(k,\theta_1,\theta_2,Z^N)^T\hat{\mathbf{e}}(k;\theta_1,Z^N) = f_e(k,\theta_1,\theta_2,Z^N)^T\hat{\mathbf{e}}(k;\theta_2,\mathbf{x}[0],Z^N), \quad \forall k$$

which also implies $\hat{\mathbf{e}}(k;\theta_1,\mathbf{x}[0],Z^N) = \hat{\mathbf{e}}(k;\theta_2,\mathbf{x}[0],Z^N)$ for all k. Given (3.4), then

we note $\hat{\mathbf{e}}(k;\theta_1,\mathbf{x}[0],Z^N) = \hat{\mathbf{e}}(k;\theta_2,\mathbf{x}[0],Z^N)$ can also be written as

$$g(k;\theta_1,\mathbf{x}[0],Z^N) = g(k;\theta_2,\mathbf{x}[0],Z^N).$$

Then, $g(k;\theta_1,\mathbf{x}[0],Z^N) = g(k;\theta_2,\mathbf{x}[0],Z^N)$ for all k if $M(\theta_1) \overset{M}{=} M(\theta_2)$ and Z^N is informative. This leads to the following result,

$$g(k;\theta_1,\mathbf{x}[0],Z^N) = g(k;\theta_2,\mathbf{x}[0],Z^N) \implies \theta_1 = \theta_2 \quad \forall k$$

which is the condition for output identifiability in Definition 6.

3.4 Design-Driven Model Identification

The standard model identification process outlined in Alg. 1 is a well-accepted approach, and Ljung provides some general guidelines on choosing the appropriate model structure and data set to accurately estimate mode parameters [54, 55]. However, the standard model identification process cannot accurately estimate parameters of ill-conditioned models such as RC building models, which are often ill-conditioned because of their complexity and structure. To address this challenge, we propose an improved identification process known as *design-driven model identification* that both detects the parameters that cannot be estimated in an ill-conditioned model and re-parameterizes the model structure to eliminate the effects of ill-conditioning. This design-driven model identification process delivers a more focused and streamlined approach to improve the identifiability of the model. We summarize our design-driven model identification process in Alg. 2. In the following subsections, we introduce introduce two key contributions used in the proposed approach: *parameter identi-*

fiability, which is used to detect model parameters that are likely inestimable and *parameter aggregation* heuristics, which are used to improve the structural identifiability of the model.

Algorithm 2 Design-Driven Model Identification Process

I. Choice of Model and Data:

A) Choose a building model $M(\theta) \in \mathcal{M}$ such that $\mathcal{S}_d \in \mathcal{M}$.

B) Choose a building data set Z^N that captures the building dynamics.

II. Parameter Identifiability:

A) Compute the structural identifiability matrix $\tilde{F}_k(\theta)$ in (3.14)

B) Determine the set of structurally unidentifiable parameters, $\theta^u \subseteq \theta$.

C) Let $\theta = \{\theta^p, \theta^u\}$ where θ^p is the identifiable set of parameters.

III. Parameter Aggregation:

A) Apply heuristics to map θ^u to a reduced set of parameters ψ^u.

B) Let the reduced set of parameter values be $\bar{\theta} = \{\theta^p, \psi^u\}$.

C) Re-parameterize the model $M(\theta)$ to be $M(\bar{\theta})$ given $\bar{\theta}$.

IV. Parameter Estimation: Solve (3.6) for $\hat{\bar{\theta}}_N$ given $M(\bar{\theta})$

V. Model Validation:

A) Choose a different building data set L^N for validation.

B) Compute the mean squared error, $V_N(\hat{\bar{\theta}}_N, L^N)$ in (3.5).

C) If $V_N(\hat{\bar{\theta}}_N, L^N) < \epsilon$, then the model $M(\hat{\bar{\theta}}_N)$ is identified.

3.4.1 Parameter Identifiability

The main idea behind parameter identifiability is to quantitatively determine the model parameters that may be poorly estimated. Parameter identifiability is implicit in the notion of model identifiability, where a model is considered identifiable if all

of the parameters are accurately estimated [43]. Likewise, unidentifiable models may have one or more parameters that are not identifiable. In [52], Li uses principle component analysis (PCA) of an output sensitivity matrix that resembles $H(\theta, U^N)$ to rank the parameters that are likely identifiable. The shortfall of this selection approach is the computational costs of evaluating several sequences of parameters that best ranks model parameters from least identifiable to most identifiable. In [24, 25], Doren uses the singular values of model identifiability metrics $F_k(\theta)$ and $H(\theta, U^N)$ to re-parameterize the model in terms of the largest singular values of the identifiability metrics. To ensure this approach works independent of parameter scaling, Van Doren scales these metrics as follows

$$\tilde{F}_k(\theta) = \Gamma(\theta)^T \left(\frac{\partial S_k(\theta)}{\partial \theta} P_S^{-1} \frac{\partial S_k(\theta)}{\partial \theta}^T \right) \Gamma(\theta) \tag{3.14}$$

$$\tilde{H}_N(\theta, U^N) = \frac{1}{N} \sum_{k=0}^{N-1} \Gamma(\theta)^T \left(\frac{\partial \hat{\mathbf{y}}[k]}{\partial \theta} Q \frac{\partial \hat{\mathbf{y}}[k]}{\partial \theta}^T \right) \Gamma(\theta) \tag{3.15}$$

where $\Gamma(\theta) = diag(|\theta(1)|, \ldots, |\theta(q)|)$, $S_k(\theta)$ is defined in (3.8), and $P_S = diag\left(s_1^2, s_2^2, \ldots\right)$ where s_i is an element of $S_k(\theta)$.

Our notion of parameter identifiability expands on Van Doren's work in [24, 25], and explicitly determines which model parameters are identifiable based on the identifiability metrics. We use the diagonal values of the identifiability metrics $F_k(\theta)$ and $H(\theta, U^N)$ to quantify which parameters are identifiable because they represent the amount of information content on each of the parameters [1]. In this section, we present an improvement to our prior approach using the singular value decomposition of the identifiability metrics. Since we are only interested in eliminating ill-conditioning in the model structure $\mathcal{M}$, we only consider the scaled structural identifiability metric $\tilde{F}_k(\theta)$ to determine structurally identifiable model parameters.

Let the SVD of $\tilde{F}_k(\theta)$ be $\tilde{F}_k(\theta) = \mathbf{U}\mathbf{\Sigma}\mathbf{V}^T$ where $\mathbf{U} \in \mathbb{R}^{q\times q}$ and $\mathbf{V} \in \mathbb{R}^{q\times q}$ are unitary matrices and $\mathbf{\Sigma} = diag(\sigma_1, \sigma_2, \ldots, \sigma_q) \in \mathbb{R}^{q\times q}$ such that $\sigma_1 \geq \sigma_2 \geq \ldots \geq \sigma_q$. Suppose the singular values $\{\sigma_{r+1}, \ldots, \sigma_q\}$ are treated as zeros if $\sigma_i < 1 \times 10^{-5}\sigma_1$ for all $i \in [r+1, q]$. Then, $\tilde{F}_k(\theta)$ can be partitioned as

$$\tilde{F}_k(\theta) \approx \begin{bmatrix} \mathbf{U}_1 & \mathbf{U}_2 \end{bmatrix} \begin{bmatrix} \mathbf{\Sigma}_1 & 0 \\ 0 & 0 \end{bmatrix} \begin{bmatrix} \mathbf{V}_1^T \\ \mathbf{V}_2^T \end{bmatrix} = \mathbf{U}_1\mathbf{\Sigma}_1\mathbf{V}_1^T \tag{3.16}$$

where $\mathbf{U}_1 \in \mathbb{R}^{q\times r}$, $\mathbf{U}_2 \in \mathbb{R}^{q\times q-r}$, $\mathbf{\Sigma}_1 \in \mathbb{R}^{r\times r}$, $\mathbf{V}_1 \in \mathbb{R}^{q\times r}$, $\mathbf{V}_2 \in \mathbb{R}^{q\times q-r}$. Van Doren determines $\mathbf{U}_1$ and $\mathbf{V}_1$ as identifiable subspaces of $F_k(\theta)$ that can be used to determine an identifiable parameterization [24, 25]. Parameters that are strongly correlated with identifiable subspaces $\mathbf{U}_1$ and $\mathbf{V}_1$ are observed to have high information content and a low parameter variance, which means those parameters are likely identifiable.

We use the diagonal of the matrix $\mathbf{U}_1\mathbf{V}_1^T$ to determine the parameters that are strongly correlated with the identifiable subspaces of $F_k(\theta)$. The diagonal entries of $\mathbf{U}_1\mathbf{V}_1^T$ lie between 0 and 1, where the i^{th} diagonal entry represents the correlation of the i^{th} parameter value with the identifiable subspace U_1 and V_1. Parameters in θ are likely identifiable if the associated diagonal entry value is close to 1, which denotes a strong correlation to the identifiable subspaces. We apply a threshold of $\mu_\sigma = 0.8$ over the diagonal entries, where entries below the threshold are determined to be likely unidentifiable. While this metric does not absolutely guarantee certain parameters can be estimated, this metric is a good indicator of the structurally identifiable parameters in the model. The following example demonstrates this concept of parameter identifiability for a small-scale building environment.

Example 2 (Parameter Identifiability of Two Room Building Model)
Consider the discrete-time model of the two room building environment in Appendix A.1. Let the sampling period be $T_s = 5$ minutes, and let estimated parameter value be $\hat{\theta}_N(i) = 0.7\theta_S(i)$ for all $i \in [1, q]$. Then, Fig. 3.1 plots the diagonal values of the structural identifiability matrix $F_k(\hat{\theta}_N)$, which denote the information content of each model parameter.

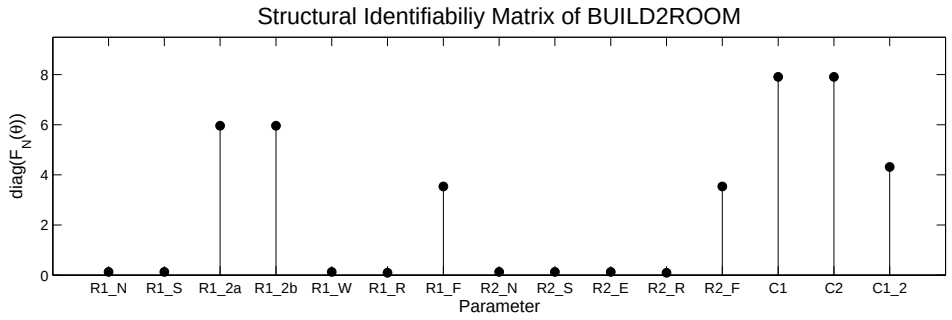

Figure 3.1: Diagonal Values of $F_k(\hat{\theta}_N)$ for Two Room Building

We observe in this plot that the parameters R_{12a}, R_{12b}, R_{1F}, R_{2F}, C_1, C_2, and C_{12} have high information content, which means these parameters are most likely to be correctly identified. The parameters R_{1N}, R_{1S}, R_{1W}, R_{1R}, R_{2N}, R_{2S}, R_{2E}, R_{1R} have low information content and signify parameters that are likely unidentifiable.

3.4.2 Parameter Aggregation

Example 2 shows that only some model parameters are structurally identifiable, which implies the overall building model $M(\theta)$ is not structurally or output identifiable. As discussed earlier, the main cause of structurally unidentifiable parameters is the over parameterization of the model [42]. Over-parameterization of building models makes

it difficult to distinguish between building model parameters given the amount of building data used to estimate the model parameters. Jacquez highlights this issue of parameter indistinguishability in [44] where he observes that state-space model parameters are numerically identifiable when they can be uniquely determined from the coefficients of the model transfer function. A similar algebraic approach is taken in compartmental models [14, 33, 72]. Godfrey et. al use simple geometric rules to determine the set of models with indistinguishable parameters based on the connectability of the model structure. Likewise, we define two rules to reduce the indistinguishability of parameters by reducing the number of parameters based on the identifiable and unidentifiable parameter values. We refer to this set of heuristics as *parameter aggregation*, and we demonstrate improvements to the structural identifiability of a model using parameter aggregation in the following section.

Rule 1: Aggregate All Parameters across a Single Building Element

In many cases, parameters across a single building element such as a roof, wall, floor, etc. cannot be distinguished, and are considered numerically unidentifiable. As a result, we can determine the unidentifiable parameters of a single building element, and re-parameterize the model using the total thermal resistance R^* and total thermal capacitance C^*. We observe that estimating the aggregate total resistance and total capacitance in a wall improves the overall structural identifiability of the model.

Consider a single building wall modeled as a 3R2C model, and let the set of wall parameters be $\theta_i = \{R_1, R_2, R_3, C_1, C_2\}$. Suppose the thermal wall resistance R_2 cannot be estimated accurately because of the inability to distinguish between individual wall resistances. To address this issue, we can re-parameterize the model of the wall in terms of the the total thermal wall resistance $R_i^* = R_1 + R_2 + R_3$ and the total thermal wall capacitance, $C_i^* = C_1 + C_2$. Given this reduced parameter

set $\psi_i = \{R_i^*, C_i^*\}$, we both reduce the model parameter and improve the structural identifiability of the model. We summarize this process for the i^{th} building element in Alg. 3, where θ_i is the set of parameters in the i^{th} building element. Given Alg.

Algorithm 3 Parameter Aggregation across a Single Building Element

1. Let $\theta_i = \{\theta_i^p, \theta_i^u\}$ where θ_i^u is the subset of unidentifiable parameters
2. Aggregate all resistances $R_k \in \theta_i$ into a single resistance $R_i^* = \sum_k R_k$.
3. Aggregate all capacitances $C_k \in \theta_i$ into a single capacitance $C_i^* = \sum_k C_k$.
4. Let $\psi_i = \{R_i^*, C_i^*\}$ be the reduced set of parameter values.

3, the unidentifiable parameters in a building model can be removed by reducing the parameter set of each building element θ_i for all i with an unidentifiable parameter to a new parameter set ψ_i that only includes the total resistance and capacitance of that particular building element. We note that this slight aggregation of the internal wall parameters changes the structure of the model, and we can test the identifiability of the restructured building model to note which lumped parameters are structurally unidentifiable.

Rule 2: Aggregate Parameters across Multiple Building Elements

We observe that based on the structure of building models, parameters between building elements may not be structurally identifiable because they are indistinguishable. For example, consider two side-by-side walls that separate two rooms. Given only measurements of the air temperatures on either side of the wall, the parameters in both walls may be considered indistinguishable since heat flow through each wall cannot be individually measured or calculated without knowledge of the model parameters. Therefore, we define a second rule, summarized in Alg. 4, where the

parameters across the indistinguishable walls are reduced to a total resistance and a total capacitance.

Algorithm 4 Parameter Aggregation across Multiple Building Elements

1. Let θ_i and θ_j be indistinguishable building elements.
2. Aggregate all resistances $R_k \in \theta_i \cup \theta_j$ into a single resistance $R^*_{ij} = \sum_k R_k$.
3. Aggregate all capacitances $C_k \in \theta_i \cup \theta_j$ into a single capacitance $C^*_{ij} = \sum_k C_k$.
4. Let $\psi_{ij} = \{R^*_{ij}, C^*_{ij}\}$ be the reduced set of parameter values.

The first step in this approach is determining indistinguishable building elements, which is directly tied to the connectability of the model structure as shown in [14, 33, 44]. In the context of building models, we find that building elements in a room bordering the outdoors such as exterior walls, windows, exterior floors, and exterior roofs tend to be indistinguishable. Therefore, the following example illustrates the application of Rule 2 to the scenario in Example 2 and illustrates how parameter aggregation can lead to significant improvement in the structural identifiability of the restructured building model

Example 3 (Parameter Aggregation of Two Room Building Model)
Consider the two room building scenario in Example 2. Given the diagonal values of the structural identifiability matrix $F_k(\theta)$ in 3.1, we note that the parameters with the lowest information content correspond to the parameters of the exterior walls, roof, and floor. The parameters in the exterior walls, floors, and roofs for Room 1 (and Room 2) cannot be distinguished because it is impossible to distinguish how much heat is being transferred through each exterior wall to identify individual wall parameters given only the temperature of the room $T_1(t)$ (and $T_2(t)$) from the

outdoors $T_o(t)$. Therefore, we apply Rule 2 to all the exterior walls, roofs, and floor elements in each room such that $\psi_{Room1} = \{R_{1o}\}$ and $\psi_{Room2} = \{R_{2o}\}$ for $R_{1o} = R_{1N} + R_{1S} + R_{1W} + R_{1R} + R_{1F}$ and $R_{2o} = R_{2N} + R_{2S} + R_{2E} + R_{2R} + R_{2F}$. We also apply Rule 1 to the interior wall such that

$$\psi_{Rule1} = \{R_{12}, C_{12}\}$$

where $R_{12} = R_{12a} + R_{12b}$. Given ψ_{Rule1} and $\psi_{Rule2} = \psi_{Room1} \cup \psi_{Room2}$, let the set of aggregated parameters be

$$\psi = \{R_{1o}, R_{12}, R_{2o}, C_1, C_2, C_{12}\}.$$

Fig. 3.2 plots the diagonal values of the structural identifiability matrix based on the restructured model, $M(\hat{\psi}_N)$.

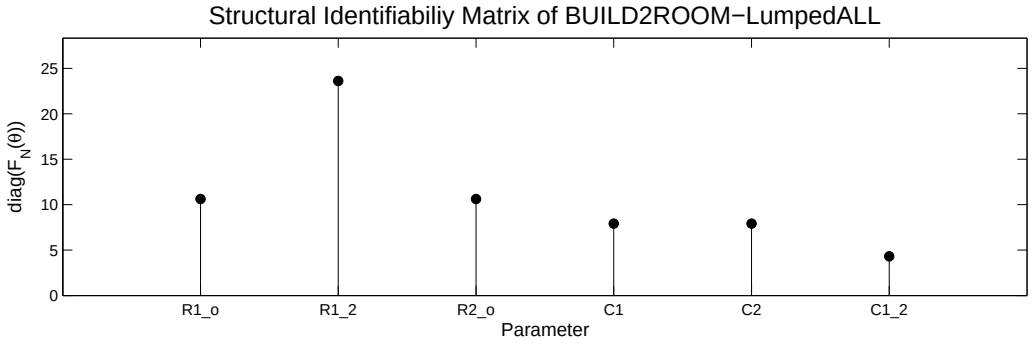

Figure 3.2: Diagonal Values of $F_k(\hat{\psi}_N)$ for Two Room Building

In comparison to Fig. 3.1, there is a much higher level of information on the aggregated parameters, which implies those parameters ψ are likely identifiable. It also implies the model $M(\psi)$ is structurally identifiable given $\psi = K(\theta)$.

3.5 Application: Identification of the IW-North Model

This section demonstrates both the current and proposed approaches to building model identification with the IW-North scenario highlighted in Chapter 2. We note the commercial office building is too large of a model to be successfully identified with the resources available.

3.5.1 Summary of Identification Metrics

We present the following metrics to analyze the accuracy of an identification process.

Mean Squared Output Error Given the set of parameter estimates $\hat{\theta}_N$ and validation data L^N, let the mean squared output error be

$$V_N(\theta, L^N) = \frac{1}{N} \sum_{k=1}^{N} \|\mathbf{y}[k] - \hat{\mathbf{y}}[k]\|^2$$

where $\{\mathbf{y}[k]\} \subset L^N$ is the building output and $\hat{\mathbf{y}}[k]$ is the model output given $\{\mathbf{u}[k], \mathbf{w}[k]\} \subset L^N$. This metric will be used to determine if the output of the model $M(\hat{\theta}_N)$ fits the actual building output $\mathbf{y}[k]$ given θ.

Mean Relative Parameter Error Given the parameter scaling deviations, let the mean absolute parameter scaling deviation be

$$\bar{\epsilon}_S(\theta) = \frac{1}{n_\theta} \sum_{i=1}^{n_\theta} \frac{|\theta_S(i) - \theta(i)|}{\theta_S(i)}$$

where n_θ is the number of parameters $\theta(i) \in \theta$ and θ_S is the set of true parameter values. This metric will be used as a benchmark that captures the quality of

identification experiment that yields the parameter estimate $\theta = \hat{\theta}_N$ where n_θ is the total number of parameters. For $\bar{\epsilon}_S(\theta) \leq 0.01$, we will assume the parameter θ is identified correctly because the parameter value $\theta(i)$ is within 1% of the true parameter value $\theta_S(i)$ on average.

3.5.2 Initial Conditions & Assumptions

Suppose the building data is sampled every 5 minutes, $T_s = 300$ sec, and collected for a period of two weeks, $k \in [0, 8063]$. Then, consider the following conditions for identification.

- Let $\theta_0(i) = 0.7\theta_S(i)$ and let $0.7\theta_S(i) \leq \theta(i) \leq 1.3\theta_S(i)$ for all $\theta(i) \in \theta \in \mathbb{R}^q$.
- Let the identification data be the first week of building data, $Z^{4032} = \{\mathbf{u}[k], \mathbf{w}[k], \mathbf{y}[k] : k \in [0, 4031]\}$ and let the validation data be the second week of building data, $L^{4032} = \{\mathbf{u}[k], \mathbf{w}[k], \mathbf{y}[k] : k \in [4032, 8063]\}$.
- Let $\bar{\mathbf{u}}[k]$ be a PRBS signal where $0W \leq \bar{u}_i[k] \leq 2000W$ for all i and for all $m \in [0, 1, \ldots]$.
- For sampling period $T_m = 3600$ sec (or 1 hr), let $\bar{T}_o[m]$ be given in Table 2.4 for all $m \in [0, \infty)$. Then, let $T_o[k] = \bar{T}_o[m]$ for $m \leq \frac{T_s}{T_m}k < m + 1$ and for all k.
- For sampling period $T_m = 600$ sec (or 10 min), let $\dot{q}_i[m] \sim \mathcal{N}(70W, 10^2W)$ for all $i \in [1, 13]$ and for all $m \in [0, \infty)$. Then, let $\dot{q}_i[k] = \dot{q}_i[m]$ for $m \leq \frac{T_s}{T_m}k < m + 1$ and for all k.
- Let $y_i[k]$ be the i^{th} building output with measurement error, $e_i[k] \sim \mathcal{N}(0, 0.1^2K)$ for all $i \in [1, 13]$.

3.5.3 Comparison of Standard and Design-Driven Identification of IW-North Model

In this subsection, we consider the following identification scenarios for the IW-North.

Case 1: Apply the standard identification process outlined in Alg. 1 to the IW-North model under the initial conditions above.

Case 2: Apply the design-driven identification process in Alg. 2 to the IW-North model under the initial conditions above.

Table 3.2 uses the metrics described above to quantify the quality of the solution $\hat{\theta}_N$, assuming the true parameter θ_S is known for both case scenarios. Table 3.3 uses the identifiability metrics presented earlier to demonstrate the usefulness of parameter identifiability. Table 3.3 assumes the true parameter θ_S is unknown.

Table 3.2: Identification of the IW-North Model

	Init. Param. $\bar{\epsilon}_S(\theta_0)$	Estim. Param. $\bar{\epsilon}_S(\hat{\theta}_N)$	Time (sec)	Model Validation $V(\hat{\theta}_N, L^N)$
Case 1	0.30	0.20	225	0.78
Case 2	0.30	0.03	79	0.03

Table 3.3: Parameter Identifiability of the IW-North Model

	# of θ n_θ	Rank of $\tilde{F}_k(\hat{\theta}_N)$	Rank of $\tilde{H}_N(\hat{\theta}_N, U^N)$
Case 1	166	142	138
Case 2	59	59	27

For Case 1, we observe that both the structural and output identifiability matrices in Table 3.3 are not full rank, which means the model $M(\theta)$ is not structurally or

output identifiable given Z^N. The second column of Table 3.2 supports this claim since a large number of parameters are cannot be identified. Furthermore, using the notion of parameter identifiability, we are able to correctly detect some of the parameters that are likely unidentifiable given the model structure and the data set. Lastly, the large values for the mean relative parameter error in column 4 of Table 3.2 and the mean squared output error in column 5 of Table 3.2 are further proof that the standard identification algorithm used in Case 1 poorly estimates parameters in the IW-North.

In comparison to Case 1, Case 2 demonstrates the identification process with parameter aggregation does a significantly better job of accurately estimating the model parameters. We observe from Table 3.3 that the rank of the structural identifiability matrix is full rank. This implies all the parameters should be correctly estimated, provided an informative input. We also note the output identifiability matrix is not full rank, which means the model $M(\theta)$ is not output identifiable for a given set of data Z^N. Finally, the mean absolute parameter deviation and the mean squared output error in Table 3.2 are much lower for Case 2 than Case 1 because the parameters are better estimated in this process and approximate the true parameter values.

3.6 Summary

This chapter poses the building model identification problem and presents the standard method of identifying grey-box building models. Using the concept of model identifiability outlined in [24–26], we propose the following improvements to the current identification process and make the following contributions.

1. Based on the structural and output identifiability metrics defined above, we introduce the notion of parameter identifiability that answers the question *which* model parameters are unidentifiable and *why* these model parameters are unidentifiable. This analysis of the model parameters provides useful guidelines to users about how to restructure the model to improve structurally unidentifiable.

2. We propose a design-driven identification process in Alg. 2 and provide heuristics to improve the structural identifiability of the model. Specifically, we provide rules to aggregate an unidentifiable set of model parameters θ into a smaller identifiable set of lumped parameters ψ. Finally, we demonstrate our proposed design-driven identification process to identify a model of the IW-North.

Chapter 4

Decentralized Identification of Building Control Models

Chapter 3 presents a novel approach to identification using identifiability metrics to improve estimation of model parameters. However, one of the biggest limitations to identification of building models is scalability. Grey-box models of large-scale buildings can have as many as hundreds or even thousands of parameters depending on the complexity of the model. This also means the parameter estimation problem in (3.6) becomes a large-scale optimization problem, which can potentially be too time-consuming and too computationally expensive to solve.

To address this challenge, we propose a decentralized approach to the identification scheme in Alg. 2. The idea behind this new approach is that decentralized identification splits the overall identification problem into smaller, more tractable identification problems, which improves the time and computational effort it takes to identify a large building model. We break down the decentralized identification problem into two major questions:

1. *How do we partition the decentralized identification problem into smaller problems?*

2. *How do we guarantee the decentralized approach yields equivalent results to the centralized identification approach?*

This chapter investigates the answer to each of these questions in the following sections: Section 4.1 provides basic background on graph theory, and Section 4.2 introduces the concept of reachability using graph theory. Next, Section 4.3 lays the framework to adequately address the first question. In Section 4.4, we introduce the theoretical framework of model inclusion to answer the second question. Sections 4.5 and 4.6 apply this decentralized approach identification to case studies. Finally, Section 4.7 summarizes the contributions of this chapter.

4.1 Background on Graphs

4.1.1 Graph Notation

We briefly review basic graph theoretic terms and notation used in our work. A directed graph or *digraph* is an ordered pair $G = \{V, E\}$ where V is the set of nodes and $E \subset V \times V$ is the set of *edges*. The digraph $G_s = \{V_s, E_s\}$ is a *subgraph* of G if $V_s \subseteq V$ and $E_s \subseteq V_s \times V_s \subseteq E$. G_s *spans* G if $V_s = V$. A set of subgraphs $G_i = \{V_i, E_i\}$ for $i = 1, \ldots, N$ is a *graph partition* of G if $\bigcup_i V_i = V$, $V_i \neq \emptyset$ for all i , $V_i \bigcap V_j = \emptyset$ for all i, j, and $E_i = V_i \times V_i \subseteq E$ for all i. Let $G_1 = \{V_1, E_1\}$ and $G_2 = \{V_2, E_2\}$. Then, $G = G_1 \oplus G_2$ is the *graph sum* of G_1 and G_2 if $V = V_1 \cup V_2$ and $E = E_1 \cup E_2$. We denote graph sums as $\sum_i G_i$. Likewise, $G = G_1 - G_2$ is the *graph difference* of G_1 and G_2 where $V = V_1 \backslash V_2$ and $E = E_1 \backslash E_2$.

A vertex v_1 is *adjacent* to vertex v_2 on digraph $G = \{V, E\}$ if there exists an edge $(v_1, v_2) \in E$ or an edge $(v_2, v_1) \in E$ for $v_1, v_2 \in V$. The *open neighborhood* of a vertex set $V_s \subset V$ on the digraph $G = \{V, E\}$ is $N(V_s) = \{v$ adjacent to $v_i : v \in V \backslash V_s, v_i \in V_s\}$. We use the term neighborhood in place of the term open neighborhood.

A *simple path* or path on graph G between the root vertex $v_1 \in V$ and the terminal vertex $v_k \in V$ is a sequence of edges $\{(v_1, v_2), (v_2, v_3), \ldots, (v_{k-1}, v_k)\}$ for which all the vertices are distinct i.e. $v_i \neq v_j$ for $i \neq j$. A path $P = \{(v_1, v_2), \ldots, (v_{k-1}, v_k)\}$ can be represented as a subgraph $G(P) = \{V(P), P\}$ where $V(P) = \{v_1, v_2, \ldots, v_k\}$. $G = \{V, E\}$ is a *weakly connected digraph* if there exists a path from v_i to v_j or there exists a path from v_j to v_i for every pair of vertices $v_i, v_j \in V$ for $i \neq j$. We use the term "connected digraphs" to refer to weakly connected digraphs. $G = \{V, E\}$ is a *strongly connected digraph* if there exists a path from v_i and v_j and there exists a path from v_j and v_i for all $v_i, v_j \in V$ for $i \neq j$.

4.1.2 Digraph of Building Dynamics

Consider the structured system matrices $A_c(\theta)$, $B_c(\theta)$, $G_c(\theta)$, and C of the continuous-time building dynamics in (2.11). Then, the structure of the building dynamics $\mathcal{S}$ can be represented as a digraph, $G(\mathcal{S}) = \{V_S, E_S\}$, where graph vertices $v \in V_S$ represent building signals (such as building temperature) and graph edges $(v_i, v_j) \in E_S$ represent the dynamic interaction between these building signals. Given the different types of building signals, we define the different types of vertices and edges associated to the digraph $G(\mathcal{S})$ below.

T_i	The *state vertex* T_i represents the i^{th} building temperature, $T_i(t)$.
u_i	The *input vertex* u_i represents the i^{th} building input, $u_i(t)$.

w_i	The *disturbance vertex* w_i represents the i^{th} building disturbance, $w_i(t)$.
y_i	The *output vertex* y_i represents the i^{th} building output, $y_i(t)$.
(T_i, T_j)	The edge (T_i, T_j) exists if $[A_c(\theta)]_{ij} \neq 0$.
(u_j, T_i)	The edge (u_j, T_i) exists if $[B_c(\theta)]_{ij} \neq 0$.
(w_j, T_i)	The edge (w_j, T_i) exists if $[G_c(\theta)]_{ij} \neq 0$.
(T_j, y_i)	The edge (T_j, y_i) exists if $[C]_{ij} \neq 0$.
X	$X = \{T_1, \ldots, T_n\} \in \mathbb{R}^n$ is the set of all state vertices.
X_a	$X_a \subseteq X$ represents building air temperatures, $\mathbf{T}_a(t)$.
X_w	$X_w \subset X$ represents non-air building temperatures, $\mathbf{T}_w(t)$.
U	$U = \{u_1, \ldots, u_m\} \in \mathbb{R}^m$ is the set of all input vertices.
W	$W = \{w_1, \ldots, w_p\} \in \mathbb{R}^p$ is the set of all disturbance vertices.
Y	$Y = \{y_1, \ldots, y_o\} \in \mathbb{R}^o$ is the set of all output vertices.
$E_{x,x}$	$E_{x,x} = \{(T_i, T_j) : [A_c(\theta)]_{ij} \neq 0\} \subset X \times X$ is the set of all edges between state vertices.
$E_{u,x}$	$E_{u,x} = \{(u_j, T_i) : [B_c(\theta)]_{ij} \neq 0\} \subset U \times X$ is the set of all edges between state and input vertices
$E_{w,x}$	$E_{w,x} = \{(w_j, T_i) : [G_c(\theta)]_{ij} \neq 0\} \subset W \times X$ is the set of all edges between state and disturbance vertices
$E_{x,y}$	$E_{x,y} = \{(T_j, y_i) : [C]_{ij} \neq 0\} \subset X \times Y$ is the set of all edges between state and output vertices.

Using this detailed notation, the digraph of $\mathcal{S}$ is formally defined as follows.

Definition 7 (Building Digraph). *Given a building $\mathcal{S}$, the building digraph is* $G(\mathcal{S}) = \{X \cup U \cup W \cup Y, E\}$ *where* $E = E_{x,x} \cup E_{u,x} \cup E_{w,x}, \cup E_{x,y}$. ♠

4.2 Reachability of Building Dynamics

Several papers have studied the relationship between controllability, observability, and identifiability [15, 21, 25] but have shown that controllability and observability are neither necessary nor sufficient conditions for output identifiability. However, Van Doren notes in [25] that structural identifiability is dependent on parameter sensitivity, controllability, and observability. This makes sense because identification exposes the relationship between system inputs and system outputs. Therefore, buildings without an input cannot be controllable or structurally identifiable because the building states cannot be influenced. Likewise, buildings without an output cannot be observable or structurally identifiable because there are no building outputs to observe changes in the building states. Intuitively, a building cannot be structurally identifiable if the building states are inaccessible from the building inputs or inaccessible to the building outputs.

Based on this logic, we highlight the importance of structural access to building states from building inputs and to building outputs for structural identifiability. This notion of structural access is more formally known as input and output reachability in [14, 44] or structural controllability and observability in [53]. Although both sets of terms are equivalent, we will exclusively use and define the terms *input reachability* and *output reachability*. Given Definition 7, we define the reachability properties of the building environment $\mathcal{S}$ as follows.

Definition 8 (Input Reachability [14]). *A dynamic system $\mathcal{S}$ is input reachable from the controllable input $u_i(t)$ if there exists a directed path on the digraph of the system $G(\mathcal{S})$ from the associated input vertex $u_i \in U$ to every state vertex $x_i \in X$.* ♠

Definition 9 (Output Reachability [14]). *A dynamic system $\mathcal{S}$ is output reachable to the output $y_i(t)$ if there exists a directed path on the digraph of the system $G(\mathcal{S})$ from every state vertex $x_i \in X$ to the output vertex $y_i \in Y$.* ♠

In [53], Liu uses digraphs of large-scale systems to analyze the structural relationship between the states and controllable inputs. Likewise, we use digraphs of building dynamics provide an easy way to characterize structural input/output relationships in a building that may lead to poor structural identifiability. The following example depicts a building digraph and illustrates the notion of input and output reachability for a small-scale building.

Example 4 (Reachability of Four Room Building)

Consider the four room building dynamics $\mathcal{S}$ in Appendix A.2. Then, the digraph of the building dynamics is $G(\mathcal{S}) = \{X \cup U \cup W \cup Y, E_{x,x} \cup E_{u,x} \cup E_{w,x}, \cup E_{x,y}\}$ where the set of graph vertices are

$$X_a = \{T_1, T_2, T_3, T_4\}, \qquad X_w = \{T_{12}, T_{13}, T_{24}, T_{34}\} \qquad X = X_a \cup X_w$$

$$U = \{u_1, u_4\}, \qquad W = \{T_o\}, \qquad Y = \{y_1, y_2, y_3, y_4\}$$

and the set of graph edges are

$$\begin{aligned}
E_{x,x} = \{&(T_1, T_{12}), (T_1, T_{13}), (T_2, T_{12}), (T_2, T_{24}), (T_3, T_{13}), (T_3, T_{34}), \ldots \\
&(T_4, T_{24}), (T_4, T_{34}), (T_{12}, T_1), (T_{12}, T_2), (T_{13}, T_1), (T_{13}, T_3), \ldots \\
&(T_{24}, T_2), (T_{24}, T_4), (T_{34}, T_3), (T_{34}, T_4)\} \\
E_{u,x} = \{&(u_1, T_1), (u_4, T_4)\} \\
E_{w,x} = \{&(T_o, T_1), (T_o, T_2), (T_o, T_3), (T_o, T_4)\} \\
E_{x,y} = \{&(T_1, y_1), (T_2, y_2), (T_3, y_3), (T_4, y_4)\}.
\end{aligned}$$

Then, the building digraph $G(\mathcal{S})$ is illustrated in Fig. 4.1. Given the building digraph $G(\mathcal{S})$, let $P_{u_1,x}$ and $P_{u_4,x}$ be the sets of all possible paths that start from input vertices u_1 and u_4, respectively, and end on a state vertex $T_i \in X$, such that

$$P_{u_1,x} = \{\{(u_1, T_1)\}, \{(u_1, T_1), (T_1, T_{12})\}, \{(u_1, T_1), (T_1, T_{12}), (T_2, T_{24}), \}\ldots\} \quad (4.1a)$$

$$P_{u_4,x} = \{\{(u_4, T_4)\}, \{(u_4, T_4), (T_4, T_{24})\}, \{(u_4, T_4), (T_4, T_{24}), (T_{24}, T_2), \}\ldots\} \quad (4.1b)$$

From observation of the building digraph $G(\mathcal{S})$ in Fig. 4.1, we conclude that the set of paths $P_{u_1,x}$ and $P_{u_4,x}$ includes a path from every input vertex to every state vertex. Therefore, the building $\mathcal{S}$ is input-reachable. Likewise, let P_{x,y_1}, P_{x,y_2}, P_{x,y_3}, and P_{x,y_4} be the sets of all possible paths that start from a state vertex and end on an output vertex y_1, y_2, y_3, and y_4, respectively, such that

$$P_{x,y_1} = \{\{(y_1, T_1)\}, \{(y_1, T_1), (T_1, T_{12})\}, \{(y_1, T_1), (T_1, T_{12}), (T_{12}, T_2), \}\ldots\} \quad (4.2a)$$

$$P_{x,y_2} = \{\{(y_2, T_2)\}, \{(y_2, T_2), (T_2, T_{24})\}, \{(y_2, T_2), (T_2, T_{24}), (T_{24}, T_4), \}\ldots\} \quad (4.2b)$$

$$P_{x,y_3} = \{\{(y_3, T_3)\}, \{(y_3, T_3), (T_3, T_{13})\}, \{(y_3, T_3), (T_3, T_{13}), (T_{13}, T_1), \}\ldots\} \quad (4.2c)$$

$$P_{x,y_4} = \{\{(y_4, T_4)\}, \{(y_4, T_4), (T_4, T_{34})\}, \{(y_4, T_4), (T_4, T_{34}), (T_{34}, T_3), \}\ldots\} \quad (4.2d)$$

We observe that the set of paths P_{x,y_1}, P_{x,y_2}, P_{x,y_3}, and P_{x,y_4} includes a path from every state vertex to every output vertex. Therefore, $\mathcal{S}$ is also output reachable.

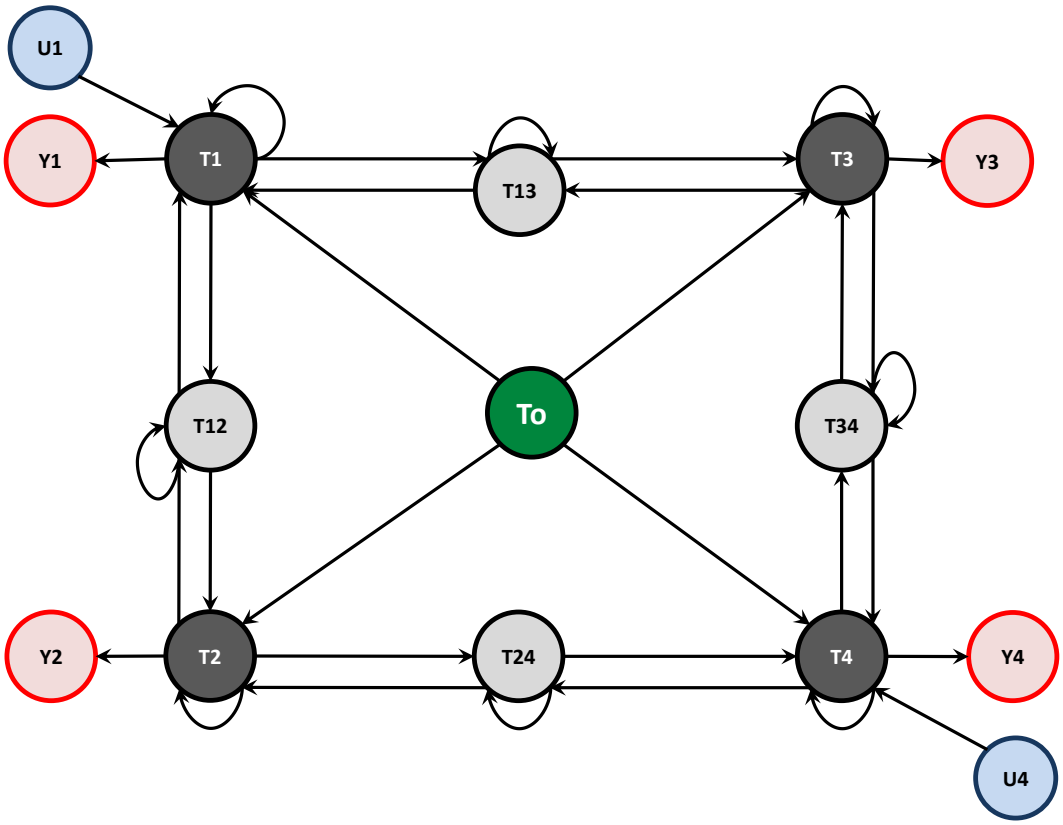

Figure 4.1: Digraph of Building Dynamics: Grey nodes represent state vertices, $T_i \in X$ and dark grey nodes represent air state vertices, $T_i \in X_a$. Blue nodes represent input vertices $u_i \in U$, and red nodes represent output vertices $y_i \in Y$. Green nodes are disturbance inputs, $w_i \in W$.

4.3 Decentralized Reachability of Building Dynamics

Although the reachability of $\mathcal{S}$ can be easily observed for the small-scale building in Example 4, it can be much more difficult to detect for large-scale systems. To address this issue, we propose a decentralized approach to determine the input-output reachability of the building. This approach first determines the input-output reachability of the component air-based subsystems of $\mathcal{S}$ and then uses the interactions between these air-based building subsystems to determine the reachability of the entire building.

4.3.1 Air-Based Building Subsystems & Building Maps

A building is a collection of rooms, offices, hallways, and other physical spaces. In each of these spaces, heat is being transferred to the space air from surrounding non-air materials with thermal mass (such as walls, roofs, floors), independent heat sources such as radiators, and heat flow from neighboring spaces. We denote the dynamics of the i^{th} air space in the building as $\mathcal{S}_i^a$, where $\mathcal{S}_i^a$ is a subsystem of $\mathcal{S}$ and the digraph $G(\mathcal{S}_i^a)$ is a subgraph of $G(\mathcal{S})$. $\mathcal{S}_i^a$ is referred to as the i^{th} *air-based subsystem* of $\mathcal{S}$. We provide a precise definition of $\mathcal{S}_i^a$ below.

Definition 10 (Air-Based Building Subsystem). *$\mathcal{S}_i^a$ is the i^{th} air-based subsystem of $\mathcal{S}$ if $G(\mathcal{S}_i^a) = \{X_i^a \cup U_i^a \cup W_i^a \cup Y_i^a, E_i^a\}$ is a connected subgraph of $G(\mathcal{S}) = \{X \cup U \cup W \cup Y, E\}$ and satisfies the following conditions:*

- *$X_i^a \cap X_a = \{T_i\}$ and $X^i - \{T_i\} \subset X_w$ where $X_a \cup X_w = X$ and T_i is the i^{th} building air temperature,*

- $N(X_i^a) \cap X \subset X_a$ *where* $N(X_i^a)$ *is the neighborhood of* X_i^a *on* $G(\mathcal{S})$,
- $U_i^a = N(X_i^a) \cap U$,
- $W_i^a = N(X_i^a) \cap (X \cup W)$,
- $Y_i^a = N(X_i^a) \cap Y$, *and*
- $E_i^a = \{(u, v) \in E : \forall u, v \in X_i^a \cup U_i^a \cup W_i^a \cup Y_i^a\}$. ♠

The concept of air-based building subsystems is important because it exposes the structured thermodynamics of individual building spaces. We will use these component subsystems later in this chapter to examine certain structural properties in the building. In Appendix B.1, we present Alg. 12 which partitions the building digraph $G(\mathcal{S})$ into the set of subgraphs $\{G(\mathcal{S}_i^a) : \forall i \in [1, a]\}$ that satisfy the conditions in Definition 10. We can infer the interactions between any two subsystems $\mathcal{S}_i^a$ and $\mathcal{S}_j^a$ based on the edges that are shared between the digraphs $G(\mathcal{S}_i^a)$ and $G(\mathcal{S}_j^a)$. These interactions represent the heat flow between physical spaces in a building, and they can be mapped on a high-level graph to expose the connections between the different air-based subsystems. We define this high-level graph as a *building map*, and we demonstrate this decentralized approach in the following example.

Definition 11 (Building Map). *Let* $\{\mathcal{S}_i^a : \forall i \in [1, a]\}$ *be the set of all air-based subsystems of* $\mathcal{S}$. *Then,* $G_R(\mathcal{S}) = \{V_R, E_R\}$ *is the building map of* $\mathcal{S}$ *if,*

- $V_R = \{1, \ldots, a\}$ *where* $i \in V_R$ *represents the* i^{th} *air based subsystem* $\mathcal{S}_i^a$,

- *The edge* $(i,j) \in E_R$ *exists for* $(i,j) \in V_R \times V_R$ *if there exists an edge* $(u,v) \in E_i^a \cap E_j^a$ *where* $G(\mathcal{S}_i^a) = \{V_i^a, E_i^a\}$ *and* $G(\mathcal{S}_j^a) = \{V_j^a, E_j^a\}$. ♠

Example 5 (Decentralized Reachability of Four Room Building)

Given the digraph $G(\mathcal{S})$, we apply the partitioning algorithm shown in Alg. 12 to find digraphs of the air-based subsystems of $\mathcal{S}$. We observe that the building digraph $G(\mathcal{S})$ is split into 4 component air-based subsystems, $G(\mathcal{S}_1^a)$, $G(\mathcal{S}_2^a)$, $G(\mathcal{S}_3^a)$, and $G(\mathcal{S}_4^a)$ which are depicted in Fig. 4.2.

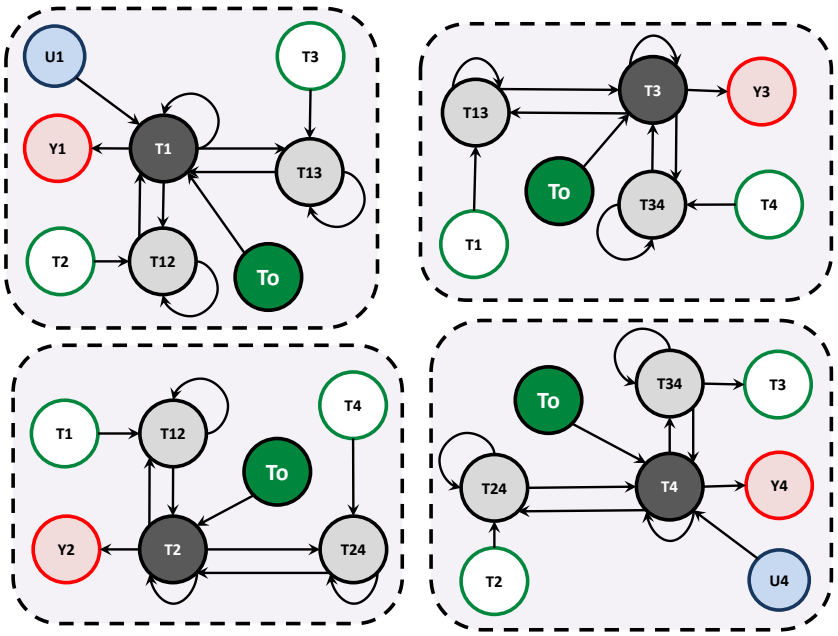

Figure 4.2: Digraph of Air-Based Building Subsystems: Grey nodes represent state vertices, $T_i \in X$ and dark grey nodes represent air state vertices, $T_i \in X_a$. Blue nodes represent input vertices $u_i \in U$, and red nodes represent output vertices $y_i \in Y$. Green nodes are disturbance inputs, $w_i \in W$, and white nodes are air temperatures from neighboring rooms, $T_j \in X_a$ which are treated as disturbance inputs

We make the following observations about the reachability of each of these air-based subsystems.

Reachability of $\mathcal{S}_1^a$: The air-based subsystem $\mathcal{S}_1^a$ is input reachable because there exists a directed path $P_i \in P_{u_1,x}$ on $G(\mathcal{S}_1^a)$ from every input vertex $U_1^a = \{u_1\}$ to every state vertex in $X_1^a = \{T_1, T_{12}, T_{13}\}$ where

$$P_{u_1,x} = \{(u_1, T_1)\} \cup \{(u_1, T_1), (T_1, T_{12})\} \cup \{(u_1, T_1), (T_1, T_{13})\}. \tag{4.3}$$

Likewise, $\mathcal{S}_1$ is output reachable because there exists a directed path $P_i \in P_{x,y_1}$ on $G(\mathcal{S}_1^a)$ from every state vertex in X_1^a to every output vertex $Y_1^a = \{y_1\}$ where

$$P_{x,y_1} = \{(T_1, y_1)\} \cup \{(T_{12}, T_1), (T_1, y_1)\} \cup \{(T_{13}, T_1), (T_1, y_1)\}. \tag{4.4}$$

Reachability of $\mathcal{S}_2^a$: The air-based subsystem $\mathcal{S}_2^a$ is output reachable because there exists a directed path $P_i \in P_{x,y_2}$ on $G(\mathcal{S}_2^a)$ from every state vertex in $X_2^a = \{T_2, T_{12}, T_{24}\}$ to every output vertex $Y_2^a = \{y_2\}$ where

$$P_{x,y_2} = \{(T_2, y_2)\} \cup \{(T_{12}, T_2), (T_2, y_2)\} \cup \{(T_{24}, T_2), (T_2, y_2)\}. \tag{4.5}$$

Reachability of $\mathcal{S}_3^a$: The air-based subsystem $\mathcal{S}_3^a$ is output reachable because there exists a directed path $P_i \in P_{x,y_3}$ on $G(\mathcal{S}_3^a)$ from every state vertex in $X_3^a = \{T_3, T_{13}, T_{34}\}$ to every output vertex $Y_3^a = \{y_3\}$ where

$$P_{x,y_3} = \{(T_3, y_3)\} \cup \{(T_{13}, T_3), (T_3, y_3)\} \cup \{(T_{34}, T_3), (T_3, y_3)\}. \tag{4.6}$$

Reachability of $\mathcal{S}_4^a$: The air-based subsystem $\mathcal{S}_4^a$ is input reachable because there

exists a directed path $P_i \in P_{u_4,x}$ on $G(\mathcal{S}_4^a)$ from every input vertex $U_4^a = \{u_4\}$ to every state vertex in $X_4^a = \{T_4, T_{24}, T_{34}\}$ where

$$P_{u_4,x} = \{(u_4, T_4)\} \cup \{(u_4, T_4), (T_4, T_{24})\} \cup \{(u_4, T_4), (T_4, T_{34})\}. \tag{4.7}$$

Likewise, $\mathcal{S}_4^a$ is output reachable because there exists a directed path $P_i \in P_{x,y_4}$ on $G(\mathcal{S}_4^a)$ from every state vertex in X_4^a to every output vertex $Y_4^a = \{y_4\}$ where

$$P_{x,y_4} = \{(T_4, y_4)\} \cup \{(T_{24}, T_4), (T_4, y_4)\} \cup \{(T_{34}, T_4), (T_4, y_4)\}. \tag{4.8}$$

We can characterize the interactions between these air-based building subsystems using the building map shown in Fig. 4.3. Using the building map, we can determine the reachability of the entire building based on how each of the air-based subsystems are connected together.

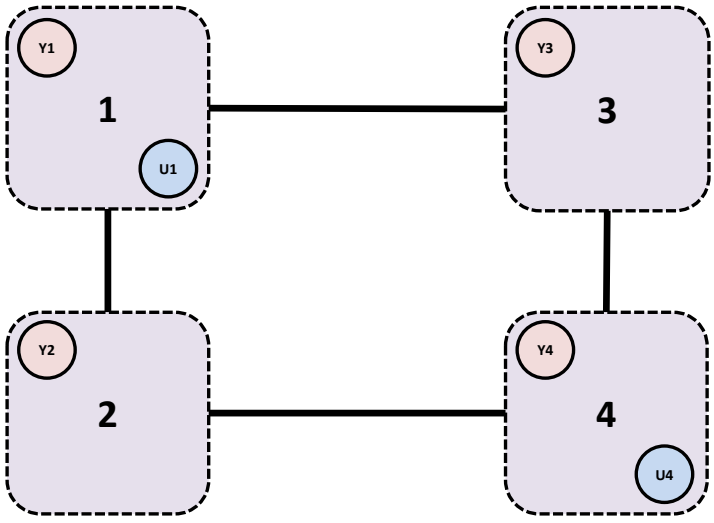

Figure 4.3: Building Map of $\mathcal{S}$

In this scenario, there exists a path from every input-output reachable air-based

building subsystem to every other air-based building subsystem. This means that there exists a path from an input or output vertex in an input-output reachable air-based building subsystem to the states in other air-based subsystems. As a result, we can conclude the entire building is both input and output reachable.

4.3.2 Input-Output Reachable Partitions of Building Map

In the prior example, we use the reachability of the air-based building subsystems to determine the reachability of the entire building. This determines whether the entire building has a room with access to at least an input and an output for identifiability. In this subsection, we are interested in partitioning the building into potentially identifiable zones such that each building zone has access to at least one input and one output. This means we are interested in creating zones of the the building that are both input and output reachable. Towards that end, we introduce this notion of input-output reachable partitions of $\mathcal{S}$ to uniformly split the building structure into input-output reachable partitions.

Definition 12 (Input-Output Reachable Partition of Building Map). *$\{\{V_R^k, E_R^k\} : \forall k\}$ is the input-output reachable partition of the building map $G_R(\mathcal{S}) = \{V_R, E_R\}$ if*

- *$\{\{V_R^k, E_R^k\} : \forall k\}$ is a graph partition of $G_R(\mathcal{S}) = \{V_R, E_R\}$*
- *There exists an input reachable $\mathcal{S}_i^a$ such that $i \in V_R^k$*
- *There exists an output reachable $\mathcal{S}_j^a$ such that $j \in V_R^k$*

where $\mathcal{S}_i^a$ is the i^{th} air-based subsystem of $\mathcal{S}$. ♠

The following example depicts the input-output partitions of the building map in Fig. 4.3.

Example 6 (Digraph of Input-Output Reachable Partitions)

The building map $G_R(\mathcal{S})$ in Fig. 4.3 can be partitioned into input-output reachable segments using Alg. 13. Fig. 4.5 provides examples of the types of input-output reachable partitions of $G_R(\mathcal{S})$.

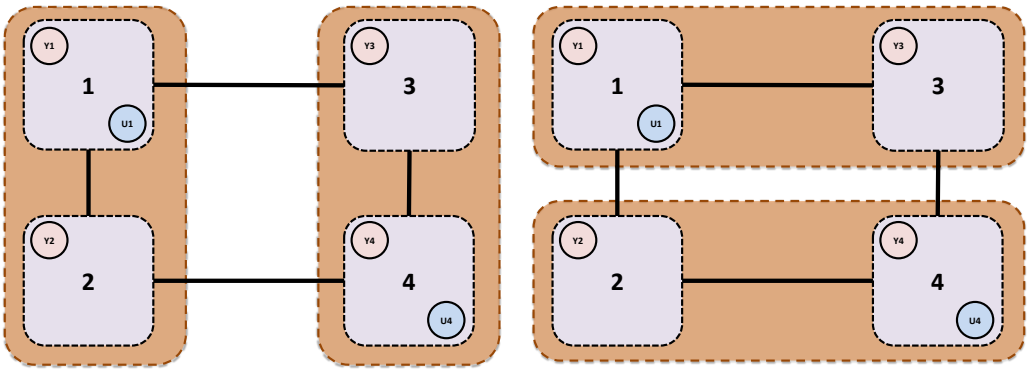

(a) Partition $\mathcal{P}_1$ (b) Partition $\mathcal{P}_2$

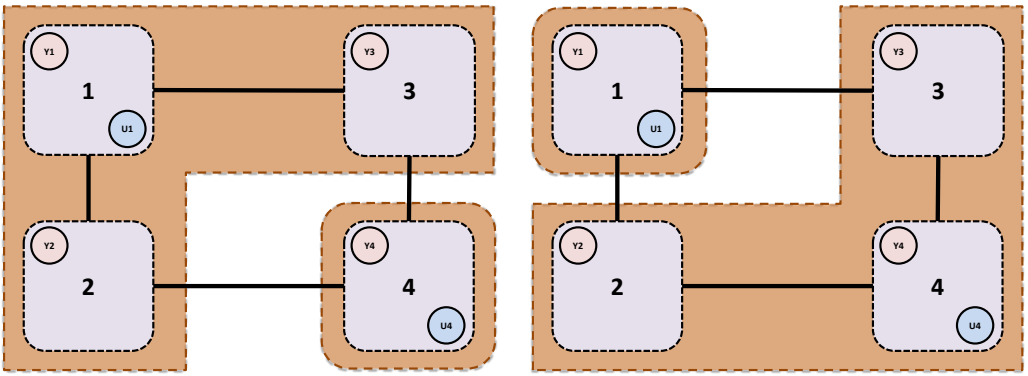

(c) Partition $\mathcal{P}_3$ (d) Partition $\mathcal{P}_4$

Figure 4.4: Partition of the Building Map $G_R(\mathcal{S})$

These partitions produce non-unique subgraphs of $G(\mathcal{S})$, and split the building model into building input-output reachable zones that can be used for decentralized identification. The easiest way to partition the building according to its reachability is to partition the building map. Alg. 13 partitions the building map $G_R(\mathcal{S})$ into a set of subgraphs $\{\{V_R^k, E_R^k\} : \forall k\}$ that satisfy the conditions in Definition 12. The idea behind this algorithm is to analyze the reachability of all the air-based subsystems and create fairly uniform groups of those air-based subsystems such that each group is connected and input-output reachable. Finally, we can partition the building $\mathcal{S}$ into input-output reachable subsystems.

4.3.3 Zone Partition of Building Dynamics

Using the input-output partition of the building map, we can create partitions of the building digraph that are both input-output reachable and possibly identifiable. We will refer to this process as the *zone partitioning* of the building dynamics $\mathcal{S}$. This leads to the following definition.

Definition 13 (Building Zone Partition). *Let $\{\{V_R^k, E_R^k\} : \forall k\}$ be the input-output partition of the building map $G_R(\mathcal{S})$. Then, $\{\mathcal{S}_k : \forall k\}$ is the zone partition of $\mathcal{S}$ if the digraph of $\mathcal{S}_k$ is $G(\mathcal{S}_k) = \{X_k \cup U_k \cup W_k \cup Y_k, E_k\}$ where*

- $X_k = \bigcup_{i \in V_R^k} X_i^a$
- $U_k = \bigcup_{i \in V_R^k} U_i^a$
- $W_k = \bigcup_{i \in V_R^k} W_i^a$
- $Y_k = \bigcup_{i \in V_R^k} Y_i^a$

- $E_k = \bigcup_{i \in E_R^k} E_i^a$

such that $G(\mathcal{S}_i^a) = \{X_i^a \cup U_i^a \cup W_i^a \cup Y_i^a, E_i^a\}$ *is the digraph of the* i^{th} *air-based subsystem.* ♠

We will use the term *building zone* to refer to an individual system $\mathcal{S}_k$ from the zone partition of the building $\mathcal{S}$. We outline the entire algorithm to partition the building dynamics into a set of non-unique building zones.

Example 7 (Zone Partition of Building Digraph)

Using the partition $\mathcal{P}_1$, we note the zone partition of the building digraph is written as follows.

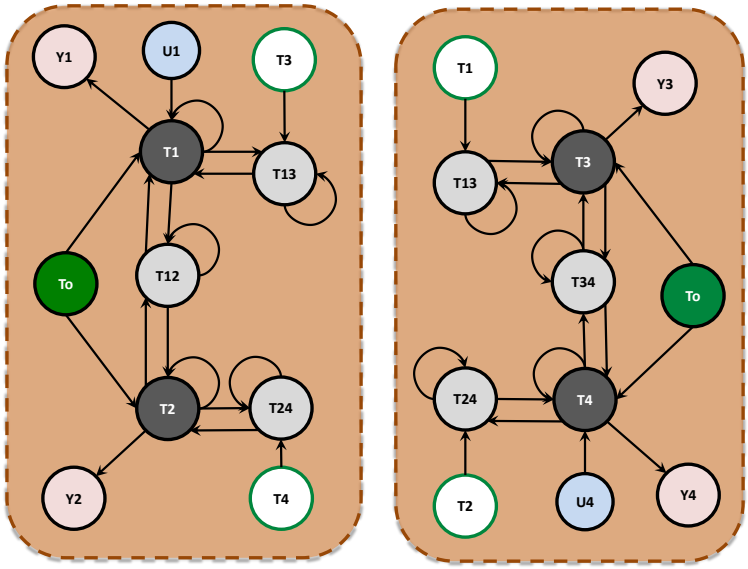

Figure 4.5: Zone Partition of the Building Digraph $G(\mathcal{S})$

4.4 Decentralized Identification Process

In the previous chapter, we note that the current and design-driven identification processes are not scalable for large building models. This is due to the size of the building and the number of parameters to be identified. To overcome this problem, we propose a decentralized approach to identification where the building environment $\mathcal{S}$ is split into input-output reachable building zones that are separately modeled and identified. This condition for input-output reachability imposed on the subsystems of the building environment is important because it guarantees the building input influences every state in the building and every state influences the building output. As a result, parameter changes in the model can be detected in the modeled building output, $\hat{\mathbf{y}}[k]$, which means the model is distinguishable in the output.

This section presents our decentralized identification scheme in the context of building modeling, and is one of the major contributions of this work. In the following subsections, we introduce the notation for modeling a building zone $\mathcal{S}_k$, and we prove that our decentralized approach is equivalent to the whole building identification used in Chapter 3. Furthermore, we observe that the parameter identifiability of the building zone models is related to the identifiability of the overall building model, and we can use the structural and output identifiability of building zone models to determine whether the zone model parameters can be estimated.

4.4.1 Continuous-Time Building Zone Models

Consider the structure of the continuous-time building dynamics $\mathcal{S}$ written in (2.11). Let $M(\theta)$ be the continuous-time model of the building $\mathcal{S}$ where both $\mathcal{S}$ and $M(\theta)$ belong to the same model structure $\mathcal{M}$. Then, we assume the following notation to

describe a subsystem of $M(\theta)$.

$M_i(\theta_i)$	The i^{th} subsystem of $M(\theta) \in \mathcal{M}$
θ_i	$\theta_i \in \mathbb{R}^{q_i}$ is the parameter vector of $M_i(\theta_i)$, and a subvector of $\theta \in \mathbb{R}^q$ where $q_i \leq q$.
$\mathbf{x}_i(t)$	$\mathbf{x}_i(t) \in \mathbb{R}^{n_i}$ is the *state vector* of $M_i(\theta_i)$, and a subvector of $\mathbf{x}(t) \in \mathbb{R}^n$ where $n_i \leq n$.
$\mathbf{u}_i(t)$	$\mathbf{u}_i(t) \in \mathbb{R}^{m_i}$ is the *input vector* of $M_i(\theta_i)$, and a subvector of $\mathbf{u}(t) \in \mathbb{R}^m$ where $m_i \leq m$.
$\mathbf{w}_i(t)$	$\mathbf{w}_i(t) \in \mathbb{R}^{p_i}$ is the *disturbance vector* of $M_i(\theta_i)$, and a subvector of $\mathbf{w}(t) \in \mathbb{R}^p$ where $p_i \leq p$.
$\mathbf{y}_i(t)$	$\mathbf{y}_i(t) \in \mathbb{R}^{o_i}$ is the *output vector* of $M_i(\theta_i)$, and a subvector of $\mathbf{y}(t) \in \mathbb{R}^o$ where $o_i \leq o$.
$A_{c,ii}(\theta_i)$	The submatrix of $A_c(\theta)$ associated to $\mathbf{x}_i(t)$ and $\mathbf{x}_i(t)$.
$A_{c,ij}(\theta_i)$	The submatrix of $A_c(\theta)$ associated to $\mathbf{x}_i(t)$ and $\mathbf{x}_j(t)$.
$B_{c,ii}(\theta_i)$	The submatrix of $B_c(\theta)$ associated to $\mathbf{x}_i(t)$ and $\mathbf{u}_i(t)$.
$B_{c,ij}(\theta_i)$	The submatrix of $B_c(\theta)$ associated to $\mathbf{x}_i(t)$ and $\mathbf{u}_j(t)$.
$G_{c,ii}(\theta_i)$	The submatrix of $G_c(\theta)$ associated to $\mathbf{x}_i(t)$ and $\mathbf{w}_i(t)$.
$G_{c,ij}(\theta_i)$	The submatrix of $G_c(\theta)$ associated to $\mathbf{x}_i(t)$ and $\mathbf{w}_j(t)$.
C_{ii}	The submatrix of C associated to $\mathbf{y}_i(t)$ and $\mathbf{x}_i(t)$.
C_{ij}	The submatrix of C associated to $\mathbf{y}_i(t)$ and $\mathbf{x}_j(t)$.

Then, let the i^{th} subsystem of $M(\theta)$ be,

$$M_i(\theta_i): \begin{aligned} \dot{\mathbf{x}}_i(t) &= A_{c,ii}(\theta_i)\mathbf{x}_i(t) + B_{c,ii}(\theta_i)\mathbf{u}_i(t) + G_{c,ii}(\theta_i)\mathbf{w}_i(t) \\ &\quad + \sum_{i \neq j} A_{c,ij}(\theta_i)\mathbf{x}_j(t) \\ \mathbf{y}_i(t) &= C_{ii}\mathbf{x}_i(t). \end{aligned} \tag{4.9}$$

where $B_{c,ij}(\theta_i) = 0_{n_i \times m_j}$, $G_{c,ij}(\theta_i) = 0_{n_i \times p_j}$, and $C_{ij} = 0_{o_i \times n_j}$ for $i \neq j$. In the prior section, we split the building $\mathcal{S}$ into input-output reachable subsystems, $\mathcal{S}_i$ for $i \in [1, P]$, which are defined as building zones. Then, given $M(\theta)$ models $\mathcal{S}$, we can model the i^{th} building zone $\mathcal{S}_i$ using the i^{th} subsystem of $M(\theta)$. Therefore, we will refer to $M_i(\theta_i)$ as the i^{th} *building zone model*. We can write the set of all zone models $\{M_i(\theta_i) : i \in [1, P]\}$ in the following form,

$$\tilde{M}(\theta): \begin{aligned} \dot{\tilde{\mathbf{x}}}(\mathbf{t}) &= \tilde{A}_c(\theta)\tilde{\mathbf{x}}(t) + \tilde{B}_c(\theta)\tilde{\mathbf{u}}(t) + \tilde{G}_c(\theta)\tilde{\mathbf{w}}(t) \\ \tilde{\mathbf{y}}(t) &= \tilde{C}\tilde{\mathbf{x}}(t) \end{aligned} \tag{4.10}$$

where

$$\tilde{\mathbf{x}}(t) = \begin{bmatrix} \mathbf{x}_1(t) \\ \vdots \\ \mathbf{x}_P(t) \end{bmatrix} \quad \tilde{\mathbf{u}}(t) = \begin{bmatrix} \mathbf{u}_1(t) \\ \vdots \\ \mathbf{u}_P(t) \end{bmatrix} \quad \tilde{\mathbf{w}}(t) = \begin{bmatrix} \mathbf{w}_1(t) \\ \vdots \\ \mathbf{w}_P(t) \end{bmatrix} \quad \tilde{\mathbf{y}}(t) = \begin{bmatrix} \mathbf{y}_1(t) \\ \vdots \\ \mathbf{y}_P(t) \end{bmatrix}$$

$$\tilde{A}_c(\theta) = \begin{bmatrix} A_{c,11}(\theta_1) & \dots & A_{c,1P}(\theta_1) \\ \vdots & \ddots & \vdots \\ A_{c,P1}(\theta_P) & \dots & A_{c,PP}(\theta_P) \end{bmatrix} \quad \tilde{B}_c(\theta) = \begin{bmatrix} B_{c,11}(\theta_1) & \dots & 0_{n_1 \times m_P} \\ \vdots & \ddots & \vdots \\ 0_{n_P \times m_1} & \dots & B_{c,PP}(\theta_P) \end{bmatrix}$$

$$\tilde{G}_c(\theta) = \begin{bmatrix} G_{c,11}(\theta_1) & \dots & 0_{n_1 \times p_P} \\ \vdots & \ddots & \vdots \\ 0_{n_P \times p_1} & \dots & G_{c,PP}(\theta_P) \end{bmatrix} \qquad \tilde{C} = \begin{bmatrix} C_{11}(\theta_1) & \dots & 0_{o_1 \times n_P} \\ \vdots & \ddots & \vdots \\ 0_{o_P \times n_1} & \dots & C_{PP}(\theta_P) \end{bmatrix}.$$

We note that $\tilde{M}(\theta) = M(\theta)$ if any two subsystems $M_i(\theta_i)$ and $M_j(\theta_j)$ are non-overlapping for $i \neq j$. Otherwise, $\tilde{M}(\theta)$ is an expanded form of $M(\theta)$ such that $\mathbf{x}(t)$ is a subvector of $\tilde{\mathbf{x}}(t)$, $\mathbf{u}(t)$ is a subvector of $\tilde{\mathbf{u}}(t)$, $\mathbf{w}(t)$ is a subvector of $\tilde{\mathbf{w}}(t)$, and $\mathbf{y}(t)$ is a subvector of $\tilde{\mathbf{y}}(t)$.

4.4.2 Decentralized Identifiability

This relationship between $M(\theta)$ and $\tilde{M}(\theta)$ is important because it allows us to infer a relationship between the identifiability of the two models. Specifically, we claim the expanded model $\tilde{M}(\theta)$ is identifiable if and only if $M(\theta)$ is also identifiable. In order, to formalize this claim, we consider a more formal definition of the relationship between the building model $M(\theta)$ and the set of zone models written as $\tilde{M}(\theta)$. Siljak uses the terms *restriction*, *aggregation*, and *inclusion* [77] to define this relationship given subsystems might overlap.

Definition 14 (Restriction & Aggregation, [77]). *A model $M(\theta)$ is a restriction of $\tilde{M}(\theta)$ with respect to Im(V) if there exists a full column rank matrix V such that $\tilde{\mathbf{x}} = V\mathbf{x}$. Likewise, $\tilde{M}(\theta)$ is an aggregation of $M(\theta)$ with respect to Im(U) if there exists a full row rank matrix U such that $\mathbf{x} = U\tilde{\mathbf{x}}$.* ♠

Theorem 1 (Inclusion Principle, [77]): *$M(\theta) \subset \tilde{M}(\theta)$ if and only if there exists a model $\bar{M}(\theta)$ such that $M(\theta) \subset \bar{M}(\theta) \subset \tilde{M}(\theta)$ where $\bar{M}(\theta)$ is a restriction of $\tilde{M}(\theta)$ and $\bar{M}(\theta)$ is an aggregation of $M(\theta)$* $\diamondsuit$

Note With an abuse of standard notation, Siljak uses $M(\theta) \subset \tilde{M}(\theta)$ to mean the model $\tilde{M}(\theta)$ includes the model $M(\theta)$.

Theorem 2 formally presents this relationship between the identifiability of a building model and its building zone models, and we prove this claim below.

Theorem 2 (Decentralized Identifiability): *The continuous-time building model $M(\theta)$ is output (structurally) identifiable if and only if every building zone model $M_i(\theta_i)$ is also output (structurally) identifiable for all $i = 1, 2, \ldots, P$.* $\diamondsuit$

PROOF Since output identifiability implies structural identifiability according to Prop. 3, we only need to show that $M_i(\theta_i)$ is output identifiable if and only if all subsystems $\{M_i(\theta_i)\}$ are output identifiable. First, given (4.10), we can write all the subsystems as $\tilde{M}(\theta)$. Let $\mathbf{y}(t)$ be the output of the model $M(\theta)$ and let $\tilde{\mathbf{y}}(t)$ be the output of the model $\tilde{M}(\theta)$. Since $M(\theta)$ is a restriction of $\tilde{M}(\theta)$ and $M(\theta)$ includes itself, then $M(\theta) \subset \tilde{M}(\theta)$. This means there exist matrices $P, \tilde{P}$ such that $\mathbf{y}(t) = \tilde{P}\tilde{\mathbf{y}}(t)$, $\tilde{\mathbf{y}}(t) = P\mathbf{y}(t)$, and $\tilde{P}P = \mathbf{I}$.

Assume the continuous-time version of the output identifiability matrix of $M(\theta)$

in (3.10) is,

$$H_c(\theta, U^T) = \frac{1}{T}\int_0^T \frac{\partial \mathbf{y}(\tau)}{\partial \theta} Q \frac{\partial \mathbf{y}(\tau)}{\partial \theta}^T \partial\tau \tag{4.11}$$

and the continuous-time output identifiability matrix of $\tilde{M}(\theta)$ is

$$\tilde{H}_T(\theta, U^T) = \frac{1}{T}\int_0^T \frac{\partial \tilde{\mathbf{y}}(\tau)}{\partial \theta} Q \frac{\partial \tilde{\mathbf{y}}(\tau)}{\partial \theta}^T \partial\tau \tag{4.12}$$

where the set of continuous-time building inputs is $U^T = \{\mathbf{u}(t), \mathbf{w}(t) : t \in [0, T]\}$. Then, given $\tilde{\mathbf{y}}(t) = P\mathbf{y}(t)$, we can rewrite (4.12) as

$$\tilde{H}_T(\theta, U^T) = P H_c(\theta, U^N) P^T. \tag{4.13}$$

Because P is a full rank column matrix, $rank(\tilde{H}_T(\theta, U^T)) = q$ if $rank(H_T(\theta, U^T)) = q$ which implies $M(\theta)$ is structurally identifiable. Likewise, we can apply $\mathbf{y}(t) = \tilde{P}\tilde{\mathbf{y}}(t)$ to (4.11) to reach the following conclusion,

$$H_T(\theta, U^T) = \tilde{P}\tilde{H}_T(\theta, U^T)\tilde{P}^T, \tag{4.14}$$

where $\tilde{P}$ is a full rank row matrix. Then, $rank(H_T(\theta, U^T)) = q$ if $rank(\tilde{H}_T(\theta, U^T)) = q$, which implies $\tilde{M}(\theta)$ is output identifiable. ■

We also note the following corollary to Theorem 2, which considers discrete-time building models.

Corollary 3: *The discrete-time building model $M_d(\theta)$ is output (structurally) identifiable if and only if every building zone model $M_{d,i}(\theta_i)$ is also output (structurally) identifiable for all $i = 1, 2, \ldots, P$.* ♣

PROOF The proof of this corollary follows directly from the proof of Theorem 2 using the discrete-time output-identifiability matrix $H_N(\theta, U^N)$ in (3.10). ■

Given Theorem 2 and Corollary 3, we can determine the structural and output identifiability of the entire building model by separately testing the structural and output identifiability of each building zone model, $M_i(\theta_i)$. If at least one zone model fails the tests for structural (or output) identifiability, then we know the entire building model cannot be structurally (or output) identifiable.

4.4.3 Decentralized Parameter Estimation

Another outcome of Theorem 2 is that we can solve the identification problem in (3.6) for a large number of parameters θ by applying the identification problem (3.6) to the subset of zone parameters θ_i provided some localized set of data Z_i^N. We propose this decentralized parameter estimation process in Alg. 5.

Algorithm 5 DECENTRALIZED PARAMETER ESTIMATION

A) Partition the model $M(\theta)$ into the set of zone models, $\{M_i(\theta_i) : \forall i\}$

B) Partition the building data Z^N into the set of zone data, $\{Z_i^N : \forall i\}$

C) For all i, discretize $M_i(\theta_i)$ and solve (3.6) for $\hat{\theta}_{i,N}$ given Z_i^N.

D) Merge all $\hat{\theta}_{i,N}$ into a single parameter estimate, $\hat{\theta}_N$

In the last step of this algorithm, estimates of the zone parameters are merged together to form an estimate of the entire set of building parameters. Zone parameters $\hat{\theta}_{i,N}$ may have overlapping parameters with another set of zone parameters. In those cases, the mean of the overlapping estimates are taken and used as the final estimate of that parameter.

4.5 Application: Decentralized Identification of the IW-North Model

This section demonstrates the decentralized identification process for the Intelligent Workplace. The objective of this work is to show that decentralized identification of the IW-North model yields equivalent results as the standard identification process applied to the IW-North model in Section 3.5. The benefit of this decentralized identification process over the standard identification process is that this approach can be scaled up to identify large building models. This section will show that the decentralized identification of the IW-North is efficient and yields results that are equivalent to the results found in Section 3.5. In the following section, we will demonstrate the scalability of this work for a large commercial office building with over 500 parameters.

4.5.1 Initial Conditions & Assumptions

In order to apply the decentralized identification process, the IW-North needs to be split into several zone models that are input-output reachable. In order to determine the reachability of the IW-North we consider the building map of the IW-North shown in Fig. 4.6a. We will also assume the input-output reachable partition of the IW-North building map in Fig. 4.6b, where Partition 1 = $\{1\}$, Partition 2 = $\{2, 4\}$, Partition 3 = $\{3\}$, Partition 4 = $\{5, 6\}$, Partition 5 = $\{7\}$, Partition 6 = $\{8\}$, Partition 7 = $\{9, 10\}$, Partition 8 = $\{11\}$, Partition 9 = $\{12\}$, and Partition 10 = $\{13\}$. Based on Fig. 4.6b, the building model for the IW-North is split into 10 zone models $M_i(\theta_i)$ where the i^{th} zone model is derived from the i^{th} input-output reachable partition of the building map according to Definition 13. Finally, we apply the same identification metrics, initial building conditions, and general building assumptions

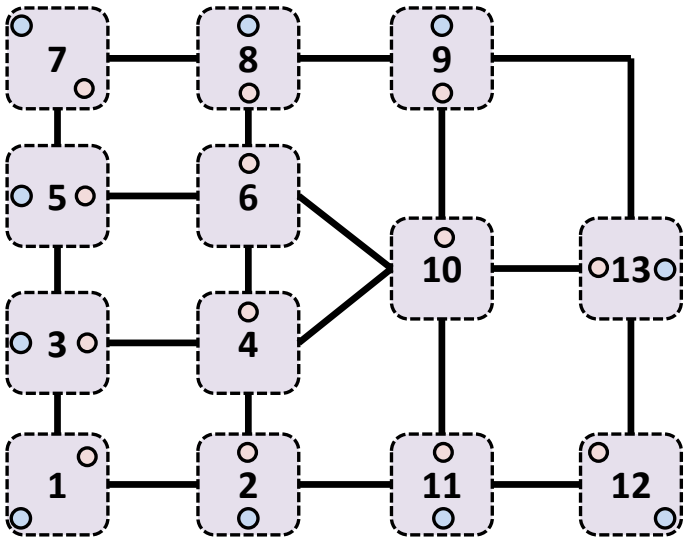

(a) IW-North Building Map

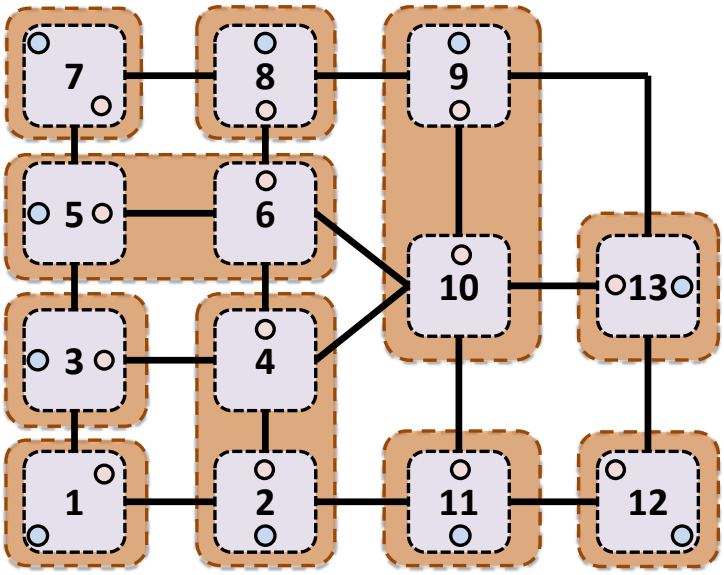

(b) Input-Output Reachable Partition of (a)

Figure 4.6: This figure illustrates the IW-North building map and an input-output reachable partition of the IW-North building map. Each numbered box in (a) refers to the corresponding air-based subsystem of the IW-North, and edges represent interconnections between these subsystems. Note that the controllable building inputs are denoted by small blue circles and the measurable building outputs are denoted by small beige circle. In (b), the orange boxes represent the individual building zones

given in Section 3.5 to the identification scenarios posed here.

4.5.2 Decentralized Standard Identification of the IW-North Model

In this scenario, the standard identification process in Alg. 1 is applied to the IW-North model $M(\theta)$ in combination with the decentralized parameter estimation scheme in Alg. 5. Table 4.3 provides the parameter identifiability results for each zone using the local zone parameter estimate $\hat{\theta}_{i,N}$. In Table 4.3, none of the structural or output identifiability metrics for each zone are full rank. This means the estimated zone models $M_i(\theta_i)$ are neither structurally nor output identifiable. Based on Theorem 2, the identified model $M(\hat{\theta}_N)$ is unidentifiable, which is the same conclusion reached in the centralized identification case shown in Case 1 of Table 3.3.

Table 4.3: Parameter Identifiability of the IW-North Zone Models

	# of θ n_θ	Rank of $\tilde{F}_k(\hat{\theta}_N)$	Rank of $\tilde{H}_N(\hat{\theta}_N, U^N)$
Zone 1	16	7	11
Zone 2	25	16	9
Zone 3	14	8	10
Zone 4	25	17	11
Zone 5	16	8	9
Zone 6	14	8	10
Zone 7	26	19	11
Zone 8	14	8	11
Zone 9	16	7	10
Zone 10	17	9	8

Assuming the set of true parameter values θ_S is known, the metrics in Table 4.4 describe the quality of the estimated zone parameter values $\hat{\theta}_{i,N}$ and the proximity of the zone parameter estimate to the true zone parameter values. Table 4.4 supports the

Table 4.4: Standard Identification of the IW-North Zone Models

	Init. Param. $\bar{\epsilon}_S(\theta_0)$	Estim. Param. $\bar{\epsilon}_S(\hat{\theta}_N)$	Time (sec)	Model Validation $V(\hat{\theta}_N, L^N)$
Zone 1	0.30	0.25	3.12	-
Zone 2	0.30	0.11	6.28	-
Zone 3	0.30	0.26	1.02	-
Zone 4	0.30	0.20	6.65	-
Zone 5	0.30	0.29	2.53	-
Zone 6	0.30	0.17	4.56	-
Zone 7	0.30	0.15	6.06	-
Zone 8	0.30	0.17	3.64	-
Zone 9	0.30	0.28	1.91	-
Zone 10	0.30	0.19	4.33	-
Merged	0.30	0.20	40.11	4.53

observations of Table 4.3, where the estimated mean relative parameter error $\bar{\epsilon}_S(\hat{\theta}_N)$ is significantly close to the initial mean relative parameter values, $\bar{\epsilon}_S(\theta_0) = 0.3$. This means that the estimated zone model parameters $\hat{\theta}_{i,N}$ cannot be accurately identified using the standard identification process with decentralized parameter estimation.

However, we note the decentralized identification approach is more computationally efficient than the standard centralized identification of the IW-North model in the previous chapter. The total time taken for standard identification of the IW-North model is 225 sec, which is an order of magnitude greater than the total time for decentralized identification, which is found to be about 40 sec.

Finally, the last row of Table 4.4 demonstrates the quality of the merged parameter estimate $\hat{\theta}_N$ in comparison to the set of true parameter values θ_S. We note the merged estimate $\hat{\theta}_N$ is not identifiable because the mean relative parameter error is significantly high and results in a high validation error $V(\hat{\theta}_N, L^N) = 4.53$. This supports the conclusion in Table 4.3 that the model is not structurally nor output

identifiable. Furthermore, it supports the original conclusion from the centralized standard identification scenario in Table 3.2.

4.5.3 Decentralized Design-Driven Identification of the IW-North Model

In this scenario, the design-driven identification process in Alg. 2 is applied to the IW-North in combination with the decentralized parameter estimation scheme in Alg. 5 to identify the building model $M(\theta)$. Table 4.5 provides the parameter identifiability results for each zone model $M_i(\hat{\theta}_{i,N})$. We note the structural identifiability metric for each zone model satisfies the rank conditions for structural identifiability in Table 4.5, which means the overall building model is also structurally identifiable. However, the model is not output identifiable for the data set Z^N since the output identifiability metric for each zone model in Table 4.5 does not satisfy the full rank conditions for output identifiability. Because the model is structurally identifiable but not output identifiable, then the data set Z^N is likely the culprit for poor model identification.

Table 4.5: Parameter Identifiability of the IW-North Zone Models

	# of θ q	Rank of $\tilde{F}_k(\hat{\theta}_N)$	Rank of $\tilde{H}_N(\hat{\theta}_N, U^N)$
Zone 1	5	5	5
Zone 2	12	12	10
Zone 3	6	6	6
Zone 4	12	12	6
Zone 5	5	5	5
Zone 6	6	6	5
Zone 7	13	13	8
Zone 8	6	6	4
Zone 9	5	5	5
Zone 10	6	6	5

Table 4.6: Design-Driven Identification of the IW-North Zone Models

	Init. Param. $\bar{\epsilon}_S(\theta_0)$	Estim. Param. $\bar{\epsilon}_S(\hat{\theta}_N)$	Total Time (sec)	Model Validation $V(\hat{\theta}_N, L_N)$
Zone 1	0.30	0.024	1.17	-
Zone 2	0.30	0.068	0.79	-
Zone 3	0.30	0.043	0.50	-
Zone 4	0.30	0.089	0.88	-
Zone 5	0.30	0.022	0.50	-
Zone 6	0.30	0.048	0.55	-
Zone 7	0.30	0.053	0.91	-
Zone 8	0.30	0.034	0.56	-
Zone 9	0.30	0.012	0.66	-
Zone 10	0.30	0.023	1.12	-
Merged	0.30	0.045	8.20	0.0805

Table 4.6 describes the accuracy of the zone model-parameters $\hat{\theta}_{i,N}$ estimated from the design-driven identification process. The mean relative parameter error, denoted as $\bar{\epsilon}_S(\hat{\theta}_N)$, is relatively small in Table 4.6 compared to the values found in Table 4.4. This means that the estimated parameter values do not deviate by much from the true parameter values, and this is reflected in the low validation result, $V(\hat{\theta}_N, L^N) = 0.0805$. Furthermore, we note the time for decentralized design-driven identification is reduced significantly from the standard identification process because of the reduction in parameters. Finally, we observe that the last rows of Table 4.4 yields a similar result to that of Case 2 in Table 3.2.

4.6 Application: Decentralized Identification of an Office Building Model

This section demonstrates the scalability of the decentralized identification process for a large commercial office building. The model for the commercial office building has a total of 543 parameters, which makes it difficult to solve (3.6) quickly and very difficult to create the identifiability metrics $F_k(\theta)$ and $H_N(\theta, U^N)$ quickly. To avoid the computationally taxing process of identifying the entire office building at once, we can split the building into several zones, identify the zone models given local building data, and test the identifiability of each building zone model.

4.6.1 Initial Conditions & Assumptions

This office building has 12 floors and 5 building spaces per floor as shown in 2.5, for a total of 60 open spaces. As noted in Chapter 2, we assume the temperature for each of these open spaces is being thermally measured and the core spaces contain building inputs. This means each floor has exactly one controllable input and 5 measurements, each of the air spaces in the building. Given this configuration, the building map of this large commercial office building shown in Fig. 4.6a is partitioned by floor as shown in Fig. 4.6b. For this commercial building scenario, we will assume the following conditions for identification.

- Let the building data be sampled every 5 minutes, $T_s = 300$ sec, and collected for a period of two weeks, $k \in [0, 8063]$.
- Let $\theta_0(i) = 0.7\theta_S(i)$ and let $0.7\theta_S(i) \leq \theta(i) \leq 1.3\theta_S(i)$ for all $\theta(i) \in \theta$.
- Let the identification data be the first week of building data, $Z^{4032} = \{\mathbf{u}[k], \mathbf{w}[k], \mathbf{y}[k] :$

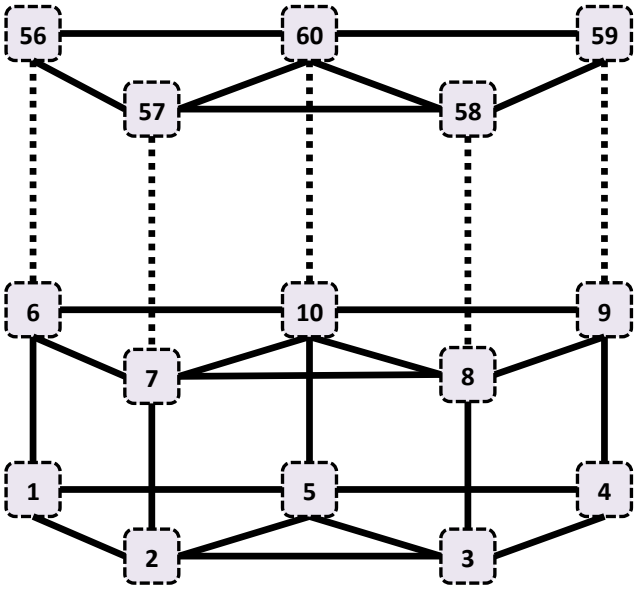

(a) Commercial Office Building Map

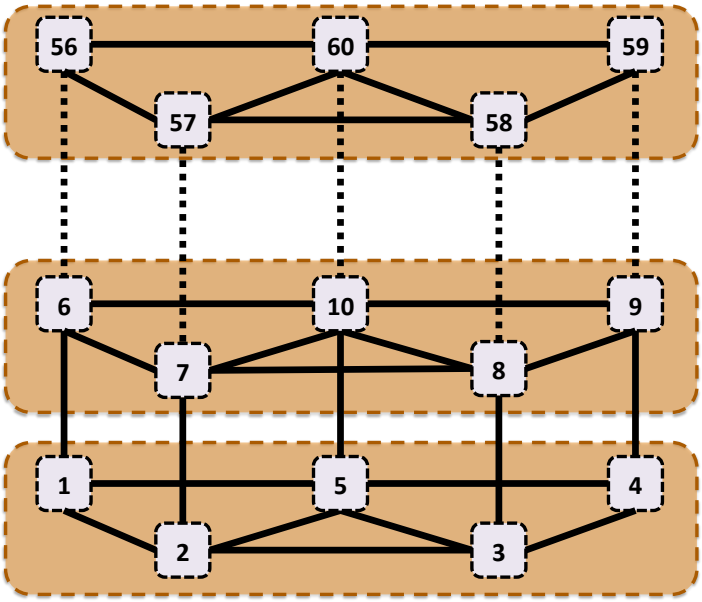

(b) Input-Output Reachable Partition of (a)

Figure 4.7: This figure illustrates the building map of the large office building and an input-output reachable partition of the building map. Each numbered box in (a) refers to the corresponding air-based subsystem of the commercial office building, and edges represent interconnections between these subsystems. Only 3 of the 12 floors are represented in these graphs. All air-based subsystems are measured and there is one controllable heating input per floor, and these inputs are in $\{5, 10, 15, \ldots, 60\}$. In (b), the orange boxes represent the individual building zones

$k \in [0, 4031]\}$ and let the validation data be the second week of building data, $L^{4032} = \{\mathbf{u}[k], \mathbf{w}[k], \mathbf{y}[k] : k \in [4032, 8063]\}$.

- Let $\bar{\mathbf{u}}[k]$ be a PRBS signal where $0W \leq \bar{u}_i[k] \leq 2000W$ for all i and for all $m \in [0, 1, \ldots]$.

- For sampling period $T_m = 3600$ sec (or 1 hr), let $\bar{T}_o[m]$ be given in Table 2.4 for all $m \in [0, \infty)$. Then, let $T_o[k] = \bar{T}_o[m]$ for $m \leq \frac{T_s}{T_m}k < m + 1$ and for all k.

- For sampling period $T_m = 600$ sec (or 10 min), let $\dot{q}_i[m] \sim \mathcal{N}(70W, 10^2W)$ for all $i \in [1, 60]$ and for all $m \in [0, 1, \ldots]$. Then, let $\dot{q}_i[k] = \dot{q}_i[m]$ for $m \leq \frac{T_s}{T_m}k < m+1$ and for all k.

- Let $y_i[k]$ be the i^{th} building output with measurement error, $e_i[k] \sim \mathcal{N}(0, 0.1^{2\circ}K)$ for all $i \in [1, 60]$.

Finally, we will assume the same identification metrics given in Section 3.5 to the identification scenarios posed here.

4.6.2 Decentralized Standard Identification of an Office Building Model

In this scenario, we apply the standard identification process in Alg. 1 with the decentralized parameter estimation scheme in Alg. 5 to the model of the office building, $M(\theta)$. Table 4.7 provides the parameter identifiability results for each zone and assumes no knowledge of θ_S. According to Table 4.7, all of the estimated zone models do not meet the rank conditions for structural and output identifiability, which means the overall model of the commercial building is neither structurally identifiable nor output identifiable given the model and the data set.

Table 4.7: Parameter Identifiability of Office Building Zone Models

	# of θ q	Rank of $\tilde{F}_k(\hat{\theta}_N)$	Rank of $\tilde{H}_N(\hat{\theta}_N, U^N)$
Zone 1	59	50	30
Zone 2	59	45	30
Zone 3	59	45	29
Zone 4	59	45	30
Zone 5	59	45	26
Zone 6	59	45	29
Zone 7	59	45	26
Zone 8	59	45	20
Zone 9	59	45	29
Zone 10	59	45	30
Zone 11	59	46	30
Zone 12	59	46	29

Table 4.8: Standard Identification of Office Building Zone Models

	Init. Param. $\bar{\epsilon}_S(\theta_0)$	Estim. Param. $\bar{\epsilon}_S(\hat{\theta}_N)$	Time (sec)	Model Validation $V(\hat{\theta}_N, L_N)$
Zone 1	0.30	0.25	21.46	-
Zone 2	0.30	0.25	21.90	-
Zone 3	0.30	0.28	20.83	-
Zone 4	0.30	0.29	21.63	-
Zone 5	0.30	0.29	21.51	-
Zone 6	0.30	0.28	22.40	-
Zone 7	0.30	0.26	21.69	-
Zone 8	0.30	0.29	23.79	-
Zone 9	0.30	0.29	22.71	-
Zone 10	0.30	0.27	21.88	-
Zone 11	0.30	0.24	22.90	-
Zone 12	0.30	0.26	20.80	-
Merged	0.30	0.25	263.5	3.7

This conclusion is supported by the identification metrics in Table 4.8, which describes the accuracy of the estimated zone model parameters $\hat{\theta}_{i,N}$. We observe

nearly all the parameters in the zones cannot be identified. Furthermore the mean relative parameter error is significantly high, which means the estimated parameter $\hat{\theta}_N$ deviates significantly from the true parameter value θ_S.

4.6.3 Decentralized Design-Driven Identification of an Office Building Model

In this last scenario, we apply the design-driven identification process in Alg. 2 in combination with the decentralized parameter estimation scheme in Alg. 5 to identify the building model $M(\theta)$. The identifiability results in Table 4.10 and the identification results in Table 4.9 demonstrate little improvement to results of the decentralized standard identification process in Table 4.8 and Table 4.7.

Table 4.9: Design-Driven Identification of Large Office Zone Models

	Init. Param. $\bar{\epsilon}_S(\theta_0)$	Estim. Param. $\bar{\epsilon}_S(\hat{\theta}_N)$	Time (sec)	Model Validation $V(\hat{\theta}_N, L_N)$
Zone 1	0.30	0.28	7.83	-
Zone 2	0.30	0.27	15.59	-
Zone 3	0.30	0.27	15.56	-
Zone 4	0.30	0.28	16.30	-
Zone 5	0.30	0.26	15.58	-
Zone 6	0.30	0.28	15.83	-
Zone 7	0.30	0.24	15.34	-
Zone 8	0.30	0.24	15.99	-
Zone 9	0.30	0.27	15.79	-
Zone 10	0.30	0.27	14.72	-
Zone 11	0.30	0.27	15.09	-
Zone 12	0.30	0.23	11.30	-
Merged	0.30	0.25	174.92	0.13

This example highlights a limitation in our current identification approach to this particular building configuration. With only one controllable heating input signal per

Table 4.10: Parameter Identifiabilty of Office Building Zone Model

	# of θ q	Rank of $\tilde{F}_k(\hat{\theta}_N)$	Rank of $\tilde{H}_N(\hat{\theta}_N, U^N)$
Zone 1	33	32	22
Zone 2	41	36	10
Zone 3	41	36	22
Zone 4	41	36	21
Zone 5	41	36	24
Zone 6	41	36	21
Zone 7	41	36	24
Zone 8	41	36	19
Zone 9	41	36	15
Zone 10	41	36	20
Zone 11	41	36	19
Zone 12	33	32	22

floor, it is very difficult to accurately distinguish between all parameters in the zone model unless the parameters are all aggregated together in a single resistance and capacitance. Aside from changing the model completely, one of the simple ways to improve the identifiability of this scenario is to increase the number of controllable heating inputs per floor.

4.7 Summary

Given the building model identification process in Chapter 3 is not scalable for large models, we are interested in answering following questions:

- *How do we partition the decentralized identification problem into smaller problems?*
- *How do we guarantee the decentralized approach yields equivalent results to the centralized identification approach?*

This chapter addresses each of these questions and makes the following contributions,

1. We apply a graph theoretic framework to building dynamics, and introduce novel concepts such as *air-based building subsystems* and *building maps* to analyze the input-output reachability of the building dynamics. Furthermore, we develop graph partitioning algorithms found in Appendix B to partition the building into input-output reachable subsystems.
2. We define the notion of *building zones* and demonstrate a link between the identifiability of building zone models and whole building models in Theorem 2 and Corollary 3. Based on this relationship, we propose a decentralized parameter estimation scheme in Alg. 5.
3. We demonstrate the process of decentralized identification for the IW-North and a large commercial office building.

Chapter 5

Robust Control of Building Environments

Building control systems can be broadly divided into two categories: *local equipment control* and *supervisory control*. At the equipment level, local building controllers regulate building HVAC equipment such as air handling units, radiators, VAV boxes, chillers, etc. to meet certain building conditioning tasks. Often, these equipments are packaged with a standard controller, but these controllers may need to be tuned or coordinated with other competing factors and equipment in the building. There has been much research to create additional control systems to incrementally improve the equipment energy efficiency and performance [9, 51, 62].

The other category for building control systems is supervisory control, which act as the brain behind building control strategies. The job of supervisory building controller is twofold. First, a supervisory building controller defines high level tasks such as heating or cooling a building space based on external building conditions. Second, the supervisory controller must coordinate local equipment level tasks to meet the

high level conditioning tasks. Examples of building supervisory controllers include building automation systems and energy management controllers, which are used to maintain comfort throughout the entire building, as well as reduce energy consumption. Wang classifies the several types of supervisory building controllers [84]. In recent years, model-based supervisory control has been of particular interest to the building community because of the large potential for energy savings [59, 70].

One of the challenging aspects to model-based supervisory building control is the need for accurate building models, that approximately describe the building dynamics. In Chapters 3 and 4, we address the question of improving the accuracy of ill-conditioned building models. This chapter tackles the problem of using uncertain building models for building control. Furthermore, we focus on model predictive control (MPC) because it has been at the center of so much research to reduce building energy consumption [37, 38, 84], but has gained little traction in the building industry because of the costs associated with developing an accurate building model.

The problem of using uncertain models for control is known in the literature as H_∞ control [5, 6, 58]. The main idea behind H_∞ control is the ability to control a system given the worst-case model uncertainty subject to a robustness factor, γ. Therefore, the robust H_∞ controller can be framed as a minimax MPC problem [6, 12, 56, 66] where the control input is chosen to mitigate the impact of the worst-case building performance due to model uncertainty. Examples of robust H_∞ control applied to building systems can be found in [49, 63]. Kim highlights two potential drawbacks of a robust control approach: increased computation to solve the robust control problem and excessive conservativeness of controller performance[49].

This chapter deals with the latter issue of controller conservativeness by tuning the robustness factor γ. In the following sections, we present the robust control framework in the context of building dynamics and frame the problem of reducing

the conservativeness of the robust building control strategy. Finally, we demonstrate improvements to the baseline control strategies of using uncertain building models.

5.1 Building Control Assumptions and Notations

We first define some of the operational notation made in this chapter.

$\|\mathbf{v}\|_P$	$\|\|\mathbf{v}\|\|_P = \sqrt{\mathbf{v}^T P \mathbf{v}}$ for matrix $P = P^T$ and vector $\mathbf{a}$.
$\|\mathbf{v}\|$	$\|\mathbf{v}\| = \|\mathbf{a}\|_I$ where I is an identity matrix.
$\|M\|$	$\|M\| = \max_{\|\mathbf{v}\|\neq 0} \frac{\|M\mathbf{v}\|}{\|\mathbf{v}\|} = \sqrt{\sigma_{max}(M)}$ where $\sigma_{max}(M)$ is the largest singular value of matrix M
$\|V\|_{[t_o,t_f]}$	$\|V\|_{[t_o,t_f]} = \sqrt{\sum_{k=t_o}^{t_f} \mathbf{v}[k]^T \mathbf{v}[k]}$ for the set, $V = \{\mathbf{v}[k] : k \in [t_o, t_f]\}$

Consider the following variation on the discrete-time system of building dynamics $\mathcal{S}_d$ found in (2.12),

$$\mathcal{S}_\Delta : \quad \mathbf{T}[k+1] = A\mathbf{T}[k] + B\mathbf{u}[k] + G\mathbf{w}[k] + G_\Delta \delta[k] \tag{5.1a}$$

$$\tilde{y}[k] = \tilde{C}\mathbf{T}[k] + \tilde{e}[k] \tag{5.1b}$$

$$\mathbf{z}[k] = \begin{bmatrix} H\mathbf{T}[k] \\ \mathbf{u}[k] \end{bmatrix} \tag{5.1c}$$

where $A = A_d(\theta) \in \mathbb{R}^{n\times n}$, $B = B_d(\theta) \in \mathbb{R}^{n\times m}$, $G = G_d(\theta) \in \mathbb{R}^{n\times p}$. Then, we make the following assumptions about $\mathcal{S}_\Delta$ presented in (5.1)

A1) The system $\mathcal{S}_\Delta$ is equivalent to $\mathcal{S}_d$ for all parameter values $\theta \in \mathbb{R}^q$.

A2) Let the deviation between the system matrices in $\mathcal{S}_\Delta$ and $\mathcal{S}$ be defined as

$$\Delta_A = A_d(\theta_S) - A \tag{5.2}$$

$$\Delta_B = B_d(\theta_S) - B \tag{5.3}$$

$$\Delta_G = G_d(\theta_S) - G. \tag{5.4}$$

We will assume that these matrix deviations are both unknown and bounded, such that $\|\Delta_A\| \leq k_a$, $\|\Delta_B\| \leq k_b$, and $\|\Delta_G\| \leq k_c$.

A3) Since $\mathcal{S}_\Delta$ is equivalent to $\mathcal{S}_d$ in **A1)**, the uncertainty in the state vector due to the matrix deviations Δ_A, Δ_B, and Δ_G is the vector

$$\delta[k] = \Delta_A \mathbf{T}[k] + \Delta_B \mathbf{u}[k] + \Delta_G \mathbf{w}[k] \in \mathbb{R}^{n\times 1}. \tag{5.5}$$

where the matrix deviations are unknown and bounded according to **A2)**. We also assume $\delta[k]$ is unknown and bounded by the building performance $\mathbf{z}[k]$, such that

$$\|\delta[k]\| \leq d\|\mathbf{z}[k]\| \tag{5.6}$$

for all k and for $d > 0$. For the special case $\theta = \theta_S$, $\delta[k] = \mathbf{0}_{n\times 1}$. We note the scaling factor for the state uncertainty is assumed to be $G_\Delta = I_{n\times n}$.

A4) The measured building output $\tilde{y}[k] \in \mathbb{R}^1$ denotes the weighted average of the building air temperatures $\mathbf{T}_a[k] \in \mathbb{R}^a$, and the scalar variable $\tilde{e}[k] \in \mathbb{R}^1$ denotes the averaged measurement error. The output matrix $\tilde{C}$ is

$$\tilde{C} = \begin{bmatrix} c_1 & \dots & c_a & \mathbf{0}_{1\times n-a} \end{bmatrix} \in \mathbb{R}^{1\times n} \tag{5.7}$$

where c_i is the weight on the i^{th} air temperatures and $\sum_{i=1}^{a} c_i = 1$ and $c_i > 0$ for all $i \in [1, a]$.

A5) We assume the matrix $H = I_{n\times n}$ and the pair (H, A) is detectable. Furthermore, we assume the vector $\mathbf{z}[k] \in \mathbb{R}^{n+m}$ represent the performance of the building at time k, and the sequence $Z = \{\mathbf{z}[k] : \forall k\}$ represents *the building performance* for all time k.

Given the the building assumptions in **A1) - A5)**, let the predictive model of the building dynamics in (5.1) be,

$$M(\theta): \qquad \bar{\mathbf{x}}[n+1] = A\bar{\mathbf{x}}[n] + B\bar{\mathbf{u}}[n] + G\bar{\mathbf{w}}[n] + G_{\Delta}\bar{\delta}[n] \tag{5.8a}$$

$$\bar{y}[n] = \tilde{C}\bar{\mathbf{x}}[n] \tag{5.8b}$$

$$\bar{\mathbf{z}}[n] = \begin{bmatrix} H\bar{\mathbf{x}}[n] \\ \bar{\mathbf{u}}[n] \end{bmatrix} \tag{5.8c}$$

where

n	The index n represents a discrete times step at present or future time such that $n \geq k$.
$\bar{\mathbf{x}}[n]$	The *predicted building state vector* at future time n.
$\bar{\mathbf{u}}[n]$	The *predicted building input vector* at future time n.
$\bar{\mathbf{w}}[n]$	The *predicted building disturbance vector* at future time n.
$\bar{\delta}[n]$	The *predicted state uncertainty* at future time n.
$\bar{y}[n]$	The average predicted building air temperatures at future time n.
$\bar{\mathbf{z}}[n]$	The *predicted building performance vector* at future time n.

5.2 Model Predictive Control Problem

In this section, we review the model-predictive control problem in the context of building environments. Consider the real-time building dynamics $\mathcal{S}_\Delta$ in (5.1) and the predictive building model $M(\theta)$ in (5.8) that predicts the state of the building over the future time horizon $n \in [k, k+n_p]$. Then, we assume the following:

- The index n_p is the length of the control and prediction horizon.
- The initial predicted state of the building at time k is $\bar{\mathbf{x}}[k] = \mathbf{T}[k]$.
- The predicted building disturbances $\bar{\mathbf{w}}[n]$ are assumed to be $\bar{\mathbf{w}}[n] = \mathbf{w}[k]$.
- The future constraints on the building control inputs $\mathbf{u}_{min}[n]$ and $\mathbf{u}_{max}[n]$ are known for all time n.
- The future building temperature setpoint $y_{set}[n]$ is known for all time n.
- The sequence of predicted state uncertainties $\bar{\Delta}_k = \{\bar{\delta}[n] : \forall n \in [k, k+n_p]\}$ is known for all time n.

Given these assumptions, consider the following finite-horizon control problem,

$\mathcal{C}_U(k, k+n_p; \mathbf{T}[k], \mathbf{w}[k], \bar{\Delta}_k)$:

$$\min_{\bar{U}_k} \quad \sum_{n=k}^{k+n_p} ||y_{set}[n] - \tilde{C}\bar{\mathbf{x}}[n]||_Q^2 + \sum_{n=k}^{k+n_p-1} ||\bar{\mathbf{u}}[n]||_R^2 \tag{5.9a}$$

$$\text{s.t.} \quad \bar{\mathbf{x}}[n+1] = A\bar{\mathbf{x}}[n] + B\bar{\mathbf{u}}[n] + G\bar{\mathbf{w}}[n] + G_\Delta\bar{\delta}[n], \qquad \forall n \tag{5.9b}$$

$$\mathbf{u}_{min}[n] \leq \bar{\mathbf{u}}[n] \leq \mathbf{u}_{max}[n], \qquad \forall n \tag{5.9c}$$

$$\bar{\mathbf{x}}[k] = \mathbf{T}[k], \quad \bar{\mathbf{u}}[n] \in \bar{U}_k, \quad \bar{\mathbf{w}}[n] = \mathbf{w}[k], \quad \bar{\delta}[n] \in \bar{\Delta}_k \qquad \forall n \tag{5.9d}$$

where $\bar{U}_k = \{\bar{\mathbf{u}}[n] : n \in [k, k+n_p]\}$ is a sequence of predicted building control inputs, $Q = Q^T > 0$, and $R = R^T > 0$. Let $\bar{U}_k^*$ be the solution to (5.9), where $\bar{U}_k^* = \mathcal{C}_U(k, k+n_p; \mathbf{T}[k], \mathbf{w}[k], \bar{\Delta}_k)$. Then, the building controller $\mathbf{u}[k]$ is a *model predictive controller* if $\mathbf{u}[k] = \bar{\mathbf{u}}[k]^*$ for $\bar{\mathbf{u}}[k]^* \in \bar{U}_k^*$ where $\bar{U}_k^* = \mathcal{C}_U(k, k+n_p; \mathbf{T}[k], \mathbf{w}[k], \bar{\Delta}_k)$ is computed every time step k. Alg. 6 summarizes the model-predictive building control policy.

Algorithm 6 Model Predictive Building Control Policy

1. Solve (5.9) for $\bar{U}_k^* = \mathcal{C}_U(k, k+n_p; \mathbf{T}[k], \mathbf{w}[k], \bar{\Delta}_k)$.
2. Apply $\mathbf{u}[k] = \bar{\mathbf{u}}[k]^*$ where $\bar{\mathbf{u}}[k]^* \in \bar{U}_k^*$.
3. Repeat Steps 1-2 for $k = k+1$.

It is important to note the sequence of predicted control inputs $\bar{U}_k^*$ minimizes the predicted costs of the building given in (5.9a). Although there are many important factors to consider in the building costs, the two major factors that we consider in (5.9) are *the predicted temperature setpoint error* denoted as $\bar{e}[n] = y_{set}[n] - \tilde{C}\bar{\mathbf{x}}[n]$, and *the predicted input energy* over the future time horizon $n \in [k, k+n_p]$. The setpoint error $\bar{e}[n]$ is a good predictor of the future thermal comfort to the occupants in the building because large predicted deviations from the setpoint temperature imply an uncomfortable building environment for building occupants while smaller deviations imply a more comfortable environment. The second factor is a measure of the predicted energy of the thermal inputs $\mathbf{u}[n]$, which is often related to the amount of money spent on building energy. Consequently, when this sequence $\bar{U}^*$ is applied to the real building, the actual building setpoint error and the amount of energy exerted to achieve setpoint regulation are minimized over the time horizon $[k, k+n_p]$. Example 8 demonstrates this control approach in a small-scale building environment.

Example 8 (Small Scale Building Case with MPC)

Consider the small scale building example in Appendix A.2. Let the dynamics of the building be the discrete-time system, $\mathcal{S}_d$ in (5.1) for sampling period $T_s = 5$ min. Furthermore, let the model of the building dynamics be $M(\theta_0)$ in (5.8) for some parameter value θ_0. Suppose a model predictive control policy with a prediction (and control) horizon of $n_p = 6$ time steps (or 30 min) is applied to the building over a period of $k \in [0, 288]$ (or 24 hrs). Then, let the building temperature setpoint be

$$y_{set}[k] = \begin{cases} 295K & \text{for } k \in [1, 96] \\ 297K & \text{for } k \in [97, 192] \\ 293K & \text{for } k \in [193, 288]. \end{cases} \tag{5.10}$$

We assume $0W \leq u_1[k] \leq 2000W$ and $0W \leq u_4[k] \leq 2000W$, $T_o[k] = 275K$ for all k, and $\dot{q}_i[k] = 500W$ for all $i \in [1, 4]$ and for all k. Finally, let the initial building temperature $\mathbf{T}[0]$ be known. Given these assumptions, we apply an MPC controller for the following cases, and we plot the result of these control scenarios in Fig. 5.1.

Case 1: Assume the building model is equivalent to the true building dynamics, $M(\theta_0) \overset{M}{=} \mathcal{S}_d$ where $\theta_0(i) = \theta_S(i)$ for all $\theta(i) \in \theta$ such that the true state uncertainty is $\delta[k] = \mathbf{0}$. Assume the predicted state uncertainty is $\bar{\delta}[n] = \mathbf{0}$ for all n.

Case 2: Assume the building model is not equivalent to the true building dynamics, $M(\theta_0) \neq \mathcal{S}_d$ where $\theta_0(i) = .7\theta_S(i)$ for all $\theta(i) \in \theta$ such that the state uncertainty $\delta[k] \neq \mathbf{0}$. Assume the predicted state uncertainty is $\bar{\delta}[n] = \mathbf{0}$ for all n.

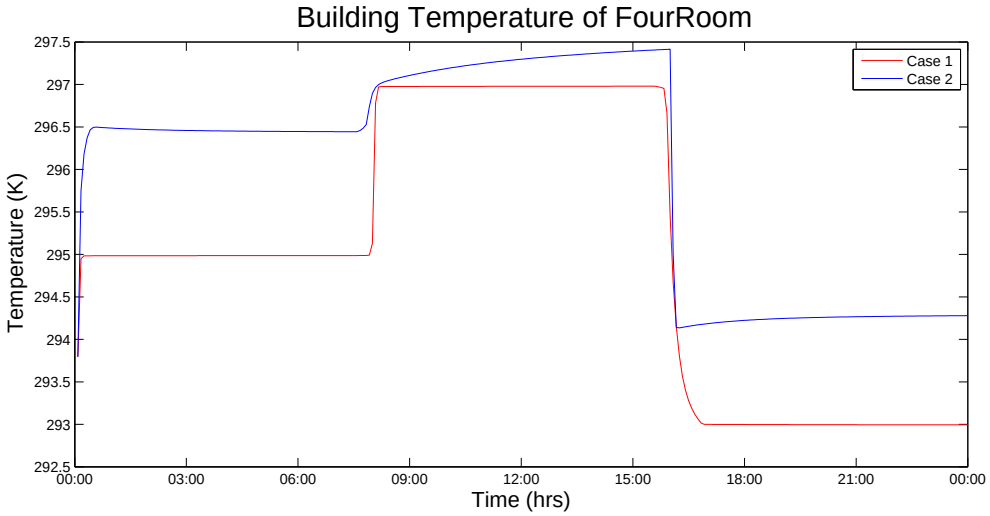

(a) The building output for $\delta[k] = \mathbf{0}$

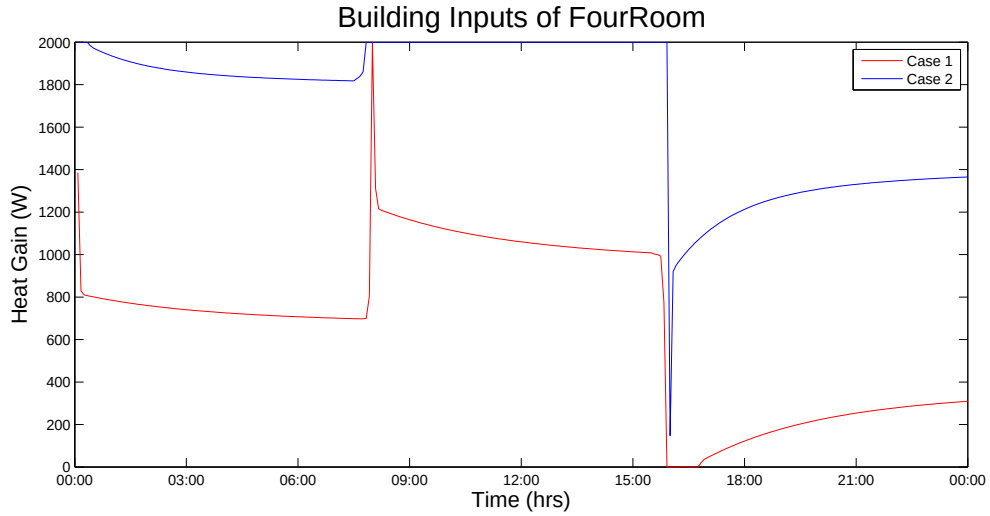

(b) The controllable building input $\mathbf{u}[k]$ for $\delta[k] = \mathbf{0}$

Figure 5.1: The model $M(\theta)$ used for MPC is equivalent to the building dynamics $\mathcal{S}$

Example 8 illustrates the sensitivity of the MPC control policy outlined in Alg. 6 to the predicted state uncertainty. When the true state uncertainty is correctly predicted such that $\bar{\delta}[k] = \delta[k]$, the building output $\mathbf{y}[k]$ achieves the desired setpoint temperature $\mathbf{y}_{set}[k]$ given the control $\mathbf{u}[k]$ as shown in Fig. 5.1a. However, when the predicted state uncertainty differs from the true state uncertainty such that $\bar{\delta}[k] \neq \delta[k]$, the control strategy $\mathbf{u}[k]$ overcompensates for the amount heat needed in the building as shown in Fig. 5.1b. As a result, the building output shown in Fig. 5.1a poorly achieves the desired setpoint temperatures. This example is important because it reflects real control scenarios where the true state uncertainty $\delta[k] \in \Delta$ is unknown. As a result, poorly predicting this uncertainty $\bar{\delta}[k]$ could lead to poor performance. This is one of the major barriers to applying MPC to real building controllers, and motivates our approach to improve the performance of a model predictive building controller given a poor building model. In the following section, we introduce the framework of H_∞ control which will be used in our proposed control strategy to address the challenge of model mismatch.

5.3 H_∞ Control Problem

This section explores the dual problem of both accurately predicting the state uncertainty over time and designing a control strategy that achieves the desired building performance. One class of control strategies that addresses this problem is known as H_∞ control and has been studied extensively in [6, 13, 45, 46, 48, 50, 78, 80]. The objective of this strategy is to predict the worst possible state uncertainty $\bar{\delta}[k]$ and design a control strategy $\mathbf{u}[k]$ that mitigates the impact of the worst possible uncertainty $\bar{\delta}[k]$ on the desired control performance. In the following subsections, we define the worst possible state uncertainty and the summarize the framework for

receding-horizon H_∞ control detailed in [6, 13, 45, 46, 78, 80].

5.3.1 Finite-Horizon H_∞ Controller

Consider the building model $M(\theta)$ used to predict the system of building dynamics $\mathcal{S}_d$ for time $n \in [k, k+n_p]$. Assume the following statements are true:

- Let the sequence of predicted control inputs be $\bar{U}_k = \{\bar{\mathbf{u}}[n] : n \in [k, k+n_p]\}$.
- Let the sequence of predicted state uncertainties be $\bar{\Delta}_k = \{\bar{\delta}[n] : n \in [k, k+n_p]\}$.
- Let the predicted building performance for all time n be $\bar{Z}_k = \{\bar{\mathbf{z}}[n] : n \in [k, k+n_p]\}$ where $\bar{\mathbf{z}}[n]$ is defined in (5.8c).

We observe that the predicted building performance $\bar{Z}_k$ is an implicit function of the initial condition $\bar{\mathbf{x}}[k]$, the predicted inputs $\bar{U}_k$, and the predicted state uncertainties $\bar{\Delta}_k$ according to the recursive state equation in (5.8a). Therefore, we define the gain from $\bar{\Delta}_k$ to $\bar{Z}_k$ as the following function,

$$G_{Z\Delta}(k, k+n_p; \bar{\mathbf{x}}[k], \bar{U}_k, \bar{\Delta}_k) = \frac{\|\bar{Z}_k\|_{[k,k+n_p]}}{\|\bar{\Delta}_k\|_{[k,k+n_p]}}. \tag{5.11}$$

Suppose there exists a sequence of predicted state uncertainties $\bar{\Delta}_k^0$ that varies from $\bar{\Delta}$ such that $\epsilon_\Delta = \|\bar{\Delta}_k^0\|_{[k,k+n_p]} - \|\bar{\Delta}_k\|_{[k,k+n_p]} \neq 0$. Furthermore, let $\bar{Z}_k^0$ be the building performance associated to $\bar{\Delta}_k^0$ given the initial condition $\bar{\mathbf{x}}[k]$ and the sequence of predicted inputs $\bar{U}_k$. If the deviation of the normed performance is $\epsilon_Z = \|\bar{Z}_k^0\|_{[k,k+n_p]} - \|\bar{Z}_k\|_{[k,k+n_p]} \neq 0$ for $\epsilon_\Delta \neq 0$, then we can infer the predicted building performance $\bar{Z}_k$ is sensitive to the predicted state uncertainty $\bar{\Delta}_k$. Moreover, the gain $G_{Z\Delta}(k, k+n_p; \bar{\mathbf{x}}[k], \bar{U}_k, \bar{\Delta}_k)$ in (5.11) is also sensitive to perturbations in $\bar{\Delta}_k$. Given this sensitivity, let the *worst-case state uncertainty* be the sequence $\bar{\Delta}_k^*$ that

maximizes (5.11) for the initial condition $\bar{\mathbf{x}}[k]$ and the predicted input $\bar{U}_k$, such that

$$G_{Z\Delta}(k, k+n_p; \bar{\mathbf{x}}[k], \bar{U}_k, \bar{\Delta}_k^*) \geq G_{Z\Delta}(k, k+n_p; \bar{\mathbf{x}}[k], \bar{U}_k, \bar{\Delta}_k) \tag{5.12}$$

for all possible $\bar{\Delta}_k$. The maximum gain over the finite horizon $n \in [k, k+n_p]$ is explicitly defined in [78, 80, 86] as the following maximization problem,

$$T_{n_p}(\bar{\mathbf{x}}[k], \bar{U}_k) = \sup_{\substack{\bar{\delta}[k] \neq 0 \\ \bar{\delta}[k] \in \bar{\Delta}_k}} \frac{\|\bar{Z}_k\|_{[k,k+n_p]}}{\|\bar{\Delta}_k\|_{[k,k+n_p]}} \tag{5.13}$$

subject to the definition of $\bar{\mathbf{z}}[k] \in \bar{Z}_k$ in terms of $\bar{\mathbf{x}}[k]$, $\bar{\mathbf{u}}[k] \in \bar{U}_k$, and $\bar{\delta}[k] \in \bar{\Delta}_k$. As $n_p \to \infty$, then $T_\infty(\bar{\mathbf{x}}[k], \bar{U}_k)$ approaches the H_∞ norm of the gain $G_{Z\Delta}(k, k+n_p; \bar{\mathbf{x}}[k], \bar{U}_k, \bar{\Delta}_k)$.

Given the worst case gain $T_{n_p}(\bar{\mathbf{x}}[k], \bar{U}_k)$ in (5.13), a *finite-horizon H_∞ controller* chooses the sequence of admissible inputs $\bar{U}_k^*$ over the horizon $n \in [k, k+n_p]$ that minimizes the predicted building performance, $\|\bar{Z}_k\|_{[k,k+n_p]}$, subject to the constraint $T_{n_p}(\bar{\mathbf{x}}[k], \bar{U}_k^*) \leq \gamma$ for the constant $\gamma > 0$. We note that $\bar{U}_k^*$ is admissible if it satisfies designated input constraints, and the admissible controller $\bar{U}_k^*$ is an H_∞ controller if it satisfies the constraint on the worst-case gain. More importantly, $\bar{U}_k^*$ mitigates the impact of the worst-case state uncertainty $\bar{\Delta}_k^*$ on the building performance $\bar{Z}_k^*$.

In [6, 12, 13], the finite-horizon H_∞ control problem over the horizon $n \in [k, k+n_p]$ is posed as the following min-max problem

$\mathcal{C}_\infty(k, k+n_p; \mathbf{T}[k], \mathbf{w}[k], \gamma)$:

$$\min_{\bar{U}_k} \quad \max_{\bar{\Delta}_k} \quad \|H\bar{\mathbf{x}}[k+n_p]\|^2 + \sum_{n=k}^{k+n_p-1} \left(\|\bar{\mathbf{z}}[n]\|^2 - \gamma^2 \|\bar{\delta}[n]\|^2 \right) \tag{5.14a}$$

$$\text{s.t.} \quad \bar{\mathbf{x}}[n+1] = A\bar{\mathbf{x}}[n] + B\bar{\mathbf{u}}[n] + G\bar{\mathbf{w}}[n] + G_\Delta\bar{\delta}[n], \qquad \forall n \tag{5.14b}$$

$$\bar{\mathbf{z}}[n] = \begin{bmatrix} \bar{\mathbf{x}}[n] \\ \bar{\mathbf{u}}[n] \end{bmatrix} \qquad \forall n \qquad (5.14c)$$

$$\bar{\mathbf{x}}[k] = \mathbf{T}[k], \quad \bar{\mathbf{u}}[n] \in \bar{U}_k, \quad \bar{\mathbf{w}}[n] = \mathbf{w}[k], \quad \bar{\delta}[n] \in \bar{\Delta}_k \qquad \forall n \qquad (5.14d)$$

for $n \in [k, k+n_p]$ where the future input constraints $\mathbf{u}_{min}[n]$ and $\mathbf{u}_{max}[n]$ are known for all n. The solution to the min-max problem in (5.24) is denoted as $\{\bar{U}_k^*, \bar{\Delta}_k^*\} = \mathcal{C}_\infty(k, k+n_p; \mathbf{T}[k], \mathbf{w}[k], \gamma)$.

Suppose the H_∞ controller $\bar{U}_k^*$ is applied to the building input $U_k = \bar{U}_k^*$ and Z_k denotes the real-time building performance given $\{U_k, \Delta_k\}$ over the horizon $n \in [k, k+n_p]$. Then, given $\bar{\mathbf{x}}[k] = \mathbf{T}[k]$, we observe the following inequality to be true,

$$G_{Z\Delta}(k, k+n_p; \mathbf{T}[k], U_k, \Delta_k) \quad \leq \quad T_{n_p}(\bar{\mathbf{x}}[k], \bar{U}_k^*) \quad \leq \quad \gamma \qquad (5.15)$$

where $G_{Z\Delta}(k, k+n_p; \mathbf{T}[k], U_k, \Delta_k)$ is the impact of the actual state uncertainty Δ_k on the actual building performance Z_k. This is an important result because it implies an upper bound on the sensitivity of the actual building performance to state uncertainties, $G_{Z\Delta}(k, k+n_p; \mathbf{T}[k], U_k, \Delta_k) \leq \gamma$. Theorem 4 outlines conditions for which (5.15) is true and $G_{Z\Delta}(k, k+n_p; \bar{\mathbf{x}}[k], U_k, \Delta_k) \leq \gamma$.

Theorem 4 (Bounded Real Lemma [45, 46, 78]): *Given the building model $M(\theta)$ in (5.8), let A be a Hurwitz matrix and let the pair (H, A) be detectable. Then, for $\gamma > 0$, the following statements are equivalent:*

1. *$M(\theta)$ is asymptotically stable, and the predicted worst-case gain defined in (5.13) satisfies $T_{n_p}(\bar{\mathbf{x}}[k], \bar{U}_k) \leq \gamma$ given the predicted control input $\bar{U}_k$.*

2. *There exists a sequence of matrices* $P_n = P_n^T > 0$ *that solves the Riccati equation*

$$P_n = A^T P_{n+1} A + H^T H + A^T P_{n+1} G_\Delta M_n^{-1} G_\Delta^T P_{n+1} A \tag{5.16}$$

where $M_n = \gamma^2 I - G_\Delta P_n G_\Delta > 0$. ♢

5.3.2 Receding Horizon H_∞ Control

Using the framework presented above, we now introduce the receding horizon H_∞ control strategy detailed in [6, 13, 47]. Consider the finite-horizon H_∞ control problem posed in (5.24), and let $(\bar{U}_k^*, \bar{\Delta}_k^*)$ represent the min-max solution to that problem. Then, a *receding horizon* H_∞ *controller* solves (5.24) for $\{\bar{U}_k^*, \bar{\Delta}_k^*\}$ at time k, applies the control to the building $\mathbf{u}[k] = \bar{\mathbf{u}}[k]^*$ at time k for $\bar{\mathbf{u}}[k]^* \in \bar{U}_k^*$, and repeats the process for time $k+1$. We outline the receding horizon H_∞ control policy for all time k in Alg. 7.

Algorithm 7 Receding Horizon H_∞ Control

1. Choose $\gamma > 0$.
2. Solve (5.24) for $\{\bar{U}_k^*, \bar{\Delta}_k^*\} = \mathcal{C}_\infty(k, k+n_p; \mathbf{T}[k], \mathbf{w}[k], \gamma)$.
3. Apply $\mathbf{u}[k] = \bar{\mathbf{u}}[k]^*$ where $\bar{\mathbf{u}}[k]^* \in \bar{U}_k^*$.
4. Repeat Steps 2-3 for $k = k+1$.

Given Theorem 4, we note that (5.24) satisfies the condition $T_{n_p}(\mathbf{T}[k], \bar{U}_k^*) < \gamma$ since the solution $(\bar{U}_k^*, \bar{\Delta}_k^*)$ satisfies the Riccati equation given in (5.16). However,

Theorem 4 alone does not prove that the closed-loop gain $G_{Z\Delta}(k, k+n_p; \mathbf{T}[k], U, \Delta)$ is upper bounded given the receding horizon control strategy, $U = \{\mathbf{u}[k] : \forall k\}$. Therefore, we introduce Theorem 5, which claims the impact of Δ on the closed-loop building performance, $Z = \{\mathbf{z}[k] : \forall k\}$ is bounded where $\mathbf{z}[k]$ is defined in (5.1c). To prove this claim, we first present Lemma 2 and Lemma 3 taken from [12, 13].

Lemma 2 ([12, 13]): *Given $(\bar{U}_k^*, \bar{\Delta}_k^*)$ is the solution to* (5.24) *for $\gamma > 0$, let the optimal predicted cost over the horizon $n \in [k, k+n_p)$ be*

$$S(k, k+n_p) = \|H\bar{\mathbf{x}}[k+n_p]^*\|^2 + \sum_{n=k}^{k+n_p-1} \left(\|\bar{\mathbf{z}}[n]^*\|^2 - \gamma^2 \|\bar{\delta}[n]^*\|^2 \right) \tag{5.17}$$

where $\bar{\delta}[n]^* \in \bar{\Delta}_k^*$, and the vectors $\bar{\mathbf{z}}[n]^*$, $\bar{\mathbf{x}}[n]^*$ are functions of $\bar{\mathbf{x}}[k]$, $\bar{U}_k^*$, and $\bar{\Delta}_k^*$ according to (5.24b) *and* (5.24c). *Then, $S(k, k+n_p) \geq S(k, k+n_p+1)$.* ♣

Lemma 3 ([12, 13]): *Given $(\bar{U}_k^*, \bar{\Delta}_k^*)$ is the solution to* (5.24) *for $\gamma > 0$, let $S(k, k+n_p)$ be the predicted cost over the horizon $n \in [k, k+n_p]$, as defined in* (5.17). *Furthermore, let $S(k+1, k+n_p+1])$ be the predicted optimal cost over the horizon $[k+1, k+n_p+1]$. Then,*

$$S(k, k+n_p) - S(k+1, k+n_p+1]) \geq \|\mathbf{z}[k]\|^2 - \gamma^2 \|\delta[k]\|^2 \tag{5.18}$$

where $\delta[k] = \bar{\delta}[k]^*$ is the actual state uncertainty at time k and $\mathbf{z}[k] = \bar{\mathbf{z}}[k]^*$ is the actual building performance at time k given $\bar{\mathbf{u}}[k]^*$, as defined in (5.1c). ♣

The complete proofs for Lemmas 2 and 3 are given in Appendix **??**. Lemma 3 ensures that that the actual performance $\mathbf{z}[k]$ and the actual state uncertainty $\delta[k]$ are upper bounded at time k, given the receding horizon H_∞ controller, $\mathbf{u}[k] = \bar{\mathbf{u}}[k]^*$. Based on Lemma 3, we now present Theorem 5 which formally claims the overall

closed-loop building performance $Z = \{\mathbf{z}[k]\}$ and the state uncertainty $\Delta = \{\delta[k]\}$ satisfy the constraint $T_{n_p}(Z, \Delta) < \gamma$.

Theorem 5 (Bounds on Receding Horizon H_∞ Control [12, 13, 47]): *Let $U = \{\mathbf{u}[k] : k \in [0, N]\}$ be a receding horizon H_∞ control strategy as defined in Alg. 7 and let $\Delta = \{\delta[k] : k \in [0, N]\}$ be the true state uncertainty over the horizon $k \in [1, N]$. Furthermore, let $Z = \{\mathbf{z}[k] : k \in [0, N]\}$ be the closed-loop building performance where $\mathbf{z}[k]$ is defined in* (5.1c) *and is a function of U and Δ. Then, for $\gamma > 0$,*

$$\frac{z_0 + \|Z\|^2_{[0,N]}}{\|\Delta\|^2_{[0,N]}} \leq \gamma^2 \tag{5.19}$$

$\diamondsuit$

where $z_0 = S(N, N + n_p) - S(0, n_p)$ and $S(k, k + n_p)$ is the predicted cost over the horizon $n \in [k, k + n_p]$ given in (5.17).

Proof (of Theorem 5) Given Lemma 3, we know that

$$S(k, k + n_p) - S(k + 1, k + n_p + 1) \geq \|\mathbf{z}[k]\|^2 - \gamma^2 \|\delta[k]\|^2. \tag{5.20}$$

We can add (5.20) over the horizon $k \in [0, N]$,

$$\sum_{k=0}^{N} \Big(S(k, k + n_p) - S(k + 1, k + n_p + 1) \Big) \geq \sum_{k=0}^{N} \Big(\|\mathbf{z}[k]\|^2 - \gamma^2 \|\delta[k]\|^2 \Big). \tag{5.21}$$

Then, (5.21) reduces to the following inequality

$$S(0, n_p) - S(N, N + n_p) \geq \sum_{k=0}^{N} \Big(\|\mathbf{z}[k]\|^2 - \gamma^2 \|\delta[k]\|^2 \Big). \tag{5.22}$$

Assuming $z_0 = S(N, N + n_p) - S(0, n_p)$, then (5.22) can be rearranged into the inequality shown in (5.19). ∎

Theorem 5 is important for two reasons. First, it ensures the uncertainty in the building dynamics Δ is bounded by the the building performance Z, which can be measured. Second, it ensures the impact of Δ to the building performance is attenuated by a factor $\gamma > 0$. In the following section, we will merge the standard MPC control policy and the receding horizon H_∞ control policy in order to define a controller that achieves the desired MPC performance and the attenuates the sensitivity of the controller to system uncertainties.

5.4 Robust Supervisory Building Control

In this section, we present a controller $\mathbf{u}[k]$ that solves the MPC problem in (5.9) and the receding-horizon H_∞ control problem in (5.24) at time k. We solve this mixed problem in order to both minimize the standard MPC cost function in (5.9a) and to satisfy the H_∞ condition for closed loop robust performance shown in (5.19).

5.4.1 Robust Model Predictive Control

Let $\bar{U}_k^* = \mathcal{C}_U(k, k+n_p; \mathbf{T}[k], \mathbf{w}[k], \bar{\Delta}_k^*)$ be the model-predictive control problem at time k in (5.9), and let $\mathcal{C}_\infty(k, k + n_p; \mathbf{T}[k], \mathbf{w}[k], \gamma)$ be the receding horizon H_∞ controller

in (5.24). Furthermore, assume

$$\mathcal{C}_\infty(k, k+n_p; \mathbf{T}[k], \mathbf{w}[k], \gamma) = \max_{\bar{U}_k} \quad \mathcal{C}_\Delta(k, k+n_p; \mathbf{T}[k], \mathbf{w}[k], \bar{U}_k, \gamma) \tag{5.23}$$

where

$\mathcal{C}_\Delta(k, k+n_p; \mathbf{T}[k], \mathbf{w}[k], \bar{U}_k, \gamma)$:

$$\max_{\bar{\Delta}_k} \quad \|H\bar{\mathbf{x}}[k+n_p]\|^2 + \sum_{n=k}^{k+n_p-1} \left(\|\bar{\mathbf{z}}[n]\|^2 - \gamma^2 \|\bar{\delta}[n]\|^2 \right) \tag{5.24a}$$

$$\text{s.t.} \quad \bar{\mathbf{x}}[n+1] = A\bar{\mathbf{x}}[n] + B\bar{\mathbf{u}}[n] + G\bar{\mathbf{w}}[n] + G_\Delta\bar{\delta}[n], \qquad \forall n \tag{5.24b}$$

$$\bar{\mathbf{z}}[n] = \begin{bmatrix} H\bar{\mathbf{x}}[n] \\ \bar{\mathbf{u}}[n] \end{bmatrix} \qquad \forall n \tag{5.24c}$$

$$\bar{\mathbf{x}}[k] = \mathbf{T}[k], \quad \bar{\mathbf{u}}[n] \in \bar{U}_k, \quad \bar{\mathbf{w}}[n] = \mathbf{w}[k], \quad \bar{\delta}[n] \in \bar{\Delta}_k \qquad \forall n \tag{5.24d}$$

Then, the *robust model-predictive building controller* at time k is $\mathbf{u}[k] = \bar{\mathbf{u}}[k]^* \in \bar{U}_k^*$ where the set $\{\bar{U}_k^*, \bar{\Delta}_k^*\}$ satisfies the pair of coupled problems

$$\bar{U}_k^* = \mathcal{C}_U(k, k+n_p; \mathbf{T}[k], \mathbf{w}[k], \bar{\Delta}_k^*) \tag{5.25a}$$

$$\bar{\Delta}_k^* = \mathcal{C}_\Delta(k, k+n_p; \mathbf{T}[k], \mathbf{w}[k], \bar{U}_k^*, \gamma) \tag{5.25b}$$

for $\gamma \geq 0$. Then, given $\{\bar{U}_k^*, \bar{\Delta}_k^*\}$, where $\bar{\mathbf{u}}[k]^* \in \bar{U}_k^*$. Alg. 8 outlines the robust MPC strategy for all time k.

5.4.2 Robust MPC with Tuned Disturbance Attenuation

We note the solutions $\{\bar{U}_k^*, \bar{\Delta}_k^*\}$ are unique to the chosen value of $\gamma \geq 0$ because (5.25a) and (5.25b) are strictly convex problems. This means the control input $\mathbf{u}[k] = \mathbf{u}[k]^*$

Algorithm 8 Robust Model Predictive Control Policy

1. Choose $\gamma > 0$.
2. Solve (5.25a) and (5.25b) for $\{\bar{U}_k^*, \bar{\Delta}_k^*\}$.
3. Apply $\mathbf{u}[k] = \bar{\mathbf{u}}[k]^*$ where $\bar{\mathbf{u}}[k]^* \in \bar{U}_k^*$.
4. Repeat Steps 2-3 for $k = k + 1$.

yields a predicted state $\bar{\mathbf{x}}[k+1]$ that underestimates the true building state $\mathbf{T}[k+1]$. Likewise, choosing small values of γ, underestimates the modeling uncertainty of (5.25a) and (5.25b). For very small values of γ, the control problems (5.25a) and (5.25b) may be infeasible and consequently will not converge to a solution, $\{\bar{U}_k^*, \bar{\Delta}_k^*\}$. Therefore, we want to choose a value of $\gamma > 0$ such that (5.25a) and (5.25b) yields a feasible solution of $\bar{\mathbf{u}}[k]^*$ and $\bar{\delta}[k]^*$ for all time k such that the predicted state uncertainty $\bar{\delta}[k]^*$ approximates the true state uncertainty $\delta[k]$. We propose the following tuning method in Alg. 9 to update the value of γ in real-time as the building is being controlled.

Algorithm 9 Robust MPC with Tuned Disturbance Attenuation

1. Choose $\gamma_k > 0$ at time $k = 0$.
2. Solve (5.25a) and (5.25b) for $\{\bar{U}_k^*, \bar{\Delta}_k^*\}$
3. Apply $\mathbf{u}[k] = \bar{\mathbf{u}}[k]^*$ for $\bar{\mathbf{u}}[k]^* \in \bar{U}_k^*$ at time k.
4. Measure the building output $\tilde{y}[k+1]$ at time $k+1$.
5. Compute the output error $\hat{e}[k+1] = \tilde{y}[k+1] - \tilde{C}\bar{\mathbf{x}}[k+1]$ at time $k+1$.
6. Let $\gamma_{k+1} = \gamma_k + \alpha_P \hat{e}[k+1] + \alpha_I \sum_{\tau=1}^{k+1} \hat{e}[\tau]$
7. Repeat Steps 2-6 for $k = k + 1$.

The idea behind this algorithm is to tune the value of γ_k such that the output

error $\hat{e}[k] = \tilde{y}[k] - \tilde{C}\bar{\mathbf{x}}[k]$ is minimized for all time k. It is important to note that the error $e[k]$ also represents the measured error between the true state uncertainty $\delta[k]$ and the estimated state uncertainty $\bar{\delta}[k]$. We note the error Therefore, tuning γ_k to drive the error $e[k]$ to 0 forces the robust MPC strategy in (5.25a) and (5.25b) to tune the pair $\mathbf{u}[k]^* \in \bar{U}_k^*$ and $\bar{\delta}[k]^* \in \bar{\Delta}_k^*$ such that $\bar{\delta}[k]^*$ converges to $\delta[k]$. The update law for γ_k at Step 6 of Alg. 9 introduces this error $\hat{e}[k]$ as feedback into the controller which allows the controller to tune itself over time. We use the coefficients α_P and α_I to control the rate of convergence over time. In the following example, we compare this proposed approach outlined in Alg. 9 to the Robust MPC approach in Alg. 8, and we demonstrate improvements to the control performance.

Example 9 (Robust Control Strategies for Small Scale Building)
Assume the building scenario and Cases 1-2 in Example 8. For this example, we will consider two additional cases given below.

Case 3: Given the scenario $\theta_0(i) = .7\theta_S(i)$ for all $i \in [1, q]$ in Case 2, we apply the Robust MPC strategy in 8 to the small-scale building environment for $\gamma = 14$.

Case 4: Given the scenario $\theta_0(i) = .7\theta_S(i)$ for all $i \in [1, q]$ in Case 2, we apply the Robust MPC-T strategy in Alg. 9 to the small-scale building environment. We assume $\gamma_0 = 14$, $\alpha_P = 2$ and $\alpha_I = 0$.

Fig. 5.2 plots the building temperature and the heating inputs for each case. The motivation for using a robust control strategy is to drive the output error between the nominal MPC strategy in Case 1 and the mismatched MPC strategy in Case 2 to 0. From the plot, we compare these control strategies over time to determine which robust controller best mimics the nominal MPC controller. In this example,

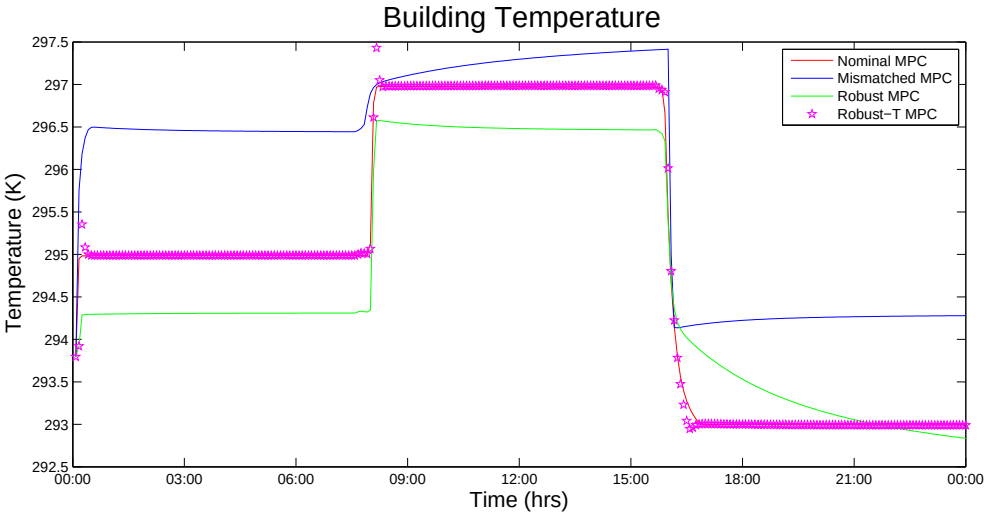

(a) Output Temperatures

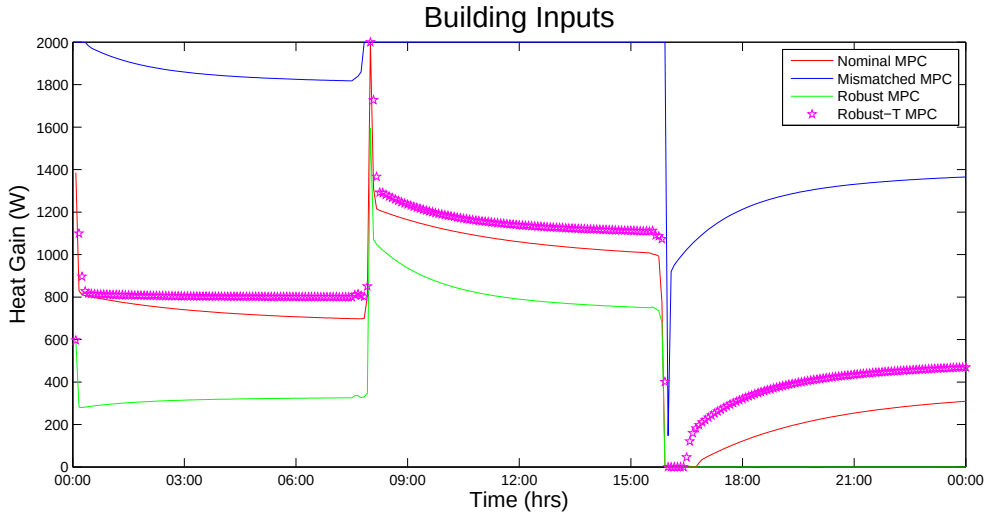

(b) Heat Inputs

Figure 5.2: Comparison of Cases 1-4

we observe the Robust MPC-T performs better than the Robust MPC strategy in terms of driving the building output temperature to the nominal MPC temperature, even though Robust MPC demands less energy that the Robust MPC-T strategy.

5.5 Robust Supervisory Control of Case Study Examples

This section demonstrates both the Robust MPC and Robust MPC-T approaches for the IW-North and office building detailed in Chapter 2. We assume the following building conditions.

5.5.1 Initial Conditions & Assumptions for the IW-North Model

Suppose the building control model of the IW-North is the discrete-time model $M(\theta_0)$ in (5.8) where $\theta_0(i) = 0.7\theta_S(i)$ for all $i \in [1, q]$. Given a sampling period $T_s = 5$, let the building be controlled for a period of one week, $k = [0, 2016]$ using model predictive control and assume a prediction and control horizon of 30 minutes or $n_p = 6$ time steps. We will assume Q is a diagonal matrix of the appropriate size where the diagonal entries are 1×10^8. We will also assume R is a diagonal matrix of the appropriate size where the diagonal entries are 1.

For sampling period $T_m = 3600$ sec (or 1 hr), let the weather $\bar{T}_o[m]$ and the input disturbance $\dot{q}_i[m]$ be given in Table 2.4 for all $m \in [0, 1, \ldots]$ and for all i. Then, let $T_o[k] = \bar{T}_o[m]$ and $\dot{q}_i[k] = \dot{q}_i[m]$ for $m \leq \frac{T_s}{T_m}k < m + 1$ and for all k. Finally, let the input constraints for the IW-North be $0W \leq u_i[k] \leq 4W$ for $i \in [1, 13]$.

5.5.2 Initial Conditions & Assumptions for the Large Office Building

We will also assume the building control model of the office building is the discrete-time model $M(\theta_0)$ in (5.8) where $\theta_0(i) = 0.7\theta_S(i)$ for all $i \in [1, q]$. Given a sampling period $T_s = 5$, let the building be controlled for a period of one week, $k = [0, 2016]$ using model predictive control and assume a prediction and control horizon of 20 minutes or $n_p = 4$ time steps. We will assume Q is a diagonal matrix of the appropriate size where the diagonal entries are 1×10^20, and R is a diagonal matrix of the appropriate size where the diagonal entries are 1. The weather and disturbance constraints are assumed to be the same as the conditions described above for the IW-North. Finally we assume the input constraints for the commercial office building is $0W \leq u_i[k] \leq 50 \times 10^3 W$ for all $i \in [1, 60]$.

5.5.3 Comparison of Control Strategies

Given the initial conditions and assumptions, we consider the following building control scenarios and compare the performance of these control strategies.

Nominal MPC Apply the MPC strategy in Alg. 6 to the building $\mathcal{S}_d$ given the exact building model $M(\theta_S)$

Baseline MPC Apply the MPC strategy in Alg. 6 to the building $\mathcal{S}_d$ given an uncertain building model $M(\theta_0)$.

Robust MPC Apply the Robust MPC strategy in Alg. 8 to the building $\mathcal{S}_d$ given $M(\theta_0)$ and the constant γ_0. For the IW-North, let $\gamma = 10$ for all time. For the commercial office building, let $\gamma = 20$ for all time as well.

Robust MPC-T Apply the Robust MPC scenario given above with the tuning strategy described in Alg. 9, where $\alpha_P = 2$, and $\alpha_I = 0$.

5.5.4 Control Performance Metrics

For this study, we will consider two metrics. The first metric is the mean-squared error between the nominally controlled building temperature $y_{mpc}[k]$ and the building temperature of interest $y[k]$ over all time k, which is computed as

$$Y_{mse} = \frac{1}{N} \sum_{k=0}^{N-1} (y_{mpc}[k] - y[k])^2. \tag{5.26}$$

The second metric is the total heat energy needed to achieve that particular control strategy, denoted as

$$U_{tot} = \sum_{k=0}^{N-1} \left(\sum_{i} u_i[k] \cdot T_s \right) \tag{5.27}$$

where T_s is the sampling period.

5.5.5 Comparison of Control Strategies

Table 5.3 provides a comparison of the different control strategies in the IW-North based on the performance metrics Y_{mse} and U_{tot}. We observe that the Robust MPC with Tuning strategy closely mimics the nominal MPC strategy in the output, and consumes only slightly more energy than the nominal MPC strategy.

Likewise, Table 5.4 provides a comparison of the different control strategies in a large commercial office building based on the performance metrics Y_{mse} and U_{tot}. We note the Robust MPC performance is worse than the baseline MPC performance because γ is not properly chosen. This highlights the importance of tuning the factor

Table 5.3: Comparison Control Strategies in the IW-North

	Y_{mse} (K)	U_{tot} (kWh)
Nominal MPC	0.00	2,500.8
Baseline MPC	1.50	3,823.3
Robust MPC	11.25	213.33
Robust MPC-T	0.02	2,526.7

γ which is demonstrated in the Robust MPC-T strategy. We note that the Robust MPC-T strategy still consumes much more energy than the Nominal MPC strategy, but the strategy also performs better than both the baseline and robust MPC strategy.

Table 5.4: Comparison of Control Strategies in the Office Building

	Y_{mse} (K)	U_{tot} (kWh)
Nominal MPC	0.00	2,250,500
Baseline MPC	2.36	4,022,300
Robust MPC	2.91	678,580
Robust MPC-T	0.55	3,549,800

5.6 Summary

In this chapter, we address the feasibility of model-based control, particularly the challenge of using inaccurate building models for building control. We deal with this challenge in the context of model-predictive building control, which is a growing area of research and concern. We observe in small-scale examples the sensitivity of MPC to poor models, and we work to correct this issue using the framework for receding-horizon H_∞ control. Using these results, we recast the original MPC problem as a min-max problem in order to guarantee the sensitivity of the controller is bounded by a factor γ. The major contribution of this chapter is the improvement of the min-max robust control strategy, where γ is tuned over real-time in order to improve the performance of the robust controller. We demonstrate this proposed strategy mimics the nominal MPC strategy for real building environments and note significant improvements from the baseline and Robust MPC strategies. In the following chapters, we extend this approach to a hierarchical and decentralized supervisory controller.

Chapter 6

Decentralized Robust Control of Building Environments

Chapter 5 proposes a robust model-predictive control strategy to address the challenge of poor supervisory building control. This chapter takes a different approach, and proposes a decentralized and hierarchical supervisory building controller to reduce building energy consumption. Mesarovic lays the framework for hierarchical control in [64, 65], and defines a *hierarchical controller* as a set of decision problems, $\mathcal{C}_H = \{\mathcal{D}_{sup}, \mathcal{D}_{inf}\}$, where $\mathcal{D}_{inf}$ is the set of *infimal decision problems* and $\mathcal{D}_{sup}$ is the set of *supremal decision problems*. Infimal decision problems $D \in \mathcal{D}_{inf}$ control low-level or unique tasks, while supremal decision problems $D \in \mathcal{D}_{sup}$ coordinate infimal decision problems to achieve a higher level task. In the context of building supervisory control, we define zone controllers used to regulate indoor air quality (IAQ) within a building zone as infimal decision problems. The benefit of using zone control in a building is that users are able to locally regulate occupied spaces, and potentially save energy waste from regulating the IAQ of unoccupied building spaces. The challenge of zone

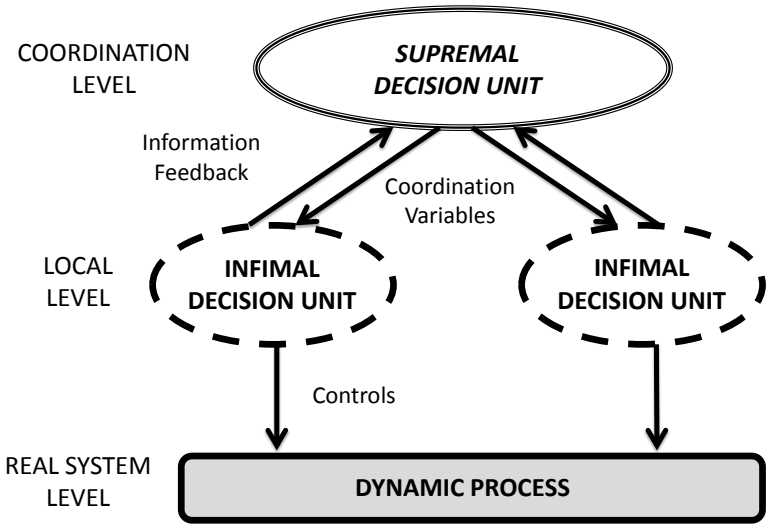

Figure 6.1: Hierarchical Control Structure

control is that building zones are interconnected, dynamic systems, and uncoordinated zone controllers waste more energy than a coordinate system of zone controllers. Therefore, we define a scheme to coordinate the zone controllers to reduce building costs, and we classify this scheme as a supremal decision problem.

6.1 Hierarchical Control Assumptions and Notations

The assumptions and notations in this chapter are a continuation of the assumptions and notations in the previous chapter, Chapter 5. Given the discrete-time building dynamics $\mathcal{S}_\Delta$ in (5.1), let $\mathcal{S}_\Delta$ be written as the interconnection of n_z building zone,

$$\mathcal{S}_\Delta : \quad \mathbf{T}_i[k+1] = A_{ii}\mathbf{T}_i[k] + B_{ii}\mathbf{u}_i[k] + G_{ii}\mathbf{w}_i[k] + A_{ip}\mathbf{p}_i[k] + G_{\Delta,ii}\delta[k] \qquad \forall i \in [1, n_z] \quad (6.1a)$$

$$\mathbf{p}_i[k] = \sum_{j \neq i} \left(E_{x,ij}\mathbf{T}_j[k] + E_{u,ij}\mathbf{u}_j[k] + E_{w,ij}\mathbf{w}_j[k] \right) \quad \forall i \in [1, n_z] \quad (6.1b)$$

$$\tilde{y}_i[k] = \tilde{C}_{ii}\mathbf{T}_i[k] + v_i[k], \quad \forall i \in [1, n_z] \quad (6.1c)$$

where

$\mathbf{T}_i[k]$	$\mathbf{T}_i[k] \in \mathbb{R}^{n_i}$ is the *state vector* of the i^{th} building zone and a subvector of $\mathbf{T}[k] \in \mathbb{R}^n$ where $n_i \leq n$.
$\mathbf{u}_i[k]$	$\mathbf{u}_i[k] \in \mathbb{R}^{m_i}$ is the *input vector* of the i^{th} building zone and a subvector of $\mathbf{u}[k] \in \mathbb{R}^m$ where $m_i \leq m$.
$\mathbf{w}_i[k]$	$\mathbf{w}_i[k] \in \mathbb{R}^{p_i}$ is the *disturbance vector* of the i^{th} building zone and a subvector of $\mathbf{w}[k] \in \mathbb{R}^p$ where $p_i \leq p$.
$\tilde{y}_i[k]$	$\tilde{y}_i[k] \in \mathbb{R}^1$ is the weighted average of the i^{th} building zone air temperatures in $T_i[k]$.
$\mathbf{p}_i[k]$	$\mathbf{p}_i[k] \in \mathbb{R}^{f_i}$ is the *interaction vector* of the i^{th} building zone where $f_i = n + m + p - n_i - m_i - p_i$, and a subvector of $\begin{bmatrix}\mathbf{T}[k]^T & \mathbf{u}[k]^T & \mathbf{w}[k]^T\end{bmatrix}^T \in \mathbb{R}^{n+m+p}$, such that $f_i < n + m + p$.
$E_{x,ij}$	$E_{x,ij} : \mathbf{T}_j[k] \to \mathbf{p}_i[k] \in \mathbb{R}^{f_i \times n_j}$ and the entries of $E_{x,ij}$ are 0 or 1.
$E_{u,ij}$	$E_{u,ij} : \mathbf{u}_j[k] \to \mathbf{p}_i[k] \in \mathbb{R}^{f_i \times m_j}$ and the entries of $E_{u,ij}$ are 0 or 1.
$E_{w,ij}$	$E_{w,ij} : \mathbf{w}_j[k] \to \mathbf{p}_i[k] \in \mathbb{R}^{f_i \times p_j}$ and the entries of $E_{w,ij}$ are 0 or 1.
A_{ii}	The submatrix of $A_d(\theta)$ associated to $\mathbf{T}_i[k]$ and $\mathbf{T}_i[k]$.
A_{ij}	The submatrix of $A_d(\theta)$ associated to $\mathbf{T}_i[k]$ and $\mathbf{T}_j[k]$.
B_{ii}	The submatrix of $B_d(\theta)$ associated to $\mathbf{T}_i[k]$ and $\mathbf{u}_i[k]$.
B_{ij}	The submatrix of $B_d(\theta)$ associated to $\mathbf{T}_i[k]$ and $\mathbf{u}_j[k]$.
G_{ii}	The submatrix of $G_d(\theta)$ associated to $\mathbf{T}_i[k]$ and $\mathbf{w}_i[k]$.
G_{ij}	The submatrix of $G_d(\theta)$ associated to $\mathbf{T}_i[k]$ and $\mathbf{w}_j[k]$.

A_{ip}	$A_{ip} = \sum_{j \neq i} \left(A_{ij} E_{x,ij}^T + B_{ij} E_{u,ij}^T + G_{ij} E_{w,ij}^T \right)$
$G_{\Delta,ii}$	The scaling factor of the state uncertainty is assumed to be $G_{\Delta,i} = I_{n_i \times n_i}$
$\tilde{C}_{ii}$	The output matrix $\tilde{C}_{ii} : \mathbf{T}_i[k] \rightarrow \tilde{y}_i[k] \in \mathbb{R}^{1 \times n_i}$ averages the i^{th} building zone air temperatures, where the entries sum to 1.

Now, consider the discrete-time model $M(\theta)$ of $\mathcal{S}_\Delta$ in (5.8). Then, the decentralized form of the predictive building model $M(\theta)$ in (5.8) is written as follows,

$$
\begin{aligned}
M(\theta): \quad \bar{\mathbf{x}}_i[n+1] &= A_{ii}\bar{\mathbf{x}}_i[n] + B_{ii}\bar{\mathbf{u}}_i[n] + G_{ii}\bar{\mathbf{w}}[n] + A_{ip}\bar{\mathbf{p}}_i[k] \\
&\quad + G_{\Delta,i}\bar{\delta}[n] && \forall i \in [1, n_z] \quad \text{(6.2a)} \\
\bar{\mathbf{p}}_i[k] &= \sum_{j \neq i} \left(E_{x,ij}\bar{\mathbf{x}}_j[k] + E_{u,ij}\bar{\mathbf{u}}_j[k] + E_{w,ij}\bar{\mathbf{w}}_j[k] \right) && \forall i \in [1, n_z] \quad \text{(6.2b)} \\
\hat{y}_i[k] &= \tilde{C}_{ii}\bar{\mathbf{x}}_i[k], && \forall i \in [1, n_z] \quad \text{(6.2c)}
\end{aligned}
$$

where

$M_i(\theta_i)$	The discrete-time model of the i^{th} building zone dynamics, $\mathcal{S}_{d,i}$.
$\bar{\mathbf{x}}_i[n]$	$\bar{\mathbf{x}}_i[n] \in \mathbb{R}^{n_i}$ predicts the state vector of the i^{th} building zone dynamics for $n \geq k$, where $\bar{\mathbf{x}}_i[n]$ is a subvector of $\bar{\mathbf{x}}[n] \in \mathbb{R}^n$.
$\bar{\mathbf{u}}_i[n]$	$\bar{\mathbf{u}}_i[n] \in \mathbb{R}^{m_i}$ predicts the input vector of the i^{th} building zone dynamics for $n \geq k$, where $\bar{\mathbf{u}}_i[n]$ is a subvector of $\bar{\mathbf{u}}[n] \in \mathbb{R}^m$.
$\bar{\mathbf{w}}_i[n]$	$\bar{\mathbf{w}}_i[n] \in \mathbb{R}^{p_i}$ predicts the disturbance vector of the i^{th} building zone dynamics for $n \geq k$, where $\bar{\mathbf{w}}_i[n]$ is a subvector of $\bar{\mathbf{w}}[n] \in \mathbb{R}^p$.
$\bar{\delta}_i[n]$	$\bar{\delta}_i[n] \in \mathbb{R}^{n_i}$ is the predicted state uncertainty of the i^{th} building zone dynamics.

$\bar{\mathbf{p}}_i[n]$ $\bar{\mathbf{p}}_i[n] \in \mathbb{R}^{f_i}$ predicts the interaction vector to the i^{th} building zone dynamics, where $\bar{\mathbf{p}}_i[n]$ is a subvector of $\begin{bmatrix} \bar{\mathbf{x}}[n]^T & \bar{\mathbf{u}}[n]^T & \bar{\mathbf{w}}[n]^T \end{bmatrix}^T \in \mathbb{R}^{n+m+p}$ such that $f_i < n + m + p$.

$\hat{y}_i[n]$ $\hat{y}_i[n] \in \mathbb{R}^1$ is the weighted average of the predicted building zone air temperatures in $\bar{\mathbf{x}}_i[n]$.

6.2 Hierarchical MPC Problem

This section briefly reviews the main results of [73, 74], which frames the original MPC problem as a hierarchical one. We consider these results within the context of the discrete-time building environment $\mathcal{S}_d$ defined in (6.1) and discrete-time building model $M(\theta)$ defined in (6.2).

Consider the model predictive control problem defined in (5.9). Given the decentralized form of the building model in (6.2), then (5.9) can also be written in the following decentralized form,

$$\min_{\bar{U}_i} \quad \sum_{i=1}^{n_z} \left(\sum_{n=k}^{k+n_p} \|y_{i,set}[n] - \tilde{C}_{ii}\bar{\mathbf{x}}_i[n]\|_{Q_i} + \sum_{n=k}^{k+n_p-1} \|\bar{\mathbf{u}}_i[n]\|^2_{R_i} \right) \tag{6.3a}$$

$$\text{s.t.} \quad \bar{\mathbf{x}}_i[n+1] = A_{ii}\bar{\mathbf{x}}_i[n] + B_{ii}\bar{\mathbf{u}}_i[n] + G_{ii}\bar{\mathbf{w}}[n] + A_{ip}\bar{\mathbf{p}}_i[n] + G_{\Delta,ii}\bar{\delta}_i[n] \qquad \forall i, \forall n \tag{6.3b}$$

$$\bar{\mathbf{p}}_i[n] = \sum_{j \neq i} \left(E_{x,ij}\bar{\mathbf{x}}_j[n] + E_{u,ij}\bar{\mathbf{u}}_j[n] + E_{w,ij}\bar{\mathbf{w}}_j[n] \right) \qquad \forall i, \forall n \tag{6.3c}$$

$$\mathbf{u}_{i,min}[n] \leq \bar{\mathbf{u}}_i[n] \leq \mathbf{u}_{i,max}[n] \qquad \forall i, \forall n \tag{6.3d}$$

$$\bar{\mathbf{x}}_i[k] = \mathbf{T}_i[k], \quad \bar{\mathbf{u}}_i[n] \in \bar{U}_i, \quad \bar{\mathbf{w}}_i[n] = \mathbf{w}_i[k], \quad \bar{\delta}_i[n] \in \bar{\Delta}_i \qquad \forall i, \forall n \tag{6.3e}$$

for $i \in [1, n_z]$ and $n \in [k, k + n_p]$ where

- $Q_i = Q_i^T > 0$ and $R_i = R_i^T > 0$,
- $y_{i,set}[n]$ is the future setpoint for the i^{th} building zone air temperature, and
- $\mathbf{u}_{i,min}[n]$ and $\mathbf{u}_{i,max}[n]$ are the future constraints on the inputs for the i^{th} building zone.

Because the building cost function in (6.3b) can be separated into indivdual building zone costs, then (6.3) can be separated into n_z individual building zone control problems. The i^{th} building zone control problem can be summarized as the controller $\bar{U}_i$ that minimizes the i^{th} building zone cost, $\sum_{n=k}^{k+n_p} \|y_{i,set}[n] - \tilde{C}_{ii}\bar{\mathbf{x}}_i[n]\|_{Q_i} + \sum_{n=k}^{k+n_p-1} \|\bar{\mathbf{u}}_i[n]\|_{R_i}^2$, subject to the i^{th} building zone constraints in (6.3b) -(6.3e). The problem with this naive approach to decentralized building control is that the constraint (6.3c) depends on the variables $\bar{\mathbf{x}}_j[n]$, $\bar{\mathbf{u}}_j[n]$, and $\bar{\mathbf{w}}_j[n]$, which are determined by the outcome of the j^{th} building zone control problem. Sadati takes a hierarchical approach to address this problem using the Lagrangian dual of (6.3) [73, 74]. Let the Lagrangian dual of (6.3) be defined as the following min-max optimization problem,

$$\min_{\{\bar{\alpha}_i\},\{\bar{\beta}_i\},\bar{\zeta}} \quad \max_{\{\bar{X}_i\},\{\bar{U}_i\},\{\bar{P}_i\}} \quad \sum_{i=1}^{n_z} L_i(k, k+n_p; \bar{\alpha}_i, \bar{\beta}_i, \bar{\zeta}, \bar{X}_i, \bar{U}_i, \bar{P}_i, \bar{\Delta}_i) \tag{6.4a}$$

$$\text{s.t.} \quad \bar{\beta}_i[n] \geq 0, \qquad \forall i \in [1, n_z] \quad \forall n \in [k, k+n_p] \tag{6.4b}$$

where

- $L_i(k, k+n_p; \bar{\alpha}_i, \bar{\beta}_i, \bar{\zeta}, \bar{X}_i, \bar{U}_i, \bar{P}_i, \bar{\Delta}_i) =$

$$\sum_{n=k}^{k+n_p} \|y_{i,set}[n] - \tilde{C}_{ii}\bar{\mathbf{x}}_i[n]\|_{Q_i} + \sum_{n=k}^{k+n_p-1} \|\bar{\mathbf{u}}_i[n]\|_{R_i}^2$$
$$+ \quad \sum_{n=k}^{k+n_p} \bar{\alpha}_i[n]^T \Big(\bar{\mathbf{x}}_i[n+1] - A_{ii}\bar{\mathbf{x}}_i[n] - B_{ii}\bar{\mathbf{u}}_i[n]$$

$$
\begin{aligned}
& - G_{ii}\bar{\mathbf{w}}[n] - G_{\Delta,ii}\bar{\delta}_i[n] - A_{ip}\bar{\mathbf{p}}_i[n]\Big) \\
+ & \sum_{n=k}^{k+n_p} \bar{\beta}_{i,min}[n]^T \Big(\mathbf{u}_{i,min}[n] - \bar{\mathbf{u}}_i[n]\Big) \\
+ & \sum_{n=k}^{k+n_p} \bar{\beta}_{i,max}[n]^T \Big(\bar{\mathbf{u}}_i[n] - \mathbf{u}_{i,max}[n]\Big) \\
+ & \sum_{n=k}^{k+n_p} \bar{\zeta}_i[n]^T \bar{\mathbf{p}}_i[n] \\
- & \sum_{n=k}^{k+n_p} \sum_{j\neq i} \bar{\zeta}_j[n]^T \Big(E_{x,ji}\bar{\mathbf{x}}_i[n] + E_{u,ji}\bar{\mathbf{u}}_i[n] + E_{w,ji}\bar{\mathbf{w}}_i[n]\Big)
\end{aligned}
\tag{6.5}
$$

- $\bar{\alpha}_i[n] \in \bar{\alpha}_i$, $\beta_i[n] = \begin{bmatrix} \bar{\beta}_{i,min}[n] \\ \bar{\beta}_{i,max}[n] \end{bmatrix} \in \bar{\beta}_i$, $\bar{\zeta}_i[n] \in \bar{\zeta}$ for all $i \in [1, n_z]$ and for all $n \in [k, k+n_p]$,
- $\bar{X}_i = \{\bar{\mathbf{x}}_i[n] : n \in [k, k+n_p]\}$, $\bar{U}_i = \{\bar{\mathbf{u}}_i[n] : n \in [k, k+n_p]\}$, $\bar{P}_i = \{\bar{\mathbf{p}}_i[n] : n \in [k, k+n_p]\}$, and $\bar{\Delta}_i = \{\bar{\delta}_i[n] : n \in [k, k+n_p]\}$ for all $i \in [1, n_z]$, and
- $\bar{\mathbf{w}}_i[n] = \mathbf{w}_i[k]$ for all $n \in [k, k+n_p]$.

It is important to note that the i^{th} Lagrangian in (6.5) is purely a function of the variables $\bar{X}_i$, $\bar{U}_i$, $\bar{P}_i$, $\bar{\Delta}_i$, which are all exclusively related to the i^{th} building zone model, $M_i(\theta_i)$. Sadati splits the dual problem in (6.5) into an equivalent hierarchical control framework shown in (6.6) and (6.7) [74]. Assuming $\bar{\Delta}_i$ is given, let the hierarchical form of the model predictive controller in (5.9) be

$\mathcal{C}_S(k, k+n_p; \bar{\alpha}, \bar{\beta}, \bar{X}, \bar{U})$:

$$
\min_{\bar{\zeta}} \quad \max_{\bar{P}} \quad \sum_{i=1}^{n_z} L_i(k, k+n_p; \bar{\alpha}_i, \bar{\beta}_i, \bar{\zeta}, \bar{X}_i, \bar{U}_i, \bar{P}_i, \bar{\Delta}_i) \tag{6.6a}
$$

$$
\text{s.t.} \quad \bar{\alpha}_i \subseteq \bar{\alpha}, \quad \bar{\beta}_i \subseteq \bar{\beta}, \quad \bar{X}_i \subseteq \bar{X}, \quad \bar{U}_i \subseteq \bar{U}, \quad \bar{P}_i \subseteq \bar{P}, \qquad \forall i \tag{6.6b}
$$

$\mathcal{C}_i(k, k+n_p; \bar{\zeta}, \bar{P}_i, \bar{\Delta}_i)$:

$$\min_{\bar{\alpha}_i, \bar{\beta}_i} \quad \max_{\bar{X}_i, \bar{U}_i} \quad L_i(k, k+n_p; \bar{\alpha}_i, \bar{\beta}_i, \bar{\zeta}, \bar{X}_i, \bar{U}_i, \bar{P}_i, \bar{\Delta}_i) \tag{6.7a}$$

$$\text{s.t.} \quad \bar{\beta}_i[n] \geq 0, \qquad \forall i, \forall n \tag{6.7b}$$

where

- $\{\alpha_i^*, \beta_i^*, \bar{X}_i^*, \bar{U}_i^*\} = \mathcal{C}_i(k, k+n_p; \bar{\zeta}, \bar{P}_i, \bar{\Delta}_i)$ is the solution to the i^{th} infimal controller at time k, and
- $\{\bar{\zeta}^*, \bar{P}^*\} = \mathcal{C}_S(k, k+n_p; \bar{\alpha}, \bar{\beta}, \bar{X}, \bar{U})$ is the solution to the supremal controller at time k

for $i \in [1, n_z]$ and $n \in [k, k+n_p]$. Furthermore, the solution $\{\bar{X}_i^*, \bar{U}_i^*, \bar{P}_i^*\}$ solves the original decentralized model-predictive control problem in (6.3).

In [73], Sadati sequentially solves the pair of control problems in (6.6) and (6.7) to find the i^{th} model predictive controller $\mathbf{u}_i^*[k] \in \bar{U}_i^*$ for the i^{th} subsystem of the controlled process for all $i \in [1, n_z]$. Alg. 10 presents the hierarchical MPC strategy for all time k.

6.3 Robust Hierarchical MPC Problem

The previous section presents a hierarchical approach to model-predictive building control using the work in [73–75]. One of the underlying assumptions in the literature is that the control model is equivalent to the dynamics of the controlled process. This implies the predicted model uncertainty is known, $\bar{\Delta}_i = \Delta_i = \{0\}$ for all $i \in [1, n_z]$. In this section, we relax the assumption that the model uncertainty is known.

Algorithm 10 Hierarchical MPC Algorithm [73]

1. Initialize $\{\alpha_i^m, \beta_i^m, \bar{X}_i^m, \bar{U}_i^m, \bar{\zeta}^m, \bar{P}_i^m, \bar{\Delta}_i^k\}$ at $m = 0$ given the initial condition $\bar{\mathbf{x}}_i[k]$ and $\bar{\Delta}_i^k$ at time k for all $i \in [1, n_z]$.
2. Using $\{\alpha_i^m, \beta_i^m, \bar{X}_i^m, \bar{U}_i^m, \bar{\zeta}^m, \bar{P}_i^m, \bar{\Delta}_i^k\}$, solve the infimal control problem (6.7) for $\{\alpha_i^{m+1}, \beta_i^{m+1}, \bar{X}_i^{m+1}, \bar{U}_i^{m+1}, \bar{\zeta}^m, \bar{P}_i^m, \bar{\Delta}_i^k\}$ for all i.
3. Using $\{\alpha_i^{m+1}, \beta_i^{m+1}, \bar{X}_i^{m+1}, \bar{U}_i^{m+1}, \bar{\zeta}^m, \bar{P}_i^m, \bar{\Delta}_i^k\}$, solve the supremal control problem (6.6) for $\{\alpha_i^{m+1}, \beta_i^{m+1}, \bar{X}_i^{m+1}, \bar{U}_i^{m+1}, \bar{\zeta}^{m+1}, \bar{P}_i^{m+1}, \bar{\Delta}_i^*\}$
4. If $\zeta_i[n]^{m+1} - \zeta_i[n]^m < \epsilon_z$ and $\mathbf{p}_i[n]^{m+1} - \mathbf{p}_i[n]^m < \epsilon_p$ for all $i = [1, n_z]$ and all $n \in [k, k + n_p]$, go to Step 5. Otherwise, repeat Steps 2-3 for $m = m + 1$.
5. Apply $\mathbf{u}_i[k] = \bar{\mathbf{u}}_i[k]^*$ for all i where $\bar{\mathbf{u}}[k]^* \in \bar{U}_i^m$.
6. Repeat Steps 1-5 for $k = k + 1$.

Specifically, we apply the robust model predictive control framework presented in Chapter 5 to the hierarchical control framework introduced in the prior section.

Consider the pair of control problems $\mathcal{C}_U(k)$ in (5.25a) and $\mathcal{C}_\Delta(k)$ in (5.25a) that comprise the robust model predictive control problem. The minimization problem $\mathcal{C}_U(k)$ solves for the predicted control sequence $\bar{U}$ given some predicted model uncertainty $\bar{\Delta}^*$. We observe that the control problem $\mathcal{C}_U(k)$ is equivalent to the MPC problem in (6.3) given a decentralized building model (6.2). Then, (5.25a) can be restructured as the hierarchical controller in (6.6) and (6.7) such that $\mathcal{C}_U(k) = \{\mathcal{C}_U^o(k), \mathcal{C}_U^1(k), \ldots, \mathcal{C}_U^{n_z}(k)\}$. This leaves the maximization problem $\mathcal{C}_\Delta(k)$ to be restructured to fit the hierarchical control framework. Suppose the control problem in (5.25b) can be written in decentralized form as follows,

$$\max_{\{\bar{\Delta}_i\}} \quad \sum_{i=1}^{n_z} \left(\sum_{n=k}^{k+n_p} \|\tilde{C}_{ii}\bar{\mathbf{x}}_i[n]\|_I + \sum_{n=k}^{k+n_p-1} \|\bar{\mathbf{u}}_i[n]\|_I^2 - \gamma_i^2 \sum_{n=k}^{k+n_p-1} \|\bar{\delta}_i[n]\|_I^2 \right) \tag{6.8a}$$

$$\text{s.t.} \quad \bar{\mathbf{x}}_i[n+1] = A_{ii}\bar{\mathbf{x}}_i[n] + B_{ii}\bar{\mathbf{u}}_i[n] + G_{ii}\bar{\mathbf{w}}_i[n]$$

$$+ G_{\Delta,ii}\bar{\delta}_i[n] + A_{ip}\bar{\mathbf{p}}_i[n] \qquad \forall i, \forall n \quad (6.8b)$$

$$\bar{\mathbf{p}}_i[n] = \sum_{j \neq i} \left(E_{x,ij}\bar{\mathbf{x}}_j[n] + E_{u,ij}\bar{\mathbf{u}}_j[n] + E_{w,ij}\bar{\mathbf{w}}_j[n] \right) \qquad \forall i, \forall n \quad (6.8c)$$

$$\bar{\mathbf{x}}_i[k] = \mathbf{T}_i[k], \quad \bar{\mathbf{w}}_i[n] = \mathbf{w}_i[k], \quad \bar{\delta}_i[n] \in \bar{\Delta}_i, \quad \bar{\mathbf{u}}_i[n] \in \bar{U}_i^*, \qquad \forall i, \forall n \quad (6.8d)$$

where $\bar{U}_i^*$ is given. Much like the control problem in (6.3), the decentralized control problem in (6.8) is not completetely separable because of the constraint in (6.8c). Therefore, to relax this constraint, we will assume that $\bar{P}_i = \{\mathbf{p}_i[n] : n \in [k, k+n_p]\}$ is given. Then, the (5.25b) can be completely decentralized, $\mathcal{C}_\Delta(k) = \{\mathcal{C}_\Delta^1(k), \ldots, \mathcal{C}_\Delta^{n_z}(k)\}$ where the i^{th} control problem $\mathcal{C}_\Delta^i(k)$ at time k is

$$\max_{\bar{\Delta}_i} \quad \sum_{n=k}^{k+n_p} \|\tilde{C}_{ii}\bar{\mathbf{x}}_i[n]\|_I + \sum_{n=k}^{k+n_p-1} \|\bar{\mathbf{u}}_i[n]\|_I^2 - \gamma_i^2 \sum_{n=k}^{k+n_p-1} \|\bar{\delta}_i[n]\|_I^2 \quad (6.9a)$$

$$\text{s.t.} \quad \bar{\mathbf{x}}_i[n+1] = A_{ii}\bar{\mathbf{x}}_i[n] + B_{ii}\bar{\mathbf{u}}_i[n] + G_{ii}\bar{\mathbf{w}}_i[n]$$

$$+ G_{\Delta,ii}\bar{\delta}_i[n] + A_{ip}\bar{\mathbf{p}}_i[n], \qquad \forall i, \forall n \quad (6.9b)$$

$$\bar{\mathbf{x}}_i[k] = \mathbf{T}_i[k], \quad \bar{\mathbf{w}}_i[n] = \mathbf{w}_i[k], \quad \bar{\delta}_i[n] \in \bar{\Delta}_i, \qquad \forall i, \forall n \quad (6.9c)$$

$$\bar{\mathbf{u}}_i[n] \in \bar{U}_i^*, \quad \bar{\mathbf{p}}_i[n] \in \bar{P}_i^* \qquad \forall i, \forall n, \quad (6.9d)$$

where $\bar{U}_i^*$ and $\bar{P}_i^*$ are given. Based on how $\mathcal{C}_U(k)$ and $\mathcal{C}_\Delta(k)$ are decentralized, we can define a two tier hierarchical framework for robust model predictive control.

Building Zone Controller The first tier of this framework is composed of n_z separate controllers $\mathcal{C}_U^i(k)$ that use approximate models of the building zone $M_i(\theta_i)$ to control the average zone air temperature. These controllers are referred to as *zone-level controllers*, and the i^{th} zone-level controller finds the set $\{\bar{X}_i^*, \bar{U}_i^*, \bar{\Delta}_i^*\}$

that solves the following pair of optimization problems,

$$\begin{aligned} &\mathcal{C}_U^i(k): \quad (6.7) \quad \text{s.t.} \quad (6.5) \\ &\mathcal{C}_\Delta^i(k): \quad (6.9a) \quad \text{s.t.} \quad (6.9b) - (6.9d). \end{aligned} \tag{6.10}$$

where $\gamma \geq 0$ and the variables $\{\bar{\zeta}, \bar{P}_i\}$ are known. Then, given $\bar{\mathbf{u}}_i^*[k] \in \bar{U}_i^*$, each zone-level controller applies a robust model predictive controller $\mathbf{u}_i[k] = \bar{\mathbf{u}}_i^*[k]$ to the building zone at time k.

Building Coordinator The second tier of this hierarchical control framework is a higher level controller $\mathcal{C}_U^o(k)$ that coordinates the efforts of the individual zone controllers $\{\mathcal{C}_U^i(k) : i \in [1, n_z]\}$ in the entire building. This high-level controller is known as a *building coordinator*, and finds the set of variables $\{\bar{\zeta}^*, \bar{P}_i^* : \forall i \in [1, n_z]\}$ that solves the following optimization problem,

$$\mathcal{C}_U^o(k): \quad (6.6) \quad \text{s.t.} \quad (6.5) \tag{6.11}$$

where the zone-level variables $\{\bar{\alpha}_i, \bar{\beta}_i, \bar{X}_i, \bar{U}_i, \bar{\Delta}_i\}$ are assumed to be known. The variables $\{\bar{\zeta}^*, \bar{P}_i^* : \forall i \in [1, n_z]\}$ are known as *coordination variables*, and these variables are used to enforce the global constraint,

$$\bar{\mathbf{p}}_i[n] = \sum_{j \neq i} \left(E_{x,ij} \bar{\mathbf{x}}_j[n] + E_{u,ij} \bar{\mathbf{u}}_j[n] + E_{w,ij} \bar{\mathbf{w}}_j[n] \right) \qquad \forall i, \forall n \tag{6.12}$$

for $i \in [1, n_z]$ and $n \in [k, k + n_p]$. Essentially, the coordinator collects zone-level control information $\{\bar{\alpha}_i, \bar{\beta}_i, \bar{X}_i, \bar{U}_i, \Delta_i\}$ from every zone, and then sends each zone-level controller a prediction of the interaction vector $\mathbf{p}[n] \in \bar{P}_i$ over the horizon $n \in [k, k + n_p]$ and a weighting variable $\bar{\zeta}$.

Similar to the sequential process in Alg. 10, the hierarchical framework for robust model-predictive control iteratively arrives at a solution $\{\bar{\alpha}_i^*, \bar{\beta}_i^*, \bar{X}_i^*, \bar{U}_i^*, \bar{\Delta}_i^*, \bar{\zeta}^*, \bar{P}_i^*\}$ at every time step k, and applies $\bar{\mathbf{u}}_i[k] \in \bar{U}_i^*$ to the i^{th} building zone. This iterative process is outlined below in Alg. 11. We demonstrate this hierarchical approach to robust model-predictive control in the following example.

Algorithm 11 Hierarchical Robust MPC Algorithm

1. Initialize $\{\alpha_i^m, \beta_i^m, \bar{X}_i^m, \bar{U}_i^m, \bar{\Delta}_i^m, \bar{\zeta}^m, \bar{P}_i^m\}$ at $m = 0$ given $\gamma > 0$ and the initial condition $\bar{\mathbf{x}}_i[k]$ at time k for all $i \in [1, n_z]$.
2. Using $\{\alpha_i^m, \beta_i^m, \bar{X}_i^m, \bar{U}_i^m, \bar{\zeta}^m, \bar{P}_i^m, \bar{\Delta}_i^m\}$ and γ, solve the zone-level control problem (6.10) for $\{\alpha_i^{m+1}, \beta_i^{m+1}, \bar{X}_i^{m+1}, \bar{U}_i^{m+1}, \bar{\Delta}_i^{m+1}, \bar{\zeta}^m, \bar{P}_i^m\}$ for all i.
3. Using $\{\alpha_i^{m+1}, \beta_i^{m+1}, \bar{X}_i^{m+1}, \bar{U}_i^{m+1}, \bar{\Delta}_i^{m+1}, \bar{\zeta}^m, \bar{P}_i^m\}$, solve the building coordination problem (6.11) for $\{\alpha_i^{m+1}, \beta_i^{m+1}, \bar{X}_i^{m+1}, \bar{U}_i^{m+1}, \bar{\Delta}_i^{m+1}, \bar{\zeta}^{m+1}, \bar{P}_i^{m+1}\}$
4. If $\zeta_i[n]^{m+1} - \zeta_i[n]^m < \epsilon_z$ and $\mathbf{p}_i[n]^{m+1} - \mathbf{p}_i[n]^m < \epsilon_p$ for all $i = [1, n_z]$ and all $n \in [k, k + n_p]$, go to Step 5. Otherwise, repeat Steps 2-3 for $m = m + 1$.
5. Apply $\mathbf{u}_i[k] = \bar{\mathbf{u}}_i[k]^*$ for all i where $\bar{\mathbf{u}}[k]^* \in \bar{U}_i^m$.
6. Repeat Steps 1-5 for $k = k + 1$.

Example 10 (Hierarchical Robust MPC of Small Scale Building)

Consider the small scale building example in Appendix A.2. Let the dynamics of the building be the discrete-time system, $\mathcal{S}_d$ in (5.1) for sampling period $T_s = 5$ min. Furthermore, assume the building is split into two building zones, where the dynamics of Zone 1 includes the dynamics for Rooms 1 and 2 and the dynamics of Zone 2 include the dynamics for Rooms 3 and 4. We will also assume that there are two local model-based controllers that delivers heating to each zone ($u_1[k]$ for Zone 1 and $u_4[k]$ for Zone 2) in order to drive the average zone temperature to achieve some setpoint. These controllers are assumed to be coordinated by a higher level

coordinator. Finally, we will assume the same model $M(\theta_0)$, input constraints, set points, and time horizon $k \in [0, 288]$ as in Example 8. Then, we will consider the following cases in this example.

Case 1: Apply MPC to $\mathcal{S}_d$ given the model, $M(\theta_0) \stackrel{M}{=} \mathcal{S}_d$ where $\theta_0 = \theta_S$.

Case 2: Apply MPC to $\mathcal{S}_d$ given the model, $M(\theta_0) \stackrel{M}{\neq} \mathcal{S}_d$ where $\theta_0(i) = .7\theta_S(i)$ for all $i \in [1, q]$.

Case 3: Apply the hierarchical form of Robust MPC for $\gamma = 14$ to $\mathcal{S}_d$ given the model, $M(\theta_0) \stackrel{M}{\neq} \mathcal{S}_d$ where$\theta_0(i) = .7\theta_S(i)$ for all $i \in [1, q]$.

Case 4: Apply the hierarchical form of Robust MPC-T for $\gamma_0 = 14$ to $\mathcal{S}_d$ given the model, $M(\theta_0) \stackrel{M}{\neq} \mathcal{S}_d$ where $\theta_0(i) = .7\theta_S(i)$ for all $i \in [1, q]$, and given $\alpha_P = 2$ and $\alpha_I = 0$.

Given these control scenarios, Fig. 6.2 and Fig. 6.3 plot the resulting zone temperature and heating input for each control strategy and for each zone. We observe that these plots are identical to Fig 5.2 in Example 9, and the hierarchical Robust MPC-T yields the same performance as Robust MPC-T in Example 9.

This hierarchical approach to robust control has several advantages over the scheme presented in the previous chapter. First, a supervisory model predictive control strategy for a large building environment can be easily decentralized into local zone controllers that only require information about the dynamics of the building zone and information from a high level coordinator. Second, this strategy takes into account modeling uncertainties $\bar{\delta}_i[k] \in \bar{\Delta}_i$ and compensates the predictive control sequence $\bar{U}_i$ for the worst case disturbance given $\gamma > 0$.

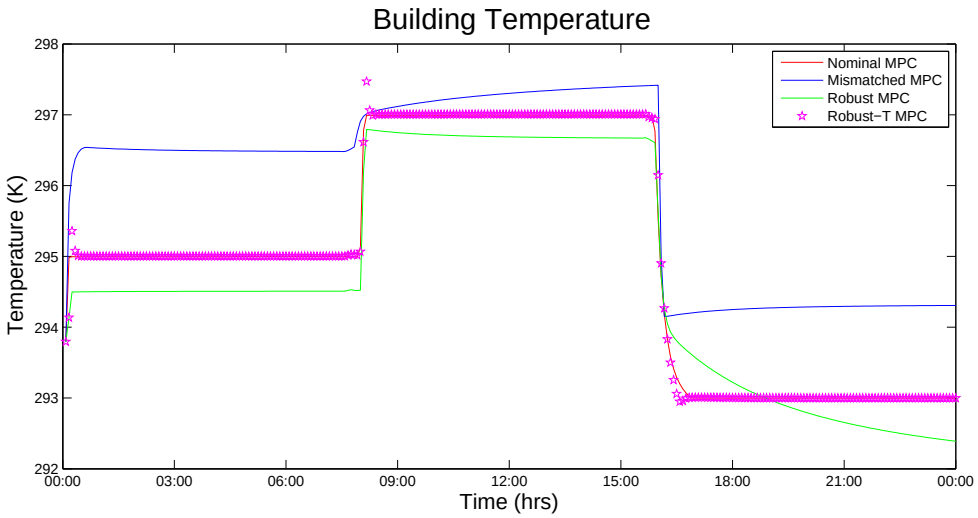

(a) Output Temperatures

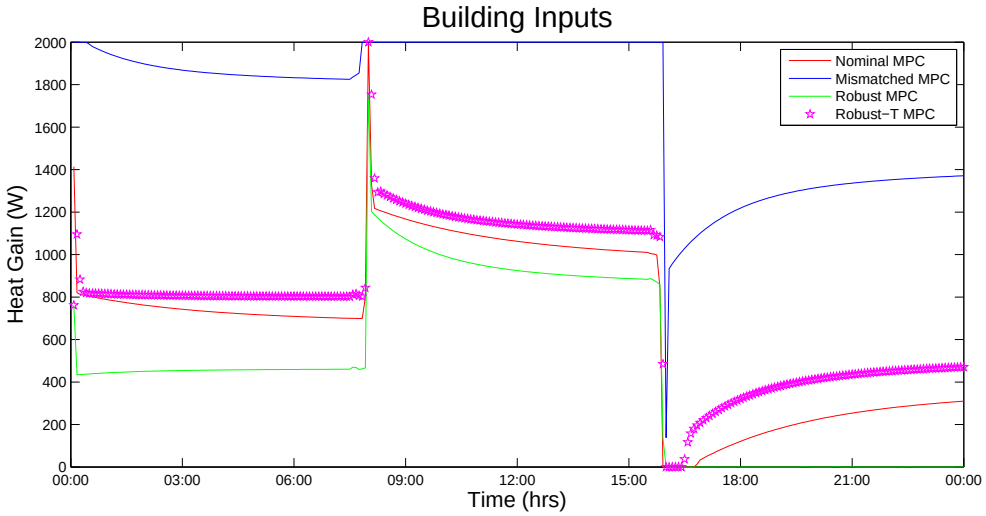

(b) Heat Inputs

Figure 6.2: Comparison of Cases 1-4 for Zone 1

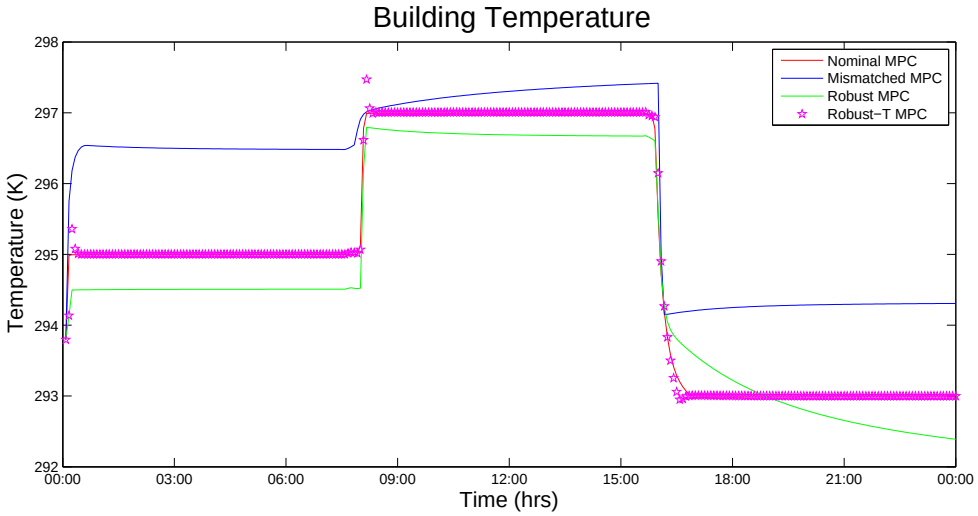

(a) Output Temperatures

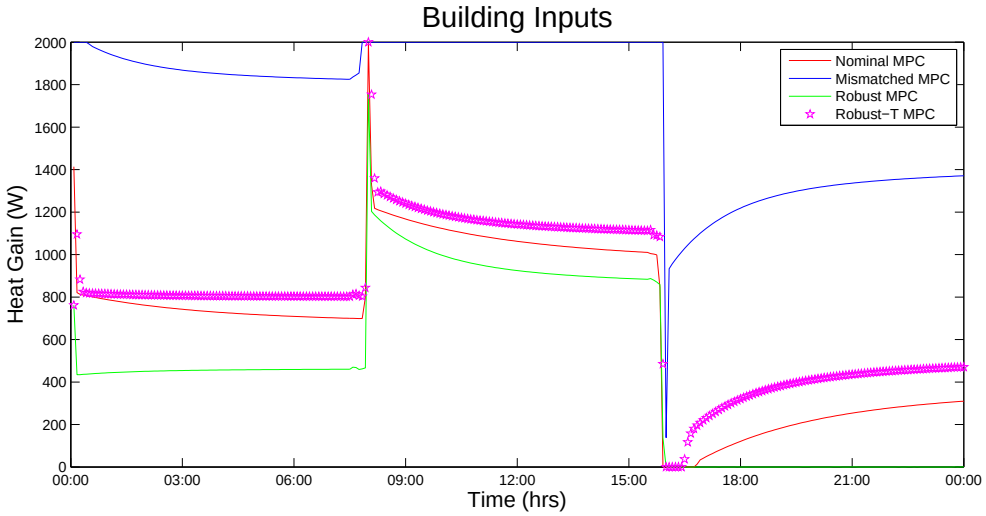

(b) Heat Inputs

Figure 6.3: Comparison of Cases 1-4 for Zone 2

6.4 Hierarchical Control of Case Study Examples

This section demonstrates the hierarchical Robust MPC and Robust MPC-T approaches for the case studies detailed in Chapter 2, where each building model is split into building zone models and used for local control of a building zone. This section will assume all the prior assumptions and cases from Section 5.5 and apply them to this study. Table 6.3 and Table 6.4 are generated from these assumptions for all Cases 1-4 outlined in Section 5.5. For Cases 3 and 4, we note $\gamma = 100$ and $\gamma_0 = 100$, respectively for the control strategy applied to the Office building. We use these tables to compare the performance of these different control strategies.

Table 6.3: Comparison of Hierarchical Control Strategies for IW-North

	Nominal MPC	Mismatch MPC		Robust MPC Constant γ		Robust MPC Tuned γ	
	U_{tot} (kWh)	Y_{mse} (K)	U_{tot} (kWh)	Y_{mse} (K)	U_{tot} (kWh)	Y_{mse} (K)	U_{tot} (kWh)
Zone 1	176.7	3.14	280.0	2.84	112.5	0.0085	195.0
Zone 2	340.0	1.76	509.2	4.80	64.2	0.0132	339.2
Zone 3	149.2	2.16	246.7	3.01	54.2	0.0099	161.2
Zone 4	351.7	1.75	519.2	3.66	74.2	0.0121	349.2
Zone 5	164.2	2.83	263.3	3.07	105.8	0.0092	185.8
Zone 6	195.0	2.72	319.2	2.80	70.8	0.0104	204.2
Zone 7	395.8	3.87	575.0	5.89	30.8	0.0443	395.0
Zone 8	181.7	2.20	296.7	4.27	32.5	0.0119	185.0
Zone 9	210.0	2.83	354.7	3.33	58.3	0.0119	221.7
Zone 10	625.8	10.42	671.7	4.40	159.2	0.0937	631.7
Total Energy:	2,790.8	-	4,034.2	-	762.5	-	2,870

In Table 6.3, we observe that the Robust MPC-T strategy has the lowest mean squared output error for all strategies, which means the building output under Robust MPC-T control mimics the building output under nominal MPC. Furthermore,

we note that the amount of energy consumed in each zone for Robust MPC-T is very similar to the amount of energy consumed under nominal conditions. With the exception of Robuse MPC with constant γ, we note the aggregate amounts of energy in the last row of 6.3 match the amounts found in 5.3, which indicates that under certain conditions the hierarchical strategy performs similar to the centralized building controller.

Table 6.4: Comparison of Hierarchical Control Strategies for Office Building

	Nominal MPC	Baseline MPC		Robust MPC		Robust MPC-T	
	U_{tot} (kWh)	Y_{mse} (K)	U_{tot} (kWh)	Y_{mse} (K)	U_{tot} (kWh)	Y_{mse} (K)	U_{tot} (kWh)
Zone 1	418,060	7.74	420,000	1.75	412,810	2.45	420,000
Zone 2	363,820	8.40	416,960	0.80	309,130	2.64	406,380
Zone 3	207,460	4.19	358,800	0.84	49,160	1.10	337,060
Zone 4	122,110	1.41	322,010	1.34	14,200	0.31	224,740
Zone 5	116,730	0.58	248,330	1.63	17,580	0.20	199,540
Zone 6	117,730	0.37	238,800	1.78	17,800	0.20	180,810
Zone 7	117,840	0.34	239,760	1.80	17,790	0.19	181,290
Zone 8	117,680	0.37	239,000	1.66	17,870	0.20	181,100
Zone 9	116,690	0.54	245,440	1.39	17,770	0.20	197,290
Zone 10	122,830	1.24	317,500	0.99	14,400	0.28	220,420
Zone 11	222,990	3.38	362,200	0.53	55,870	0.82	338,410
Zone 12	384,670	5.56	417,450	0.86	325,600	1.40	414,450
Total	2.4×10^6	-	3.8×10^6	-	1.3×10^6	-	3.3×10^6

In Table 6.4, we observe something slightly different for the large office building. Both the Robust MPC and the Robust MPC-T approaches outperform the baseline MPC strategy. For a majority of zones the Robust MPC-T strategy is closer to the nominal controller performance than the Robust MPC strategy and consumes more energy to achieve improved thermal performance.

6.5 Summary

This chapter serves as a continuation of Chapter 5 into the domain of hierarchical and decentralized control. In this chapter, we review the framework of hierarchical control as posed in [64, 73, 74], and apply some of the key results and frameworks for robust control in Chapter 5 here. Furthermore, we develop a robust, hierarchical framework for model-based building control, specifically model-predictive control. Our proposed hierarchical model-based controller is a desirable one because the supervisory zone controllers are individually robust to model uncertainties, scalable to building environments with a large number of zones, and flexible to changes in the model. Finally, this hierarchical strategy is demonstrated in the simulated case studies, and we observe the decentralized control strategy performs similarly to the centralized building control strategy us in Chapter 5.

Chapter 7

Conclusion & Future Work

7.1 Summary of Contributions

The main contributions for this work are summarized as follows.

Parameter Identifiability of Grey-Box Building Models

Based on the framework of model identifiability, we have developed an approach to quantitatively determine model parameters that may not be identifiable. This evaluation is important because it allows users to pinpoint parameters in a model that may not be identifiable due to model structure. Furthermore, it allows users to test for model structures and data sets that would improve the identifiability of certain parameters.

Design-Driven Building Model Identification Process

In the standard identification process, users would have to completely discard an unidentifiable model and choose a new model structure. This leads to a frustrating process of trial and error in testing, where many different model

structures are tested. To address this challenge, we introduce the design-driven model identification process. This process uses parameter identifiability to first determine which parameters are not identifiable and then uses heuristics to deal with these unidentifiable parameters through aggregation.

Decentralized Identification of Control-Oriented Building Models

We observe from experience that building models are generally too large to be identified efficiently with the current identification process.Therefore, we propose a decentralized approach to make identification scalable using the notion of reachability and directed graphs of the building dynamics. This new decentralized identification process very quickly parses building models into sizable building zones that can be individually identified and pieced back together. Furthermore, we introduce the notion of decentralized model identifiability where the structural and output identifiability metrics are applied to all the building zone models in order to quickly determine the identifiability of the entire building model.

Robust Model-Based Supervisory Control

The second half of this dissertation addresses the challenge of using uncertain building models for model predictive control. The objective of this work is to improve controller sensitivity to model uncertainty. To address this issue, techniques from H_∞ control are used to design a robust model-predictive control strategy that can attenuate the effect of modeling errors subject to a robustness factor. More importantly, we develop and implement a strategy to reduce the conservativeness of the controller by automatically tuning the robustness factor. This tuning process allows for significant improvements over the baseline control strategies.

Hierarchical and Robust Model-Based Supervisory Control

As a next step to the robust model-based control framework, we consider the question of decentralized and robust model-based supervisory control. We build on the current approach to hierarchical model predictive control and introduce a hierarchical version of the robust control problem. Using this framework, the local supervisory zone controllers can independently tune their robustness factor for improved performance. This is an attractive feature since it allows local supervisory controllers to independently determine the level of robustness needed for the model-based zone controller.

MATLAB Simulator & Case Study

Finally, a major contribution of this work is the demonstration of the proposed strategies using simulated examples of real building environments. We have developed an extensive simulator in MATLAB to construct the building environments and building models. Using these models, we developed algorithms to demonstrate each of the contributions to building model identification and control listed above.

7.2 Future Work

There are several directions for future work that build on the contributions listed above. We provide an overview for some of the big ideas

7.2.1 Iterative, Systematic Parameter Aggregation

In Chapter 3, the proposed design-driven model identification approach uses the notions of parameter identifiability and parameter aggregation to determine and alle-

viate the challenges of identifying a building model. The strength of this approach lies in the ability to appropriately tweak the model and deal with the poorly identifiable parameters in the model in order to improve the structural identifiability of the models. We propose two rules to improve parameter identifiability via parameter reduction, but these rules are not guaranteed to work every time for all building models. Instead, these rules provide a first step towards a fully systematic process to automatically aggregate those parameters in the model that are likely not identifiable.

One direction towards this systematic approach is to create an iterative process to test different types of linear and non-linear aggregation methods that may improve structural parameter identifiability. Examples of non-linear aggregation methods include aggregating parameters into time constants, $\tau = RC$, which may be more easily identified for a building element than individual parameters. Furthermore, more work needs to be done to determine which parameters should be aggregated together. Our current approach presents an intuitive method of aggregating the parameters in a single building element and aggregating parameters across building elements that may not be distinguishable or separately identifiable. To achieve this systematic approach, formal methods are needed to first determine parameters that belong to indistinguishable building elements, and then to aggregate those parameters using linear and/or non-linear methods.

7.2.2 Optimal and Decentralized Input Design

The proposed design-driven model identification process exclusively considers methods to improve the structural identifiability, but does not address output identifiability. Although structural identifiability is necessary for output identifiability, it is not a sufficient condition by itself that the model $M(\theta)$ be identifiable for a given

data set Z^N. One of the key barriers to output identifiability is the richness of the identification data Z^N and designing identification experiments with sufficiently rich identification data. This particular problem is known as *optimal input design* or *optimal design of experiments* [4, 40, 83], and is an important one to consider to improve the output identifiability of a model given a data set.

We can extend the design-driven model identification process to actively design identification inputs to improve the estimation of structurally identifiable parameters. Furthermore, based on the output identifiability metric, we can determine which structurally identifiable parameters may not output identifiable. In those cases, the choice of identification data impacts the quality of the parameter estimate. To support a fully automatic design-driven identification process, further work needs to be done to automatically design controllable building inputs that yield sufficiently rich identification data given building disturbances.

Another future direction to consider is input design for decentralized model identification in Chapter 4. Local identification experiments need to be designed for individual zones in order to better estimate the parameters of a building zone model. This leads to posing a *decentralized input design problem*, where correlations may exist between disturbances to the building zone. Future work might look at coordinating controllable inputs in neighboring zones to improve local data used for zone model identification.

7.2.3 Mixed Building Control Strategies

We demonstrate in Chapters 5 and 6 that model-based control is a viable strategy for supervisory building control. However, model-based control strategies may not be widely installed in buildings because of high capital costs and maintenance. To

reduce these costs, operators and owners may decide to install model-based control in critical areas of the building such as high occupancy areas where energy consumption and/or thermal comfort must be more finely controlled. This may lead to a mixed-control scenario where different supervisory control strategies are used within in a single building to save energy. We can pose this mixed building control scenario as an extension of the hierarchical control problem introduced in Chapter 6 where supervisory zone controllers are either model-based or model-free control strategies and the building coordinator ensures the controllers are cooperatively working together. Based on this scenario, there are several questions and areas for future research that may be of interest to the building community.

One issue is providing guidelines on building scenarios for which model-based control might be better to use than model-free control such as PID, rule-based control, etc. Factors such as occupancy, level of thermal tolerance, and sensing may be important to determining the effectiveness of a model-based control strategy for a particular space. Another issue is determining the optimal number of model-based strategies that maximize the amount of energy saved per dollar spent towards capital costs of installation. Further work on these two issues may yield some insightful guidelines and tradeoffs on retrofitting old buildings with advanced building control strategies.

7.2.4 Integration of Additional Building Systems

Buildings are highly complex because they are a network of nonlinear processes and systems. This work exclusively focuses on supervisory model-based controls for heating building spaces in cold climates, but there are several other scenarios for which model-based control may be helpful. In warmer climates, model-based control can be used to manage both cooling and humidification systems, which are building processes

that are strongly coupled together and have to be managed together. Another important building process is ventilation, which is required in buildings where fresh air has to be forced in through the air-handling unit. Standards for ventilation are met by increasing the amount of fresh air being taken into the building, but often lead to increased thermal conditioning since less of the conditioned air in the building cannot be recycled. One advantage of model-based control is the ability to balance several competing objectives for conditioning the building and energy needed to properly condition the building. Therefore, it is crucial that real building control strategies optimize more than just thermal performance in order to both comply with current building standards and to maximize energy savings.

Appendix A

Small-Scale Building Examples

A.1 Two Room Building Environment

Consider a building with two rooms, $T_1(t)$ and $T_2(t)$, separated by a wall as shown in Fig. A.1. Let the thermal properties of the building be given in Table A.1:

Building Element	RC Model	Resistivity $(\frac{m^2K}{W})$	Capacitivity $(\frac{J}{Wm^2})$
Interior Walls	2R1C	0.24	3,600
Exterior Walls	1R0C	1.17	102,000,000
Roofs	1R0C	2.85	104,870
Floors	1R0C	1.11	72,000

Table A.1: Thermal Properties of Two Room Building Construction. We note the exterior walls separate the outdoors from the indoors, while the interior walls partition the indoor air spaces.

Let the parameters of the interior wall be R_{12a}, R_{12b}, and C_{12}, where $T_{12}(t)$ is the internal temperature of the interior wall. Let the parameters of the exterior wall in Room 1 be R_{1N}, R_{1S}, R_{1W}, R_{1F}, R_{1R} and the parameters of the exterior wall

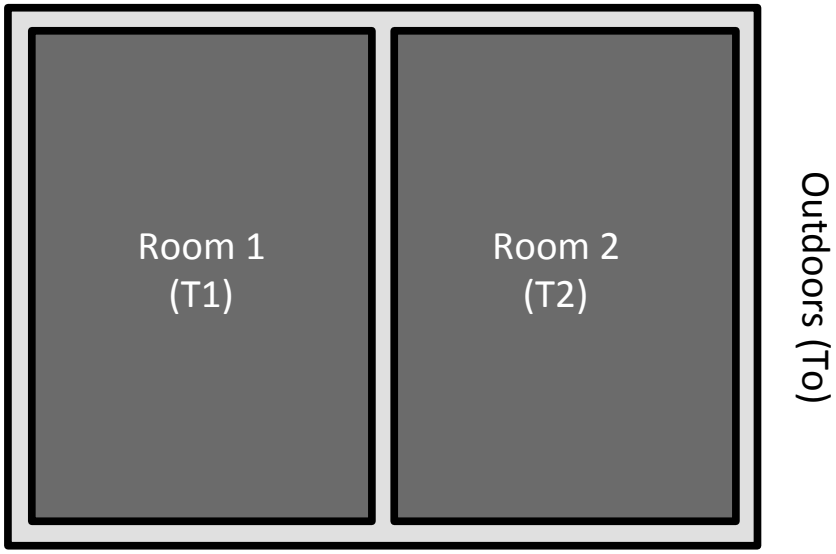

Figure A.1: 2 Room Building

in Room 2 as R_{2N}, R_{2S}, R_{2W}, R_{2F}, R_{2R}. Then, the continuous-time model of the building dynamics is written as follows,

$$\mathcal{S}: \quad \begin{bmatrix} \dot{T}_1(t) \\ \dot{T}_2(t) \\ \dot{T}_{12}(t) \end{bmatrix} = \begin{bmatrix} -a_{11} & 0 & \frac{1}{R_{12a}C_1} \\ 0 & -a_{22} & \frac{1}{R_{12b}C_2} \\ \frac{1}{R_{12a}C_{12}} & \frac{1}{R_{12b}C_{12}} & -a_{1N} \end{bmatrix} \begin{bmatrix} T_1(t) \\ T_2(t) \\ T_{12}(t) \end{bmatrix} + \begin{bmatrix} \frac{1}{C_1} & 0 \\ 0 & \frac{1}{C_2} \\ 0 & 0 \end{bmatrix} \begin{bmatrix} u_1(t) \\ u_2(t) \end{bmatrix} + \begin{bmatrix} g_1 & \frac{1}{C_1} & 0 \\ g_2 & 0 & \frac{1}{C_2} \\ 0 & 0 & 0 \end{bmatrix} \begin{bmatrix} T_o(t) \\ \dot{q}_1(t) \\ \dot{q}_2(t) \end{bmatrix} \tag{A.1}$$

$$\begin{bmatrix} y_1(t) \\ y_2(t) \end{bmatrix} = \begin{bmatrix} 1 & 0 & 0 \\ 0 & 1 & 0 \end{bmatrix} \begin{bmatrix} T_1(t) \\ T_2(t) \\ T_{12}(t) \end{bmatrix}$$

where

$$
\begin{aligned}
a_{11} &= \frac{1}{R_{12a}C_1} + \frac{1}{R_{1N}C_1} + \frac{1}{R_{1S}C_1} + \frac{1}{R_{1W}C_1} + \frac{1}{R_{1R}C_1} + \frac{1}{R_{1F}C_1} \\
a_{12} &= \frac{1}{R_{12b}C_2} + \frac{1}{R_{2N}C_2} + \frac{1}{R_{2S}C_2} + \frac{1}{R_{2E}C_2} + \frac{1}{R_{2R}C_2} + \frac{1}{R_{2F}C_2} \\
a_{1N} &= \frac{1}{R_{1Na}C_{1N}} + \frac{1}{R_{1Nb}C_{1N}} \\
g_1 &= \frac{1}{R_{1N}C_1} + \frac{1}{R_{1S}C_1} + \frac{1}{R_{1W}C_1} + \frac{1}{R_{1R}C_1} + \frac{1}{R_{1F}C_1} \\
g_2 &= \frac{1}{R_{2N}C_2} + \frac{1}{R_{2S}C_2} + \frac{1}{R_{2E}C_2} + \frac{1}{R_{2R}C_2} + \frac{1}{R_{2F}C_2}
\end{aligned}
\tag{A.2}
$$

.

A.2 Four Room Building Environment

Consider the layout of a a four room building in Fig. A.2. Let the thermal properties of the building construction be given in Table A.1. Given the floor plan and the modeling assumptions, then the dynamics of the building is written as:

$$
\mathcal{S}: \quad \begin{aligned} \dot{\mathbf{T}}(t) &= A(\theta)\mathbf{T}(t) + B(\theta)\mathbf{u}(t) + G(\theta)\mathbf{w}(t) \\ \mathbf{y}(t) &= C\mathbf{T}(t) \end{aligned}
$$

where the system vectors are

$$
\begin{aligned}
\mathbf{T}(t) &= \begin{bmatrix} T_1(t) & T_2(t) & T_3(t) & T_4(t) & T_{12}(t) & T_{13}(t) & T_{24}(t) & T_{34}(t) \end{bmatrix}^T \\
\mathbf{u}(t) &= \begin{bmatrix} u_1(t) & u_4(t) \end{bmatrix}^T \\
\mathbf{w}(t) &= \begin{bmatrix} T_o(t) \end{bmatrix}^T \\
\mathbf{y}(t) &= \begin{bmatrix} y_1(t) & y_2(t) & y_3(t) & y_4(t) \end{bmatrix}^T
\end{aligned}
$$

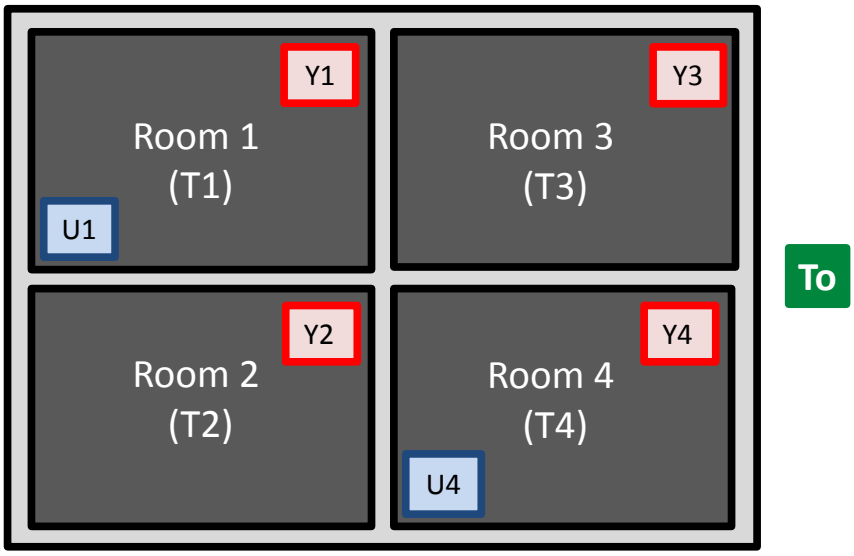

Figure A.2: Floor Plan of 4 Room Building

and the system matrices are

$$A(\theta) = \begin{bmatrix} -a_{11} & 0 & 0 & 0 & \frac{1}{R_{12a}C_1} & \frac{1}{R_{13a}C_1} & 0 & 0 \\ 0 & -a_{22} & 0 & 0 & \frac{1}{R_{12b}C_2} & 0 & \frac{1}{R_{24a}C_2} & 0 \\ 0 & 0 & -a_{33} & 0 & 0 & \frac{1}{R_{13b}C_3} & 0 & \frac{1}{R_{34a}C_3} \\ 0 & 0 & 0 & -a_{44} & 0 & 0 & \frac{1}{R_{24b}C_4} & \frac{1}{R_{34b}C_4} \\ \frac{1}{R_{12a}C_{12}} & \frac{1}{R_{12b}C_{12}} & 0 & 0 & -a_{55} & 0 & 0 & 0 \\ \frac{1}{R_{13a}C_{13}} & 0 & \frac{1}{R_{13b}C_{12}} & 0 & 0 & -a_{66} & 0 & 0 \\ 0 & \frac{1}{R_{24a}C_{24}} & 0 & \frac{1}{R_{24b}C_{24}} & 0 & 0 & -a_{77} & 0 \\ 0 & 0 & \frac{1}{R_{34a}C_{34}} & \frac{1}{R_{34b}C_{34}} & 0 & 0 & 0 & -a_{88} \end{bmatrix}$$

$$B(\theta) = \begin{bmatrix} \frac{1}{C_1} & 0 \\ 0 & 0 \\ 0 & 0 \\ 0 & \frac{1}{C_2} \\ 0 & 0 \\ 0 & 0 \\ 0 & 0 \\ 0 & 0 \end{bmatrix} \quad G(\theta) = \begin{bmatrix} g_{11} \\ g_{22} \\ g_{33} \\ g_{44} \\ 0 \\ 0 \\ 0 \\ 0 \end{bmatrix} \quad C = \begin{bmatrix} 1 & 0 & 0 & 0 & 0 & 0 & 0 & 0 \\ 0 & 1 & 0 & 0 & 0 & 0 & 0 & 0 \\ 0 & 0 & 1 & 0 & 0 & 0 & 0 & 0 \\ 0 & 0 & 0 & 1 & 0 & 0 & 0 & 0 \end{bmatrix}$$

$$a_{11} = g_{11} + \frac{1}{R_{12a}C_1} + \frac{1}{R_{13a}C_1}, \qquad g_{11} = \frac{1}{R_{1N}C_1} + \frac{1}{R_{1W}C_1} + \frac{1}{R_{1R}C_1} + \frac{1}{R_{1F}C_1}$$

$$a_{22} = g_{22} + \frac{1}{R_{12b}C_2} + \frac{1}{R_{24a}C_2}, \qquad g_{22} = \frac{1}{R_{2S}C_2} + \frac{1}{R_{2W}C_2} + \frac{1}{R_{2R}C_2} + \frac{1}{R_{2F}C_2}$$

$$a_{33} = g_{33} + \frac{1}{R_{13b}C_3} + \frac{1}{R_{34a}C_3}, \qquad g_{33} = \frac{1}{R_{3N}C_3} + \frac{1}{R_{3E}C_3} + \frac{1}{R_{3R}C_3} + \frac{1}{R_{3F}C_3}$$

$$a_{44} = g_{44} + \frac{1}{R_{24b}C_4} + \frac{1}{R_{34b}C_4}, \qquad g_{44} = \frac{1}{R_{4S}C_4} + \frac{1}{R_{4E}C_4} + \frac{1}{R_{4R}C_4} + \frac{1}{R_{4F}C_4}$$

$$a_{55} = \frac{1}{R_{12a}C_{12}} + \frac{1}{R_{12b}C_{12}}$$

$$a_{66} = \frac{1}{R_{13a}C_{13}} + \frac{1}{R_{13b}C_{13}}$$

$$a_{77} = \frac{1}{R_{24a}C_{24}} + \frac{1}{R_{24b}C_{24}}$$

$$a_{88} = \frac{1}{R_{34a}C_{34}} + \frac{1}{R_{34b}C_{34}}$$

Appendix B

Building Digraph Algorithms

B.1 Partition into Digraphs of Air-Based Subsystems

Algorithm 12 describes an approach that resembles a breadth first search to partition $G(\mathcal{S})$ into the component subgraphs $G(\mathcal{S}_i^a)$. We can claim the algorithm is correct by proving the claim of algorithm correctness in Proposition 4.

Proposition 4 (Correctness of Algorithm 12): *Algorithm 12 decomposes* $G(\mathcal{S})$ *into the set of subgraphs,* $\{G(\mathcal{S}_i^a) : \forall i \in [1, a]\}$*, where the set of air-based subsystems,* $\{\mathcal{S}_i^a : i \in [1, a]\}$ *as defined in Definition 10.* ♣

Proof Line 2 satisfies the condition, $X_i^a \cap X_a = \{T_i\}$, and Line 5 does not violate this condition since the set of state vertices $X_{w,i}$ added to X_i^a are not in X_i^a by Line 4. Furthermore, the while-loop in Lines 3-6 is terminated only when the condition, $N(X_i^a) \cap X \subset X_a$ on $G(\mathcal{S})$, is satisfied. Therefore, X_i^a satisfies the first two conditions

Algorithm 12 Decomposition of $G(\mathcal{S})$ into the set of air-based subsystems $G(\mathcal{S}_i^a)$

Input: $G(\mathcal{S}) = \{X \cup U \cup W \cup Y, E\}$
Output: $\{G(\mathcal{S}_i^a) : \forall i \in [1, a]\}$
1: **for all** $i := 1 \rightarrow a$ **do**
2: $X_i^a := \{T_i\}$
3: **while** $N(X_i^a) \cap X \not\subset X_a$ **do**
4: $X_{w,i} \leftarrow N(X_i^a) \cap X_w$
5: $X_i^a \leftarrow X_i^a \cup X_{w,i}$
6: **end while**
7: $U_i^a := N(X_i^a) \cap U$
8: $W_i^a := N(X_i^a) \cap (X \cup W)$
9: $Y_i^a := N(X_i^a) \cap Y$
10: $E_i^a := \{(u, v) \in E : \forall u, v \in X_i^a \cup U_i^a \cup W_i^a \cup Y_i^a\}$
11: $G(\mathcal{S}_i^a) := \{X_i^a \cup U_i^a \cup W_i^a \cup Y_i^a, E_i^a\}$
12: $i \leftarrow i + 1$
13: **end for**
14: **return** $\{G(\mathcal{S}_i^a) : \forall i \in [1, a]\}$

of Definition 10. Lines 7-11 follows from the conditions outlined in Definition 10. Therefore, Lines 2-11 satisfy definition for the i^{th} air based subsystem $\mathcal{S}_i^a$. Given the for-loop introduced in Line 1, Algorithm 12 returns the set of all possible air based subsystems in Line 14. ∎

B.2 Partitioning the Building Digraph

In this section, we present two algorithms to partition the building digraph into input-output reachable graphs. We accomplish this challenge in two parts. First, we partition the building map into uniform input-output reachable partitions. Second, we use these input-output reachable partitions of the building map to create zones, that are by definition input and output reachable.

Algorithm 13 Create a uniform input-output reachable partition of the building map

Input: $G_R(\mathcal{S}) = \{V_R, E_R\}$
Output: $\{\{V_R^k, E_R^k\} : \forall k\}$

1: $V_{ir} := \{i \in V_R :$ for all input-reachable air based subsystems $\mathcal{S}_i^a\}$
2: $V_{or} := \{i \in V_R :$ for all output-reachable air based subsystems $\mathcal{S}_i^a\}$
3: $N := 0$
4: **for all** $i \in V_{ir} \cap V_{or}$ **do** ▷ Create initial partitions, $\{V_R^k, E_R^k\}$
5: $\quad N \leftarrow N + 1$
6: $\quad V_R^N := \{i\}$
7: $\quad E_R^N := \emptyset$
8: $\quad G_N := \{V_R^N, E_R^N\}$
9: **end for**
10: $\mathbf{n} := \{1, 2, \ldots, N\}$
11: $V_{nodesleft} \leftarrow V_R - (V_{ir} \cap V_{or})$
12: **while** $V_{nodesleft} \neq \emptyset$ **do** ▷ Add remaining vertices to a partition $\{V_R^k, E_R^k\}$
13: $\quad$ **for all** $k \in \mathbf{n}$ **do**
14: $\quad\quad N(V_R^k) :=$ Neighborhood of vertex set V_R^k on $G_R(\mathcal{S})$
15: $\quad\quad j :=$ Choose a single element from $N(V_R^k) \cap V_{nodesleft}$
16: $\quad\quad V_R^k \leftarrow V_R^k \cup \{j\}$
17: $\quad\quad E_R^k \leftarrow E_R^k \cup \{(i,j) \in E_R : i, j \in V_R^k\}$
18: $\quad\quad V_{nodesleft} \leftarrow V_{nodesleft} - \{j\}$
19: $\quad$ **end for**
20: **end while**
21: **return** $\{\{V_R^k, E_R^k\} : \forall k\}$

B.2.1 Partitioning Building Map

Proposition 5: *Algorithm 13 returns* $\{\{V_R^k, E_R^k\} : \forall k\}$ *which is an input-output reachable partition of the building map* $G_R(\mathcal{S})$. ♣

Proof Given Lines 1 and 2, Lines 4-9 create initial subgraphs $G_k = \{V_R^k, E_R^k\}$ for $k \in \mathbf{n}$ around vertices that correspond to an input-output reachable air based system. For the remaining vertices $j \in V_{nodesleft}$, Lines 12-20 iterate through the subgraphs $\{V_R^k, E_R^k\}$ and chooses a vertex j in the neighborhood of the vertex set V_R^k to add to V_R^k. When the while loop is terminated, then $V_{nodesleft} = \emptyset$ and the set of subgraphs

$\{V_R^k, E_R^k\}$ constitute a graph partition of $G_R(\mathcal{S})$. This guarantees each partition includes the index of at least one input reachable air-based subsystem and one output reachable air based subsystem. Therefore, Algorithm 13 satisfies the conditions for an input-output reachable partition of the building map as outlined in Definition 12.■

B.2.2 Creating Building Zone Dynamics

Algorithm 14 Create a zone partition, $\{\mathcal{S}_k : \forall k\}$

Input: $\mathcal{S}$
Output: $\{\mathcal{S}_k : \forall k\}$

$G(\mathcal{S}) := \{X \cup U \cup W \cup Y, E\}$
Decompose $\mathcal{S}$ into a set of air based subsystems, $\{\mathcal{S}_i^a : i \in [1, a]\}$
Create air based building map, $G_R(\mathcal{S}) := \{V_R, E_R\}$
Partition $G_R(\mathcal{S})$ into input-output reachable parts, $\{\{V_R^k, E_R^k\} : \forall k\}$
for all $k \in$ **n do**
    $X_k := \emptyset$
    for all $i \in V_k'$ **do**
        $X_k \leftarrow X_k \cup X_i^a$
        $U_k \leftarrow U_k \cup U_i^a$
        $W_k \leftarrow W_k \cup W_i^a$
        $Y_k \leftarrow Y_k \cup Y_i^a$
        $E_k \leftarrow E_k \cup E_i^a$
    end for
    $G(\mathcal{S}_k) := \{X_k \cup U_k \cup W_k \cup Y_k, E_k\}$
end for
return $\{\mathcal{S}_k : \forall k\}$

Appendix C

Receding Horizon H_∞ Control Proofs

This chapter presents the detailed proofs to Lemma 2 and Lemma 3 in Chapter 5.

PROOF (OF LEMMA 2) This proof is adapted from [12, 13]. Given $S(k, k+n_p)$ in (5.17), Let

$$\begin{aligned} S(k,k+n_p) - S(k,k+n_p-1) &= \|H\bar{\mathbf{x}}[k+n_p]^*\|^2 - \|H\bar{\mathbf{x}}[k+n_p+1]^*\|^2 \\ &+ \gamma^2\|\bar{\delta}[K+n_p]^*\|^2 - \|\bar{\mathbf{z}}[k+n_p]^*\|^2 \end{aligned} \tag{C.1}$$

where the vectors $\bar{\mathbf{z}}[k+n_p]^*$ and $\bar{\mathbf{x}}[k+n_p+1]^*$ are functions of $\bar{\mathbf{x}}[k+n_p]^*$, $\bar{\mathbf{u}}[k+n_p]^*$, and $\bar{\delta}[k+n_p]^*$ according to (5.24b) and (5.24c).

Consider the function $V(\bar{\mathbf{x}}[k]^*) = \|\bar{\mathbf{x}}[k]^*\|_P^2 = S(k,\infty)$ for some matrix $P = P^T > 0$. Then, (5.17) can be written recursively in terms of $V(\bar{\mathbf{x}}[k]^*)$ as follows,

$$V(\bar{\mathbf{x}}[k]^*) = \|\bar{\mathbf{z}}[k]^*\|^2 - \gamma^2\|\bar{\delta}[k]^*\|^2 + V(\bar{\mathbf{x}}[k+1]^*). \tag{C.2}$$

Since the model $M(\theta)$ is asymptotically stable, then (C.2) becomes,

$$V(\bar{\mathbf{x}}[k]^*) \geq \|\bar{\mathbf{z}}[k]^*\|^2 - \gamma^2 \|\bar{\delta}[k]^*\|^2 + V(\bar{\mathbf{x}}[k+1]^*) \tag{C.3}$$

for all $\mathbf{x}[k]^*$, $\mathbf{u}[k]^*$, $\delta[k]^*$, and $\mathbf{z}[k]^*$. Assume $V(\mathbf{x}[k+n_p]^*) = \|H\bar{\mathbf{x}}[k+n_p]^*\|^2$ and $V(\mathbf{x}[k+n_p+1]^*) = \|H\bar{\mathbf{x}}[k+n_p+1]^*\|^2$. Then, for time $k+n_p$, (C.3) becomes

$$\|H\bar{\mathbf{x}}[k+n_p]^*\|^2 \geq \|\bar{\mathbf{z}}[k+n_p]^*\|^2 - \gamma^2 \|\bar{\delta}[K+n_p]^*\|^2 + \|H\bar{\mathbf{x}}[k+n_p+1]^*\|^2 \tag{C.4}$$

for $(\bar{\mathbf{u}}[k+n_p]^*, \bar{\delta}[k+n_p]^*)$. Then, (C.1) becomes the following inequality

$$S(k, k+n_p) - S(k, k+n_p-1) \geq 0 \tag{C.5}$$

which directly implies the original claim. ∎

Proof (of Lemma 3) This proof is also adapted from [12, 13]. Let the predicted cost $S(k, k+n_p)$ in (5.17) be written as the following maximization problem,

$$S(k, k+n_p) = \max_{\bar{\Delta}_k} \left\{ \|H\bar{\mathbf{x}}[k+n_p]\|^2 + \sum_{n=k}^{k+n_p-1} \left(\|\bar{\mathbf{z}}[n]\|^2 - \gamma^2 \|\bar{\delta}[n]\|^2 \right) \right\} \tag{C.6}$$

where the vectors $\bar{\mathbf{z}}[n]$, $\bar{\mathbf{x}}[n]$ are functions of $\bar{\mathbf{x}}[k]$, $\bar{U}_k^*$, and some sequence $\bar{\Delta}_k$ according to (5.24b) and (5.24c). The sequence $\bar{\Delta}_k$ that maximizes (C.6) is the solution $\bar{\Delta}_k^*$.

Suppose the actual state uncertainty at time k is $\delta[k] = \bar{\delta}[k]^*$ where $\bar{\delta}[k] \in \bar{\Delta}_k^*$ and the actual building performance at time k is $\mathbf{z}[k] = \bar{\mathbf{z}}[k]^*$ given $\mathbf{u}[k] = \bar{\mathbf{u}}[k]^* \in \bar{U}_k^*$. Then, (C.6) can be rewritten as

$$S(k, k+n_p) = \|\mathbf{z}[k]\|^2 - \gamma^2 \|\delta[k]\|^2 + \max_{\bar{\Delta}_{k+1}} \left\{ \|H\bar{\mathbf{x}}[k+n_p]\|^2 \right.$$

$$+ \sum_{n=k+1}^{k+n_p-1} \left(\|\bar{\mathbf{z}}[n]\|^2 - \gamma^2 \|\bar{\delta}[n]\|^2 \right) \Bigg\} \tag{C.7}$$

$$= \|\mathbf{z}[k]\|^2 - \gamma^2 \|\delta[k]\|^2 + S(k+1, k+n_p) \tag{C.8}$$

where $\bar{\Delta}_{k+1} \subset \bar{\Delta}_k$. Given the result $S(k+1, k+n_p) \geq S(k+n_p, k+n_p+1)$ from Lemma 2 and (C.8), then

$$S(k, k+n_p) \geq \|\mathbf{z}[k]\|^2 - \gamma^2 \|\delta[k]\|^2 + S(k+1, k+n_p+1), \tag{C.9}$$

which directly implies (5.18). ■

Bibliography

[1] Clarence Agbi, Zhen Song, and Bruce Krogh. "Parameter Identifiability for Multi-Zone Building Models". In: *IEEE Conference on Decisions and Control*. Maui, Hawaii, 2012.

[2] Klaus Kaae Andersen, Henrik Madsen, and Lars H. Hansen. "Modeling the heat dynamics of a building using stochastic differential equations". In: *Energy and Buildings* 31.1 (Jan. 2000), pp. 13–24.

[3] James Anderson, Yo-Cheng Chang, and Antonis Papachristodoulou. "Model decomposition and reduction tools for large-scale networks in systems biology". In: *Automatica* 47.6 (June 2011), pp. 1165–1174.

[4] Märta Barenthin. "On input design in system identification for control". PhD thesis. KTH, 2006. URL: `http://kth.diva-portal.org/smash/record.jsf?pid=diva2:10322`.

[5] Märta Barenthin et al. "Identification for control of multivariable systems: Controller validation and experiment design via LMIs". In: *Automatica* 44.12 (Dec. 2008), pp. 3070–3078. URL: `http://linkinghub.elsevier.com/retrieve/pii/S0005109808003221`.

[6] Tamer Basar and Pierre Bernhard. *H-Infinity Optimal Control and Related Minimax Design Problems: A Dynamic Game Approach*. 2nd. Boston: Birkhäuser, 1995.

[7] Farinaz Behrooz. "A survey on applying different control methods approach in building automation systems to obtain more energy efficiency". In: *International Journal of the Physical Sciences* 6.9 (2011), pp. 2308–2314.

[8] M.R. Brambley et al. *Advanced Sensors and Controls for Building Applications: Market Assessment and Potential R&D Pathways*. Tech. rep. April. Richland, Washington: Pacific Northwest National Laboratory, 2005. URL: `http://citeseerx.ist.psu.edu/viewdoc/download?doi=10.1.1.111.8772%5C&rep=rep1%5C&type=pdf`.

[9] James E. Braun. "Intelligent Building Systems - Past, Present, and Future". In: *2007 American Control Conference*. New York City, USA: IEEE, July 2007, pp. 4374–4381.

[10] Vikas Chandan and Andrew G. Alleyne. "Decentralized Architectures for Thermal Control of Buildings". In: *2012 American Control Conference*. Vol. 1. Montreal, Canada: IEEE, 2012, pp. 3657–3662.

[11] Francois Chaplais and K. Alaoui. "Two Time Scaled Parameter Identification By Coordination of Local Identifiers". In: *Automatica* 32.9 (1996), pp. 1303–1309.

[12] H. Chen, C.W. Scherer, and F. Allgower. "A Game Theoretic Approach to Nonlinear Robust Receding Horizon Control of Constrained Systems". In: *American Control Conference*. June. Alberquerque, New Mexico: IEEE, 1997, pp. 3073–3077.

[13] H. Chen, C.W. Scherer, and F. Allgower. "A Robust Model Predictive Control Scheme for Constrained Linear Systems". In: *IFAC Dynamics and Control of Process Systems*. Corfu, Greece, 1998, pp. 61–66.

[14] C. Cobelli, A. Lepschy, and G. Romanin Jacur. "Identifiability of Compartmental Systems and Related Structural Properties". In: *Mathematical Biosciences* 44 (1979), pp. 1–18.

[15] C. Cobelli, A. Lepschy, and G. Romanin-Jacur. "Comments on "On the Relationships Between Structural Identifiability and the Controllability, Observability Properties"". In: *IEEE Transactions on Automatic Control* 23.5 (1978), pp. 965–966.

[16] McGraw Hill Construction. *Energy Efficiency Trends in Residential and Commercial Buildings*. Tech. rep. August. US Department of Energy, Office of Energy Efficiency and Renewable Energy, 2010.

[17] S. Dautin et al. "Comparison of building thermal response model reduction methods, Experimental building application". In: *Proceedings of CLIMA 2000 World Congress*. Brussels, Belgium, 1997, pp. 1–10.

[18] Kun Deng, Prabir Barooah, and Prashant G. Mehta. "Mean-Field Control for Energy Efficient Buildings". In: *American Control Conference*. Montreal, Canada: IEEE, 2012, pp. 3044–3049.

[19] Kun Deng et al. "Building Thermal Model Reduction via Aggregation of States". In: *American Control Conference*. Baltimore, Maryland: IEEE, 2010, pp. 5118–5123.

[20] F. Déqué, F. Ollivier, and A. Poblador. "Grey boxes used to represent buildings with a minimum number of geometric and thermal parameters". In: *Energy and Buildings* 31 (2000), pp. 29–35.

[21] Joseph J. DiStefano. "On the Relationships Between Structural Identifiability and the Controllability, Observability Properties". In: *IEEE Transactions on Automatic Control* 22.4 (1977), p. 652.

[22] Joseph J. DiStefano and Claudio Cobelli. "On Parameter and Structural Identifiability: Nonunique Observability/Reconstructability for Identifiable Systems, Other Ambiguities, and New Definitions". In: *IEEE Transactions on Automatic Control* 25.4 (1980), pp. 830–833.

[23] Bing Dong. "Integrated Building Heating, Cooling and Ventilation Control". PhD thesis. Carnegie Mellon University, 2010. URL: `http://repository.cmu.edu/dissertations/4`.

[24] Jorn F. M. Van Doren et al. "Determining identifiable parameterizations for large-scale physical models in reservoir engineering". In: *Proceedings of the 17th International Federation on Automatic Control (IFAC) World Congress*. Seoul, Korea, 2008, pp. 11421–11426.

[25] Jorn F. M. Van Doren et al. "Identifiability: from qualitative analysis to model structure approximation". In: *Proceedings of the 15th International Federation on Automatic Control (IFAC) Symposium on System Identification*. Saint-Malo, France, 2009, pp. 664–669.

[26] Jorn F.M. Van Doren and Paul M. J. Van den Hof. "Parameter identification in large-scale models for oil and gas production". In: *Proceedings of 18th International Federation on Automatic Control (IFAC) World Congress*. Milano, Italy, 2011, pp. 10857–10862.

[27] Hans G.M. Dotsch and Paul M. J. Van den Hof. "Test for Local Structural Identifiability of High-order Non-linearly Parameterized State Space Models". In: *Automatica* 32.6 (1996), pp. 875–883.

[28] A.I. Dounis and C. Caraiscos. "Advanced control systems engineering for energy and comfort management in a building environment - A review". In: *Renewable and Sustainable Energy Reviews* 13.6-7 (Aug. 2009), pp. 1246–1261.

[29] D&R Internatonal Ltd. *2011 Buildings Energy Data Book*. Tech. rep. Building Technologies Program, Energy Efficiency and Renewable Energy, U.S. Department of Energy, 2012. URL: `http://buildingsdatabook.eere.energy.gov/`.

[30] U.S. Department of Energy. *Commercial Reference Buildings*. 2014. URL: `http://energy.gov/eere/buildings/commercial-reference-buildings`.

[31] U.S. Department of Energy. *EnergyPlus Engineering Reference: The Reference to EnergyPlus Calculations*. Tech. rep. 2013.

[32] Cristian Ghiaus and Christian Inard. "Energy and Environmental Issues of Smart Buildings". In: *A Handbook for intelligent Building*. 2004. Chap. 2, pp. 26–51.

[33] Keith R. Godfrey and Michael J. Chapman. "The Problem of Model Indistinguishability in Pharmacokinetics". In: *Journal of Pharmacokinetics and Biopharmaceutics* 17.2 (Apr. 1989), pp. 229–67.

[34] Xiangyang Gong. "Investigation of a Radiantly Heated and Cooled Office with an Integrated Desiccant Ventilation Unit". PhD thesis. Texas A&M University, 2007.

[35] M.M. Gouda, S. Danaher, and C.P. Underwood. "Building thermal model reduction using nonlinear constrained optimization". In: *Building and Environment* 37.12 (Dec. 2002), pp. 1255–1265.

[36] Siddharth Goyal and Prabir Barooah. "A method for model-reduction of nonlinear thermal dynamics of multi-zone buildings". In: *Energy and Buildings* 47 (Apr. 2012), pp. 332–340.

[37] Markus Gwerder and Dimitrios Gyalistras. "Potential Assessment of Rule-Based Control for Integrated Room Automation". In: *10th REHVA World Congress CLIMA 2010*. May. Antalya, Turkey, 2010.

[38] Dimitrios Gyalistras and Markus Gwerder. "Analysis of energy savings potentials for integrated room automation". In: *10th REHVA World Congress CLIMA 2010*. Antalya, Turkey, 2010.

[39] K.E. Häggblom and J.M. Böling. "Multimodel identification for control of an ill-conditioned distillation column". In: *Journal of Process Control* 8.3 (Jan. 1998), pp. 209–218.

[40] Hå kan Hjalmarsson and J Martensson. "Optimal input design for identification of non-linear systems: Learning from the linear case". In: *Proceedings of the 2007 American Control Conference*. New York City, USA, 2007, pp. 1572–1576. URL: http://ieeexplore.ieee.org/xpls/abs%5C_all.jsp?arnumber=4282525.

[41] J.M. van den Hof. "Structural Identifiability of Linear Compartmental Systems". In: *IEEE Transactions on Automatic Control* 43.6 (June 1998), pp. 800–818.

[42] X. Hong et al. “Model selection approaches for non-linear system identification: a review”. In: *International Journal of Systems Science* 39.10 (Oct. 2008), pp. 925–946.

[43] Rolf Isermann and Marco Münchhof. *Identification of Dynamic Systems*. Berlin, Heidelberg: Springer, 2011.

[44] John A. Jacquez and Peter Greif. “Numerical Parameter Identifiability and Estimability: Integrating Identifiability, Estimability, and Optimal Sampling Design”. In: *Mathematical Biosciences* 77 (1985), pp. 201–227.

[45] Pramod P. Khargonekar, Krishan M. Nagpal, and Kameshwar R. Poolla. “H Infinity Control with Transients”. In: *SIAM J. Control And Optimization* 29.6 (1991), pp. 1373–1393.

[46] Pramod P. Khargonekar, Krishan M. Nagpal, and Kameshwar R. Poolla. “H-Infinity Control of Linear Systems with Nonzero Initial Conditions”. In: *Proceedings of the 29th Conference on Decision and Control*. December. Honolulu, Hawaii: IEEE, 1990, pp. 1821–1826.

[47] Ki Baek Kim. “Disturbance Attenuation for Constrained Discrete-Time Systems via Receding Horizon Controls”. In: *Proceedings of the 42nd IEEE Conference on Decision and Control*. December. Maui, Hawaii: IEEE, 2003, pp. 935–940.

[48] Ki Baek Kim and Wook Hyun Kwon. “Intervalwise Receding Horizon H-Infinity Tracking Controls for Linear Continuous Time-Varying Systems”. In: *Proceedings of the American Control Conference*. Anchorage, Alaska: IEEE, 2002, pp. 2186–2191.

[49] Sean H. Kim. "Development of Robust Building Energy Demand-Side Control Strategy under Uncertainty". PhD thesis. Georgia Institute of Technology, 2011. URL: http://adsabs.harvard.edu/abs/2011PhDT.....221K.

[50] Mayuresh V. Kothare, Venkataramanan Balakrishnan, and Manfred Morari. "Robust Constrained Model Predictive Control using Linear Matrix Inequalities". In: *Automatica* 32.10 (1996), pp. 1361–1379.

[51] Bin Li and Andrew G. Alleyne. "Optimal On-Off Control of an Air Conditioning and Refrigeration System". In: *Proceedings of the American Control Conference*. Baltimore, Maryland: IEEE, 2010, pp. 5892–5897.

[52] Rujun Li, Michael A. Henson, and Michael J. Kurtz. "Selection of Model Parameters for Off-Line Parameter Estimation". In: *IEEE Transactions on Control Systems Technology* 12.3 (May 2004), pp. 402–412.

[53] Yang-Yu Liu, Jean-Jacques Slotine, and Albert-László Barabási. "Controllability of complex networks". In: *Nature* 473.7346 (May 2011), pp. 167–73.

[54] Lennart Ljung. *System Identification: Theory For The User*. 2nd. Upper Saddle River, New Jersey: Prentice Hall, 1999.

[55] Lennart Ljung. *System Identification: Theory for the User*. 1st. Englewood Cliffs, New Jersey: Prentice Hall, 1987.

[56] J Löfberg. "Minimax approaches to robust model predictive control". PhD thesis. Linkoping University, 2003. URL: http://www.researchgate.net/publication/228869742%5C_Minimax%5C_approaches%5C_to%5C_robust%5C_model%5C_predictive%5C_control/file/d912f5098b781a4e95.pdf.

[57] Yan Lu et al. *Advanced, Integrated Control for Building Operations to Achieve 40% Energy Saving*. Tech. rep. Princeton, New Jersey: Siemens Corportation, Corporate Research, 2012.

[58] Miaomiao Ma, Hong Chen, and Xiangjie Liu. "Robust H-infinity control for constrained uncertain systems and its application to active suspension". In: *Journal of Control Theory Applications* 10.12 (2012), pp. 470–476. URL: http://link.springer.com/article/10.1007/s11768-012-0286-5.

[59] Yudong Ma and Francesco Borrelli. "Fast Stochastic Predictive Control for Building Temperature Regulation". In: *Proceedings of 2012 American Control Conference*. Montreal, Canada: IEEE, 2012, pp. 3075–3080.

[60] Mehdi Maasoumy, Alessandro Pinto, and Alberto Sangiovanni-Vincentelli. "Model-Based Hierarchical Optimal Control Design for HVAC Systems". In: *Proceedings of the ASME 2011 Dynamic Systems and Control Conference*. Arlington, Virginia, 2011, pp. 271–278.

[61] Paul Malisani et al. "Thermal building model identification using time-scaled identification methods". In: *49th IEEE Conference on Decision and Control*. Atlanta, Georgia: IEEE, Dec. 2010, pp. 308–315.

[62] K Marik et al. "Advanced HVAC Control: Theory vs. Reality". In: *Proceedings of the 18th IFAC World Congress*. Milano, Italy, 2011, pp. 3108–3113.

[63] DG Marinova and GE Stavroulakis. "Robust Control Design of a Smart Building Structure". In: *Journal of Theoretical and Applied Mechanics* 45.1 (2007), pp. 73–90. URL: http://www.ptmts.org/marinova-s-1-07.pdf.

[64] M.D. Mesarović, D. Macko, and Y. Takahara. *Theory of Hierarchical, Multilevel Systems*. Vol. 68. New York, New York: Academic Press, Inc., 1970.

[65] Mihaljo D. Mesarovic. “Multilevel Systems and Concepts in Process Control”. In: *Proceedings of the IEEE* 58.1 (1970), pp. 111–125.

[66] Riccardo Muradore and Giorgio Picci. “Mixed H2/H-Infinity Control: The Discrete Case”. In: *Proceedings of the 42nd IEEE Conference on Decision and Control*. December. Maui, Hawaii, 2003, pp. 1789–1794.

[67] Truong Nghiem. *Modeling and Advanced Control of HVAC System*. 2011. URL: `http://www.seas.upenn.edu/~cis800/lectures/hvac%5C_mdl%5C_mpc.pdf`.

[68] Truong X. Nghiem. *MLE+: a Matlab-EnergyPlus Co-simulation Interface.* 2014. URL: `http://www.seas.upenn.edu/~nghiem/mleplus.html`.

[69] Truong X. Nghiem and George J. Pappas. “Receding-horizon Supervisory Control of Green Buildings”. In: *Proceedings of 2011 American Control Conference*. San Francisco, California: IEEE, 2011, pp. 4416–4421.

[70] Frauke Oldewurtel et al. “Energy Efficient Building Climate Control using Stochastic Model Predictive Control and Weather Predictions”. In: *Proceedings of 2010 American Control Conference*. Baltimore, Maryland: IEEE, 2010.

[71] Glenn Platt et al. “Adaptive HVAC zone modeling for sustainable buildings”. In: *Energy and Buildings* 42.4 (Apr. 2010), pp. 412–421.

[72] Atilla Raksanyi et al. “Identifiability and Distinguishability Testing via Computer Algebra”. In: *Mathematical Biosciences* 77 (Dec. 1985), pp. 245–266.

[73] N. Sadati and E. Dehghan Marvast. “Nonlinear Optimal Control of Large-Scale Systems; Part II -Interaction Balance Principle”. In: *International Conference on Industrial Electronics and Control Applications (ICIECA)*. Quito, Ecuador: IEEE, 2005.

[74] N. Sadati and AR Momeni. "Nonlinear Optimal Control of Two-Level Large-Scale Systems; Part I-Interaction Prediction Principle". In: *International Conference on Industrial Electronics and Control Applications (ICIECA)*. Quito, Ecuador: IEEE, 2005.

[75] N. Sadati and M. H. Ramezani. "Hierarchical Optimal Control of Nonlinear Systems; An Application to a Benchmark CSTR Problem". In: *3rd IEEE Conference on Industrial Electronics and Applications*. Singapore: IEEE, June 2008, pp. 455–460.

[76] Timothy Salsbury. "A Survey of Control Technologies in the Building Automation Industry". In: *Proceedings of the 16th IFAC World Congress*. Czech Republic: IFAC, 2005.

[77] D.D. Siljak. *Decentralized Control of Complex Systems*. Academic Press, Inc., 1991.

[78] Carlos E. de Souza and Lihua Xie. "On the Discrete-time Bounded Real Lemma with application in the characterization of static state feedback H-Infinity controllers". In: *Systems & Control Letters* 18.1 (Jan. 1992), pp. 61–71.

[79] Przemyskaw Stec and Yucai Zhu. "Some Study on Identification of Ill-Conditioned Processes for Control". In: *Proceedings of the American Control Conference*. IEEE, 2001, pp. 1202–1207.

[80] M. Bala Subrahmanyam. *H-Infinity Optimal Control Theory Over a Finite Horizon.* Tech. rep. 0602936. Warminster, Pennsylvania: Naval Air Development Center, 1991.

[81] Samuel C. Sugarman. *HVAC Fundamentals*. United States of America: The Fairmont Press, Inc., 2005.

[82] Bourhan Tashtoush, M. Molhim, and M. Al-Rousan. "Dynamic model of an HVAC system for control analysis". In: *Energy* 30 (2005), pp. 1729–1745.

[83] Bo Wahlberg, Hakan Hjalmarsson, and Mariette Annergren. "On Optimal Input Design in System Identification for Control". In: *Proceedings of the 49th IEEE Conference on Decision and Control*. Atlanta, Georgia: IEEE, Dec. 2010, pp. 5548–5553.

[84] Shengwei Wang and Zhenjun Ma. "Supervisory and Optimal Control of Building HVAC Systems: A Review". In: *HVAC&R Research* 14.1 (2008), pp. 37–41.

[85] J.K.W. Wong, H. Li, and S.W. Wang. "Intelligent building research: a review". In: *Automation in Construction* 14.1 (Jan. 2005), pp. 143–159.

[86] Zhiguo Yan, Guoshan Zhang, and Jiankui Wang. "Infinite horizon H-two/H-infinity control for descriptor systems: Nash game approach". In: *Journal of Control Theory and Applications* 10.2 (Apr. 2012), pp. 159–165.

[87] Yucai Zhu and Przemyskaw Stec. "Simple control-relevant identification test methods for a class of ill-conditioned processes". In: *Journal of Process Control* 16.10 (Dec. 2006), pp. 1113–1120.